Distribution Category:
Energy Storage—Electrochemical
(UC-94c)

ANL-76-9

ARGONNE NATIONAL LABORATORY
9700 South Cass Avenue
Argonne, Illinois 60439

HIGH-PERFORMANCE BATTERIES FOR OFF-PEAK ENERGY STORAGE AND ELECTRIC-VEHICLE PROPULSION

Progress Report for the Period
July—December 1975

P. A. Nelson	Manager, Battery Program
R. O. Ivins	Associate Manager, Battery Program
N. P. Yao	Assistant Manager, Battery Program
J. E. Battles	Group Leader, Materials Development
A. A. Chilenskas	Group Leader, Battery Design
E. C. Gay	Group Leader, Electrode Development
R. K. Steunenberg	Group Leader, Cell Chemistry
W. J. Walsh	Group Leader, Cell Development

April 1976

Previous Reports in this Series

ANL-8057	July—December 1973
ANL-8109	January—June 1974
ANL-75-1	July—December 1974
ANL-75-36	January—June 1975

FOREWORD

Argonne National Laboratory's program on high-temperature secondary batteries is carried out principally in the Chemical Engineering Division, with assistance on specific problems being given by the Materials Science Division and, from time to time, by other Argonne divisions. The individual efforts of many scientists and technicians are essential to the success of the program, and recognition of these efforts is reflected in the individual contributions cited throughout the report.

TABLE OF CONTENTS

LIST OF FIGURES

LIST OF TABLES

HIGH-PERFORMANCE BATTERIES FOR OFF-PEAK ENERGY STORAGE AND ELECTRIC-VEHICLE PROPULSION

July-December 1975

ABSTRACT

This report describes the research and management efforts of Argonne National Laboratory's program on high-performance lithium/metal sulfide batteries during the period July-December 1975. The batteries are being developed for two applications: off-peak energy storage in electric utility networks and electric-vehicle propulsion. The battery designs for the two applications differ, particularly in cell configuration and electrode design, because of the differing performance requirements. The present cells are vertically oriented, prismatic cells with two negative electrodes of a solid lithium-aluminum alloy and a central positive electrode of iron sulfide (FeS_2 or FeS). The electrolyte is molten LiCl-KCl eutectic, which requires a cell temperature of about 400-450°C.

Effort was continued on the development of engineering-scale cells with hot-pressed electrodes assembled in the uncharged state (positive electrode of Li_2S-Fe, negative electrode of Al). Studies of electrodes were directed principally toward developing positive electrodes of FeS_2 and FeS in carbon-bonded structures and toward improving the performance and lowering the cost of negative Li-Al electrodes. Materials studies included work on improved separators and feedthroughs, corrosion tests of materials in the cell environment, and postoperative examinations of cells. Work in the area of cell chemistry included the continuing studies of cell reactions and investigations of advanced cell systems. Battery design work was directed toward the design of a battery for an electric vehicle, development of battery components, and design and construction of battery testing facilities. Efforts were continued on contractual arrangements with industrial firms to develop and fabricate cells, electrodes, and cell components; the first contractor-produced cells were delivered to ANL.

SUMMARY

Cell Development

Recent work in cell development has been concentrated on the development of prismatic, vertically oriented cells that can be directly stacked in compact battery arrays. Particular emphasis has been placed on improving the specific power and lifetime of the cells and on establishing improved fabrication procedures. A major effort has been directed toward the

development of Li-Al/FeS_x cells with electrodes assembled in the uncharged state. All of the prismatic cells (designated R-series) described herein were assembled in the uncharged state, and these cells have yielded highly promising results. The electrodes in these cells have experienced little or no change in shape, and gas evolution was greatly reduced in both Li-Al/FeS_2 and Li-Al/FeS cells. Electrical performances were equal to or higher than those of equivalent charged cells in every case. The uncharged cells appear to be very attractive with respect to ease of fabrication and cost of mass-manufactured cells.

Cell R-2, an FeS_2-type cell, demonstrated the highest specific-power capability of any engineering cell constructed at ANL; the cell was operated at currents as high as 170 A, with a peak power of about 135 W/kg sustainable for 10 sec. Cell R-7, an FeS-type cell, demonstrated major advances in specific-energy and specific-power capabilities for this type of cell.

Technical assistance was given to the commercial development program, especially in helping to solve individual problems associated with the first electrodes and cells fabricated by Gould Inc. These cells have electrodes consisting of porous structures into which powdered active materials are loaded. In the course of this effort, a number of problems related to the fabrication of cells and electrodes of this type were identified. Cells having pressed or carbon-bonded electrodes appear to be more amenable to industrial fabrication, and work is now being concentrated on cells of this type.

Electrode Development

A major effort is being directed to the development of carbon-bonded FeS_2 electrodes for electric vehicle application, and hot-pressed Li_2S-Fe electrodes (assembly of FeS electrodes in the uncharged state) for off-peak energy storage application. A minor effort is being directed to the development of vibratorily loaded FeS_2 and Li_2S-Fe electrodes for the respective applications. Negative electrode studies include investigations of cast Li-Al electrodes and aluminum-foil structures for uncharged Li-Al electrodes.

Cells KK-1 and KK-2 have demonstrated the feasibility of using carbon-bonded FeS and FeS_2 electrodes, respectively, for vertical, prismatic cells of compact design. Cell KK-1 was operated for about 1300 hr and 60 cycles, with a coulombic efficiency greater than 96%. Normal cell operation was at an 8-hr discharge rate (0.04 A/cm^2) at which 54% of the theoretical capacity was utilized. Cell KK-2 has been operated for 1500 hr and 75 cycles. At a discharge current density of 0.025 A/cm^2, 52% of the theoretical capacity density was achieved.

Cell S-77 had the longest life of any Li-Al/FeS_2 cell, namely, 300 cycles and 6400 hr. Results of postoperative examinations of this cell and evaluations of various operating conditions have been instrumental in determining factors which appear to be necessary for high performance over a large number of cycles. One of the cells currently operated in the lifetime studies is Cell S-82. Cell S-82 has been operated for over 148 cycles and 3777 hr and operation is continuing. At charge and discharge current densities of 0.052 and 0.075 A/cm^2, respectively, capacities of 117 to

131 A-hr (61 to 68% Li-Al theoretical capacity) have been measured; the performance of the cell with cycling is very stable.

Studies of Li-Al electrodes are being directed toward development of low-cost electrodes having improved performance. Li/Li-Al cells with all-lithium-ion electrolyte (LiCl-LiF-LiI) showed no improvement in performance over cells with LiCl-KCl electrolyte, thereby strengthening the postulation that the performance of Li-Al electrodes is limited by solid-state diffusion of the lithium in the Li-Al. Relatively thick (0.6 cm) Li-Al electrodes prepared by casting discs of Li-Al alloy show performances similar to those of 0.64-cm thick Li-Al electrodes prepared electrochemically from pressed aluminum York mesh. An uncharged Li-Al electrode prepared from aluminum foil (0.7 cm thick) demonstrated the same performance as electrodes of similar thickness prepared electrochemically from pressed aluminum York mesh. Studies have recently been initiated to investigate the morphology of aluminum particles in a discharged Li-Al electrode operated under controlled conditions. The first studies, in which the effect of discharge current density during deep discharge is being examined showed that the average particle size decreases as the discharge current density is increased. Moreover, the particles are porous, sponge-like material with an extremely high surface area.

Materials Testing and Fabrication

The development of an electrical feedthrough has progressed significantly with several conceptually different prototypes that have sufficient merit to warrant in-cell testing. Continued refinements in cell design and assembly procedures and improvements in the feedthroughs themselves preclude the likelihood that a selection based on demonstrated superiority will be made in the near future. Nonetheless, data are being accumulated that indicate that the feedthrough costs will be consistent with other cell costs.

A study of the mechanical properties of Y_2O_3 has been initiated. The flexure strength will be correlated with processing and microstructure and will ultimately serve to establish allowable design stresses in Y_2O_3 components. Prototype insulators for feedthroughs have been prepared by isostatic compaction and machining prior to final firing. Two MgO bodies and a commercial specimen of BeO were exposed to lithium at 500°C. One of the MgO materials appears to be sufficiently attractive to warrant further testing. The BeO also underwent very little corrosion and is a primary candidate for commercial feedthroughs.

Boron nitride fabric has been used successfully in test cells for up to 6400 hr, but its present cost of $\$515/ft^2$ and projected cost of about $\$10\text{-}15/ft^2$ precludes its use in commercial cells. Efforts have been concentrated on the development of papers prepared from BN or other stable, lower-cost ceramic fibers to obtain the necessary cost reductions. Papers made from fibers of BN were obtained through contracts with the Carborundum Company and the University of Florida. These papers contained either an organic or inorganic binder; particulate fillers of BN, MgO and $LiAlO_2$ were added in some cases. Carborundum is continuing with the development of a stable BN binder, whereas the University of Florida is working on composite papers of BN fibers and particulate fillers using a small amount of asbestos fibers for added strength. Major efforts will continue on the development and evaluation of paper separators.

Results of a study of the lithium-aluminum phase diagram are summarized. The liquidus and solidus temperatures over the entire diagram, except for those near the 335°C isotherm, are in agreement with previous work. Recently identified features of the diagram are the peretectic formation of Li_9Al_4 at 335°C and the polymorphic transition of Li_9Al_4 at 275°C. Also, the aluminum-rich boundary of LiAl was established at 48 at. % Li; the lithium-rich boundary, not yet firmly established, is near 57 at. % Li.

Solid lithium-aluminum electrodes were prepared by casting the molten alloy into a mold of the desired size and configuration and tested in a small-scale cell (JW-2). This cell operated reasonably well, but it was believed that increased electrode performance could be achieved by incorporating a metal current collector within the cast electrode. Electrodes of this type were prepared by immersing small discs of a macroporous metal in the molten Li-Al alloy. In-cell tests with these electrodes yielded very good results.

The formation of brittle, aluminum-rich, intermetallic compounds on the negative electrode housing has been observed in the postoperative examination of cells operated near 500°C. Dissimilar metal couple tests have established that this reaction occurs near the end of the discharge cycle when a galvanic couple is established between the Li-depleted Li-Al alloy and the electrode housing. Test results confirmed that the reaction was negligible at 400°C. In tests conducted at 500°C using high-purity (polarographic-grade) LiCl-KCl eutectic salt, the reaction rate was increased by 1 to 2 orders of magnitude, over those at 400°C. However, duplicate tests using a less pure eutectic salt showed reaction rates near those of the 400°C tests. Anoinic impurities in the less pure salt are believed to be involved in the formation of a passivating film on the aluminum surface, thereby reducing the reaction rate.

Long term (1000-hr) corrosion tests at 500°C have been conducted in both FeS and FeS_2 positive electrode environments. The materials evaluated included six alloys of Fe-Mo-Ni prepared at ANL and the following commercial materials: Armco Electromagnet iron, Ni, Nb, Mo, and Hastelloys B and C. The FeS/LiCl-KCl tests indicated that the following materials have acceptable corrosion resistance: Mo, Hastelloys B and C, Nb, Ni, 10Mo-20Ni-Fe, 15Mo-20Ni-Fe, and 15Mo-30Ni-Fe. In the FeS_2/LiCl-KCl environment, only Mo showed adequate corrosion resistance at 500°C.

Postoperative examinations were conducted on prismatic cells PR-1, R-1, and R-2 to determine materials and electrode behavior. These examinations included microscopic, X-ray diffraction, chemical and electron microprobe analysis. No evidence of electrode slumping was observed in visual and microscropic examination. Metallographic examination showed considerable nonuniformity in the microstructure within the electrochemically formed Li-Al electrodes (*i.e.*, unreacted or partially reacted Al wire was observed). Also, the lithium concentration was greater at or near the negative/positive electrode interfaces.

Cell Chemistry

The overcharge characteristics of the FeS electrode were investigated by charging a series of Li-Al/FeS cells to successively higher cutoff voltages. The products of the overcharge reaction appear to be elemental sulfur and

$FeCl_2$ (complexed in the electrolyte as $FeCl_3^-$). An increased porosity of the FeS electrode at the higher cutoff voltages is attributed to the formation of sulfur vapor in the electrode.

Studies of the overdischarge reactions of the Li-Al electrode in Li-Al/FeS_x cells showed that cells having Li-Al electrodes made from high purity aluminum can be discharged to 0.7 V or less before the aluminum undergoes anodic oxidation. If the aluminum contains magnesium as an alloying agent, however, the discharge cutoff potential should be kept above 0.9 V to avoid anodic oxidation of the magnesium.

Several laboratory-scale Li/FeS cells were started successfully from the uncharged condition, using mixtures of sintered Li_2S and iron in the positive electrode. Since this procedure requires a source of Li_2S, tests were conducted on the preparation of Li_2S by the reduction of Li_2SO_4 with graphite. This reaction proceeded satisfactorily either under vacuum at about 820°C, or under helium at 1000-1100°C.

Cyclic voltammetric techniques have been developed for the quantitative determination of water in LiCl-KCl electrolyte, as well as a study of its electrochemical behavior. The reversible reduction of water on platinum electrodes was observed, with peak currents proportional to concentration. The diffusion coefficients of water calculated from these results were 3.1×10^{-5} cm^2/sec at 390°C and 8×10^{-5} cm^2/sec at 480°C. Further measurements of the diffusivity of oxide ion yielded values of 2.8×10^{-6} cm^2/sec and 7.0×10^{-6} cm^2/sec, respectively, at the above temperatures.

Investigations of purification methods for LiCl-KCl electrolyte showed that filtration and electrolysis should be adequate to achieve purity levels similar to those obtained by much more extensive procedures. Alternative electrolyte compositions for use in Li-Al/FeS cells were also investigated by determining the liquidus temperatures of samples consisting of Li^+, F^-, Cl^-, Br^- and small concentrations of other cations. Preliminary results indicate that substitution of 10% K^+ ions for the Li^+ ions in these systems reduces the liquidus temperatures by as much as 54°C.

The penetrability of various separator and particle retainer cloths by molten LiCl-KCl electrolyte was determined. Zirconia cloth was readily penetrated and permeated by the molten salt. In contrast, boron nitride and carbon cloths were penetrated only when a layer of molten salt was present on both sides of the cloth while the system was evacuated and repressurized. After this procedure, the salt passed easily in either direction through both types of cloth. A large contact angle hysteresis was observed for sessile drops of the molten salt or solid surfaces of all three of the materials. A layered separator concept based on these observations is effective in achieving the desired wetting characteristics.

Experiments on calcium alloy/molten/salt/FeS secondary cells have progressed to the stage that a 50 A-hr sealed cell is being constructed. This cell employs Ca_2Si as the negative electrode and LiCl-KCl-$CaCl_2$ as the electrolyte. Laboratory studies of calcium alloy/FeS cells are being continued to develop improved electrodes and electrolyte.

A statistical model of the resistance of a randomly packed bed of active material has been developed to treat the behavior of Li-Al electrodes. The bed resistance is related to the lithium utilization by a cumulative lognormal function. The model agrees well with experimental Li-Al electrode polarization data over a wide range of current densities, and applies to both charge and discharge.

Studies have continued on the phase relationships of various sulfide systems used in the positive electrodes of Li-Al/metal sulfide cells. Chemical analysis of a sample of J phase prepared by the reaction of iron with Li_2FeS_2 in the presence of molten LiCl-KCl eutectic at 400°C gave the following result in wt %: Fe, 54.69; K, 9.44; S, 32.82; Cl, 1.37; Li, 0.29. A differential thermal analysis experiment showed that the material begins to decompose irreversibly at 560°C on heating. In a study of a modified Li_2FeS_2 phase that has been detected in the positive electrodes of $Li/FeS{\cdot}Cu_2S$ cells, its composition corresponded approximately to the compound $2Li_2S{\cdot}FeS{\cdot}Cu_2S$.

The kinetics of lithium electrodeposition on aluminum and Li-Al alloys is being investigated by galvanostatic pulse techniques. Preliminary results have indicated that the charge-transfer process is fast and that there is no mass-transport limitation in the electrolyte phase. Solid-state diffusion and crystallization probably are the slow processes limiting the incorporation of lithium into aluminum.

The mechanism and reaction rates involved in the operation of the FeS electrode are also under investigation. Cyclic voltammograms of Li_2S dissolved in LiCl-KCl at 450°C with an iron electrode show anodic deposition-cathodic stripping-type waves in the region of 1.65 V *vs.* Li/Li^+, thereby indicating the formation of an FeS film. A resistive-type overpotential was observed above 2 V *vs.* Li/Li^+, presumably as a result of dissolution of the iron and accumulation of $FeCl_2$ or $KFeCl_3$ near the electrode.

Emf measurements on Li-Al alloys as a function of composition and temperature have been completed. Liquidus compositions at 510 and 553°C are 85.5 and 77 at. % lithium, respectively. The activities and activity coefficients of lithium in the alloys were obtained from the emf values at the liquidus points.

Electrode potentials of the metal/metal ion couples, Fe/Fe^{++}, Cu/Cu^+, Ag/Ag^+, and Pd/Pd^{++} were measured in LiF-LiCl-LiBr electrolyte at 450°C. The standard potentials at unit molality concentrations of the metal ions differed slightly from those in the LiCl-KCl eutectic, but followed the same trend. The temperature coefficient of the emf for Cu/Cu^+ was -0.93 mV/degree.

Battery Engineering

A continuing effort is under way to define the proper goals for the application of ANL-developed high-temperature batteries to electric-vehicle propulsion and utility load-leveling.

Calculations have been made to estimate the driving ranges for a first-generation (1978) electric automobile powered by a Li-Al/iron sulfide battery and for an electric automobile that is mass-produced in 1985. The range of

the test automobile (1978) at highway speeds is about 85 miles and that of the mass-produced automobile of 1985 is >200 miles.

The cost of operating electric- and gasoline-powered vehicles over a 10-year period was compared. Reference conditions were selected for the initial cost of vehicle and battery, and operating costs for gasoline, electricity, and maintenance. Operating costs were adjusted for assumed rates of price increases over the 10-year period. Under the range of conditions that were examined, the electric vehicle had a cost advantage over the gasoline vehicle when advanced, high-capacity batteries were used and the initial cost of the electric vehicle without batteries did not exceed the cost of the gasoline vehicle by more than about $2000.

A reference design of a prismatic cell that provided the basis for development/fabrication contracts to three participating industrial firms is described. This design served as the basis for the first industrially fabricated cells, currently under test.

A conceptual design of a 30 kW-hr electric vehicle battery with prismatic cells was completed. This design specifies the size of industrially fabricated cells to be incorporated into an electric vehicle battery. This battery is expected to be used to power a test automobile in 1978.

The emphasis during the past year has been upon the development of high-temperature bus/connectors and equipment that simplify cell fabrication and assembly. High-temperature connection resistances will be determined in a test program presently being developed. A study of the battery geometry for the BEST Facility has defined the first test pieces. These have been fabricated and will be tested in a new facility now under construction. A procedure has been developed and apparatus designed for use in filling the industrially fabricated prismatic cells with molten-salt electroltye. The apparatus provides for filtering the salt before the cell is filled to a prescribed level. The apparatus will fill cells without the need for inert-atmosphere glovebox operations.

A battery test laboratory has been constructed that provides the facilities for battery testing (up to 15 cells), electrical/electronic circuit development, and space for development of equipment such as the salt-filling apparatus. Battery test chambers and their controls have been installed, a battery cycler console has been completed, and fabrication of a battery charge/equalization console has begun.

Battery charging/equalizing circuits have been developed for four-cell and six-cell batteries. The four-cell charger/equalizer is intended for laboratory use in test work with the industrially fabricated prismatic cells. The six-cell charger/equalizer is being developed for application to charging electric vehicle batteries. The design work in the latter case is being performed by an industrial participant from Gulton, Industries, Inc.

A multicell charging module has been designed, tested, and is currently being fabricated by a commercial firm. The module has all solid-state components. In addition to being cheaper and more compact than the previously used electromechanical charging equipment, it is expected to improve accuracy, reliability and versatility.

Commercial Development

To accelerate the commercial availability of lithium-aluminum/iron sulfide batteries, a rapid and efficient transfer of technology to industry is required. Toward this end, the participation of industrial firms capable of manufacturing components, electrodes, cells and batteries has been sought at an early stage in the development program. Commercial development is being implemented by contracting with industrial firms to (1) develop manufacturing techniques for electrodes, (2) develop components such as insulated battery casings, electrical feedthroughs, and charging control systems and (3) fabricate test hardware.

Development contracts have been made with three industrial firms to develop manufacturing procedures and fabricate test electrodes and cells. The industrial firms at Gould Inc., Eagle-Picher Industries, Inc., and Catalyst Research Corp. Electrodes and cells fabricated under the contract with Gould have been received and are undergoing testing at ANL. Delivery of prototype cells from Eagle-Picher is scheduled for February 1976.

A contract has been made with Carborundum Co. to develop a flexible paper separator of boron nitride fiber. Test samples using various organic and inorganic binders have been prepared and are being evaluated. Contracts have also been made with several firms for the fabrication of both mechanical and brazed-type electrical feedthroughs.

I. INTRODUCTION

Lithium/metal sulfide batteries are being developed at Argonne National Laboratory (ANL) for use as (1) energy storage devices for load-leveling on electric utilities and (2) power sources for electric automobiles. Batteries that are currently available are too expensive for the first application and have insufficient energy storage and power per unit weight for the second application. The installation of batteries on electric utility networks would permit the utilities to store energy generated at night by coal-burning or nuclear baseload plants and discharge the battery to the network during the day when demand is highest. This would reduce the need for gas- or oil-burning turbine generators. Electric automobile batteries could be recharged at night using electricity produced from coal or nuclear energy. The successful development of batteries for either application would reduce our dependence on foreign sources of oil.

The development effort on the energy storage battery, which is funded by ERDA, includes cell chemistry studies, materials studies, electrode development, cell development, battery development, and systems studies. The development of the electric-vehicle battery, which is also funded by ERDA, consists of systems design studies and cell and battery development; most of the more basic studies performed under the energy storage battery program are also applicable to the vehicle-propulsion effort.

The performance goals that we have set for off-peak energy storage and electric automobile batteries, presented in Table I-1, are unchanged from those given in the preceding semiannual report (ANL-75-36, p. 11).

Table I-1. Performance Goals for Lithium/Metal Sulfide Batteries

Battery Goals	Electric Vehicle Propulsion	Off-Peak Energy Storage
Power		
Peak	60 kW[a]	40 MW
Normal	21 kW	10 MW
Voltage, V	140	1000
Specific Energy, W-hr/kg	120-160	120-150
Energy Output	42 kW-hr	100 MW-hr
Discharge Time, hr	2	10
Charge Time, hr	5	5-7
Watt-Hour Efficiency, %	70	80
Cycle Life	1000[b]	1500[b]
Cost of Capacity, $/kW-hr	20-30[b]	15-20[b]
Heat Loss Through Insulation	150 W	100 kW

[a]Based on the power required to accelerate a 1570-kg car from 0 to 60 mph in 23 sec.

[b]Tentative; to be specified by systems and cost studies.

Most of the present effort in the program is directed toward the development of cells having negative electrodes of a solid lithium-aluminum alloy, positive electrodes of either FeS_2 or FeS, and an electrolyte of LiCl-KCl eutectic (mp, 352°C) that fills the pores in the electrodes and the separator. The use of this electrolyte requires operation of the cell at about 400 to 450°C. Boron nitride fabric has proved to be a satisfactory electrode separator material in these cells, and the addition of metal sulfides to the positive electrodes, namely, Cu_2S to FeS and CoS_x to FeS_2, has resulted in significant improvements in cell lifetime and performance. Recent experimental work on electrode and cell development has been directed primarily toward vertically oriented cells having a prismatic shape. This type of cell was selected because it is more amenable than the previous cylindrical, horizontal cells to incorporation into a compact battery. The electrode and cell designs for the two applications differ; the major difference is that the power requirements for electric vehicle propulsion necessitate the use of thinner electrodes.

The efforts in electrode and cell development have resulted in the identification of new designs for electrodes and cells and new procedures for cell assembly and start up. Several promising types of positive electrodes have been designed for prismatic cells; these include (1) electrodes having porous current collector structures into which the active material is vibratorily loaded, (2) electrodes in which a mixture of the active material and electrolyte is hot-pressed onto a metal current collector, and (3) electrodes formed from a mixture of active material and carbon cement to give a carbon-bonded structure that is easily penetrated by electrolyte. A major improvement has been achieved in the design of cells with hot-pressed FeS positive electrodes. The cells are assembled in the uncharged state, *i.e.*, the positive electrode is a mixture of Li_2S, electrolyte, and iron powders, and the negative electrode is a pressed aluminum-wire plaque. During the first charge, lithium is transferred to the negative electrode, and FeS is formed in the positive electrode. This method of assembly, along with the addition of copper to the positive electrode, has produced greatly improved performance in Li-Al/FeS cells and has significantly reduced the swelling previously encountered in FeS electrodes. A continuing effort is being made to incorporate these advances in technology into new battery designs.

Battery design and engineering work is directed principally toward systems and cost studies, cell and battery design, and battery component development. A conceptual design was recently completed for a 30 kW-hr electric-vehicle battery with prismatic cells; present plans call for a test of this battery in a compact-sized automobile in 1978. The effort on battery components has included development of bus bars and connectors, and equipment for equalizing the voltage among battery cells.

Development work at ANL on the Li-Al/metal sulfide cells has progressed to the stage where contracts have been made with several industrial firms to develop fabrication techniques and fabricate electrodes and cells. These contracts effectively utilize the expertise of battery manufacturers and at the same time facilitate the transfer of ANL-developed technology to industry. The first contract was made in April 1975 with Gould Inc., and since that date contracts have also been made with Eagle-Picher Industries, Inc. (in

May 1975) and Catalyst Research Corporation (in October 1975). The first cells fabricated under the Gould contract were received at Argonne in mid-November 1975. These cells were designed to meet certain near-term performance specifications that are somewhat less stringent than the long-range goals given in Table I-1. ANL is also subcontracting cell development work of a more basic nature to Atomics International, and contracts have been made with several industrial firms to develop improved electrode separators and electrical feedthroughs.

II. CELL DEVELOPMENT
(W. J. Walsh)

The effort in this part of the program is directed primarily toward the development of engineering-scale, sealed cells capable of meeting the requirements for batteries for both of our applications. Recent work has been concentrated on improving the specific power and lifetime of the cells, and on establishing improved fabrication techniques. The cells (~100 A-hr capacity) employ a design[1] having a central positive electrode of iron sulfide (FeS_2 or FeS) between negative electrodes of a solid Li-Al alloy. During the past six months, emphasis in development work has shifted from cylindrical cells operated in a horizontal position to prismatic cells (13 by 13 cm, 2 to 4 cm thick) that are designed for vertical operation. A schematic diagram of a typical prismatic cell is presented in Fig. II-1; a photograph of a typical cell, presented previously in ANL-75-36, p. 21, is also included here in Fig. II-2. To date, seven vertically oriented, prismatic cells (designated R-series) have been operated. The physical characteristics and performance results are summarized in Table II-1. (Cell R-1 was described in the preceding semiannual report, ANL-75-36, p. 20.)

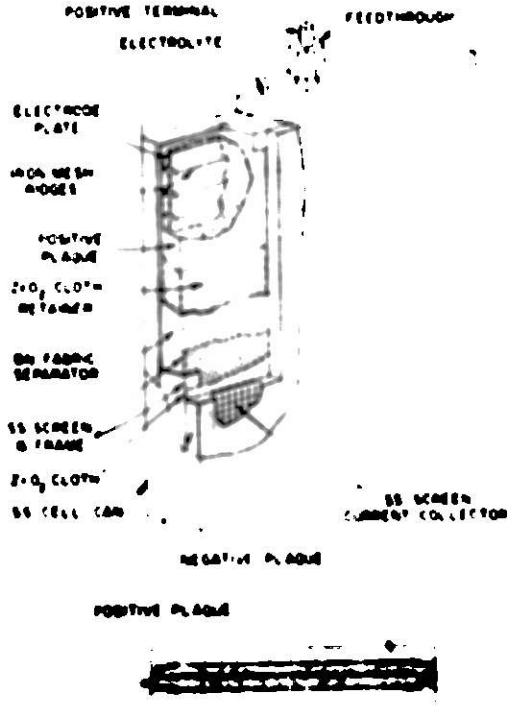

Fig. II-1. Design of Prismatic Li-Al/FeS Cell

A major effort during the past 10 months has been the development of Li-Al/FeS_x cells assembled in the uncharged state. In this type of cell, the active materials in the positive electrode are Li_2S and iron and the negative electrodes are porous plaques of aluminum. Upon charging the cell, lithium is transferred to the negative electrodes, and FeS or FeS_2 (depending on the

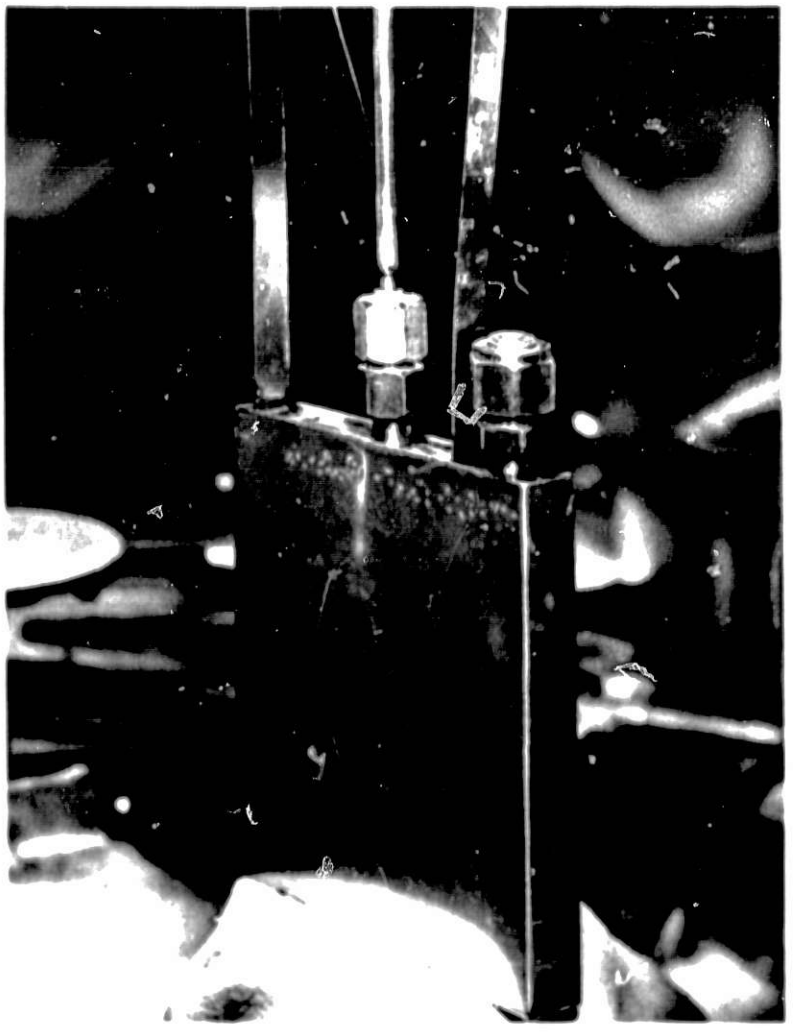

Fig. II-2. Photograph of Typical Prismatic Cell. ANL Neg. No. 308-4090.

original ratio of Li_2S to Fe) is formed in the positive electrode. All of the R-series cells were assembled in the uncharged state, and have achieved highly promising results. The electrodes in these cells experienced little or no changes in shape, and gas evolution was greatly reduced for both Li-Al/FeS_2 and Li-Al/FeS cells assembled in the uncharged state. In every case, electrical performance was equal to or higher than that of equivalent cells assembled in the charged state. The uncharged cells appear to be very attractive with respect to ease of fabrication and cost of mass-manufactured cells.

In other work, technical assistance was given to the commercial development program, especially in solving individual problems that arose during the fabrication of the first electrodes and cells by Gould Inc. In the course of this effort, it was found that cells having electrodes in which powered active materials were loaded into porous structures were relatively difficult to fabricate. Cells having pressed electrodes or carbon-bonded electrodes appear to be more amenable to industrial fabrication, and recent work at ANL has been concentrated on cells of this type.

Table II-1. Physical Characteristics and Performance of R-Series Cells

	Cell Designation						
	R-1	R-2	R-3	R-4	R-5	R-6	R-7
Cell Weight, kg	0.98	1.05	1.10	1.2	1.0	1.0	1.0
Lifetime,[a] hr	1010	1400	440	688	>2400	>2000	>1700
No. of Cycles[a]	53	143	24	46	>140	>125	>70
Specific Energy, W-hr/kg							
Maximum	105	110	105	55	63	67	100
Normal	90	90	80	45	55	57	85
Positive Electrode							
Active Material	Li_2S-Fe-CoS_2[c]	Li_2S-Fe-CoS_2[c]	Li_2S-Fe-CoS_2[c]	Li_2S-Fe	Li_2S-Fe	Li_2S-Fe-Cu[d]	Li_2S-Fe-Cu[d]
Theor. Capacity, A-hr	100	75	89	80	76	73	112
Current Collector	Mo Mesh	Mo Sheet	Mo Sheet	Fe[f]	Fe[f]	Fe[f]	Fe[f]
Negative Electrodes							
Active Material	Al	Al	Al	Al	Al	Al	Al
Li-to-Al Atom Ratio[b]	0.92	0.92	0.85	0.92	0.92	0.92	0.92
Current Collector	Fe Mesh	Fe Mesh	Fe Mesh	SS Screen	SS Screen	SS Screen	SS Screen
Cell Operating Temp., °C	450	450	450	450	450	450	450

[a]Cells R-5, R-6, and R-7 are still in operation.

[b]Value is based on the fully charged State.

[c]10 mol % CoS_2 based on fully charged FeS_2-CoS_2 electrode.

[d]10 mol % Cu_2S based on fully charged FeS-Cu_2S electrode.

[e]20 mol % Cu_2S based on fully charged FeS-Cu_2S electrode.

[f]Positive electrodes were hot-pressed onto an iron current collector plate.

A. Design of R-Series Prismatic Cells

(H. Shimotake, E. S. Carr, L. G. Bartholme, and J. D. Arntzen)

The prismatic cell design was selected to allow the direct stacking of cells into compact battery arrays; the previous cylindrical cells (W-series) had central feedthroughs and could not be compactly stacked without a miniature, interlocking feedthrough.

The housing of the prismatic cell (13 by 13 cm, 2-4 cm thick) is capable of containing active materials equivalent to a cell capacity of 100 to 150 A-hr, depending on the degree of compactness achieved. The LiCl-KCl eutectic (58.5 mol % LiCl-41.5 mol % KCl, mp = 352°C) was the electrolyte in most of the cells. A boron nitride cloth impregnated with liquid electrolyte served as the separator between the positive and negative electrodes, and a zirconia cloth was used as a porous barrier to retain the particles of active material in all of the positive electrodes and in some of the negative electrodes. In the FeS-type cells, the positive-electrode current collector was an iron substrate; in FeS_2-type cells, it was a single sheet or mesh of molybdenum.

B. Uncharged Li-Al/FeS_2 Cells

(W. J. Walsh, J. D. Arntzen, and E. S. Carr*)

In Cells R-2 and R-3, the material in the positive electrode was a mixture of Li_2S, iron powder, electrolyte, and CoS_2 additive.[2] A compact, high-performance positive electrode was obtained by hot-pressing the mixture above the melting point of the electrolyte. A cold-pressed aluminum-wire plaque containing stainless steel mesh as a current collector served as the negative electrode in these uncharged cells. The cells were filled with electrolyte under vacuum and then sealed through the use of heliarc welding and a compression feedthrough. As part of the start-up procedure, the capacity charge and discharge was controlled at a low value and was gradually increased as cycling continued.

Neither Cells R-2 nor R-3 experienced significant gas evolution, in contrast to previous charged cells. In the case of Cell R-3, no significant outgassing was observed following the electrolyte-filling step. It is concluded that uncharged cells may have the potential of being sealed during manufacture, without an electrochemical cycling step to release gases.

As seen in Table II-1, Cells R-2 and R-3 achieved specific energies of slightly higher than 100 W-hr/kg. These values are not as high as the specific energies of 125-150 W-hr/kg achieved by previous horizontal, cylindrical (W-series) cells, which had thicker electrodes and higher Li/Al ratios. However, the prismatic cells show promise of attaining these higher specific energies when fully developed.

Cell R-2 demonstrated the highest specific power of any engineering cell constructed at ANL; the cell was operated at currents as high as 170 A, with a peak power of about 135 W/kg sustainable for 10 sec. Figure II-3 shows the peak power capability of Cell R-2 as a function of state of charge; Figure II-4 gives typical voltage curves for Cell R-2.

---

*Industrial participant from Eagle-Picher Industries, Inc.

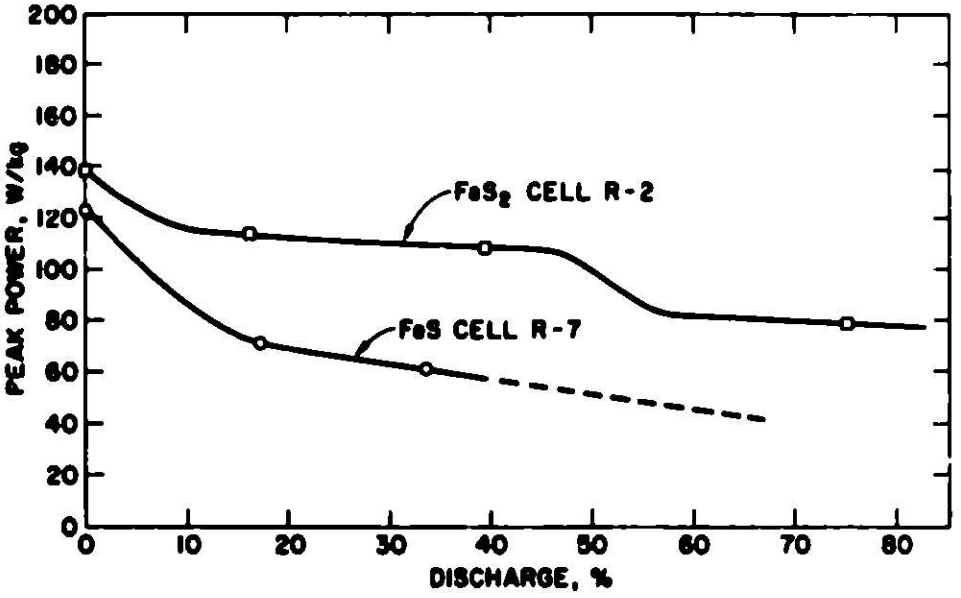

Fig. II-3. Present Power Capabilities of FeS and FeS_2 Cells

Cells R-2 and R-3 achieved high utilization of reactants (80 to 90%), but had relatively short lives. Both cells developed internal short circuits as a result of stresses on the positive electrode. This problem illustrated the need for a design modification in prismatic cells to minimize stresses on the positive electrode current collector.

The Li_2S and Fe used in Cells R-2 and R-3 were prepared by direct reaction of FeS_2 and lithium, which is a somewhat tedious procedure. Because of the highly promising results attained with the uncharged cells, it was recommended that an improved method for preparation of Li_2S be developed. (Studies addressing this problem are discussed in Section V.B.)

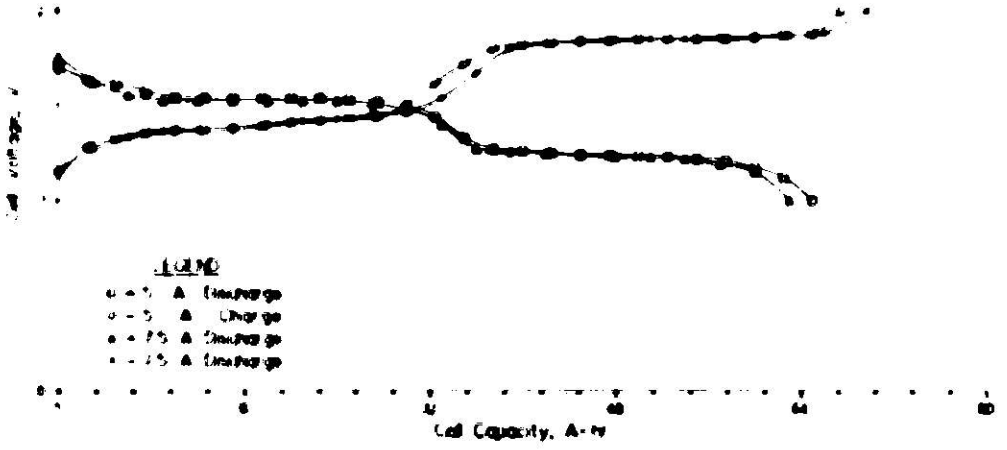

Fig. II-4. Voltage-*vs.*-Capacity Curves for Cell R-2 (theoretical capacity, 75 A-hr)

C. Uncharged Li-Al/FeS Cells
(H. Shimotake and L. G. Bartholme)

In past studies of cells with FeS electrodes, excessive swelling occurred in the positive electrode, utilization of the positive active material was low, and excessive gassing occurred. Postoperative examinations of FeS-type cells showed that a reaction had occurred between the FeS electrodes and potassium in the LiCl-KCl electrolyte to form a K-Li-Fe-S compound, designated J phase (ANL-8109, p. 72). This reaction caused excessive swelling of the positive electrode and high polarization, the latter of which resulted in low utilization of the positive active materials.

Accordingly, means of eliminating or minimizing this problem were sought. In previous chemical studies, the addition of Cu_2S to the FeS resulted in a modification of the J phase (ANL-75-1, p. 106); as a consequence, the polarization of the FeS electrode was reduced and the utilization was improved. Similar results were also obtained by raising cell temperature from 450 to 500°C (ANL-75-1, p. 32). However, the problem of excessive swelling remained. During this period, FeS-type cells were operated with electrolytes containing only lithium ions, *e.g.*, LiF-LiCl-LiI or LiF-LiCl-LiBr. Because of the absence of potassium, J phase did not form and these cells exhibited significantly higher electrical performance and little positive-electrode swelling. However, the use of these electrolytes is impractical, at present, because of high costs of the LiI and LiBr.

A more practical solution to the problem is the assembly of Li-Al/FeS cells in the uncharged state.[3,4] As a result of chemical studies (Section V.B), an improved procedure for preparing Li_2S was developed. Commercial Li_2S was sintered at 1200°C to form a high-density cake, which was ground and mixed with iron powder and electrolyte. We found that a highly efficient and compact positive electrode could be prepared by hot-pressing (at 380°C) the powder mixture of Li_2S, Fe, and electrolyte (in some electrodes copper powder also) onto an iron current collector plate. To prevent slumping of active material in the vertically oriented cell, the current collector plate was made with ridges of steel mesh, 10 mm high and 25 mm apart, extending across the width. The pressed plaque was encased in a thin zirconia fabric for particle retention, and then wrapped with boron nitride fabric for electrical insulation. The boron nitride fabric was impregnated with LiCl-KCl electrolyte prior to assembly to promote wetting during the electrolyte-addition step. A set of thin steel frames held the fabrics in position, as shown in Fig. II-5.

The electrical performance results for the four uncharged FeS-type cells that have been tested (Cells R-4, -5, -6, and -7) were summarized earlier in Table II-1. In Cell R-4, the electrolyte was LiF-LiCl-LiBr. Because of the absence of potassium, Cell R-4 achieved a higher performance than previous cells containing FeS electrodes. However, as discussed previously, LiBr is too costly for use in a practical cell.

The positive electrode of Cell R-5 did not contain an additive, but copper was added to the positive electrode of Cell R-6, to give a fully charged electrode of FeS-10 mol % Cu_2S. Cells R-5 and R-6 achieved respective utilizations that were 55 and 62% of theoretical at current densities of 0.035 A/cm^2. The ohmic resistance of Cell R-6, which contained copper, was 6 mΩ compared with 100 mΩ for Cell R-5. In view of these results, more copper

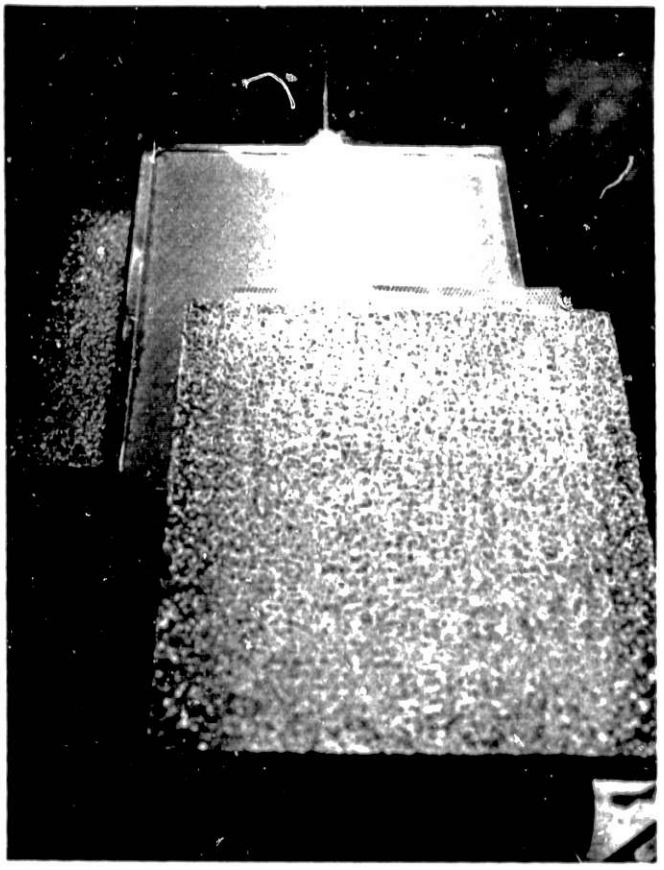

Fig. II-5.

Positive Electrode Assembly and Two Negative-Electrode Aluminum Plaques for an Uncharged Li-Al/FeS Cell

powder (to give 20 mol % Cu_2S in FeS) was added to the positive electrode in Cell R-7.

The performance curves for Cell R-7 at current densities up to 0.07 A/cm^2 are shown in Fig. II-6. At a current density of 0.035 A/cm^2, the utilization was 85% of theoretical. The ohmic resistance of the cell was quite low, less

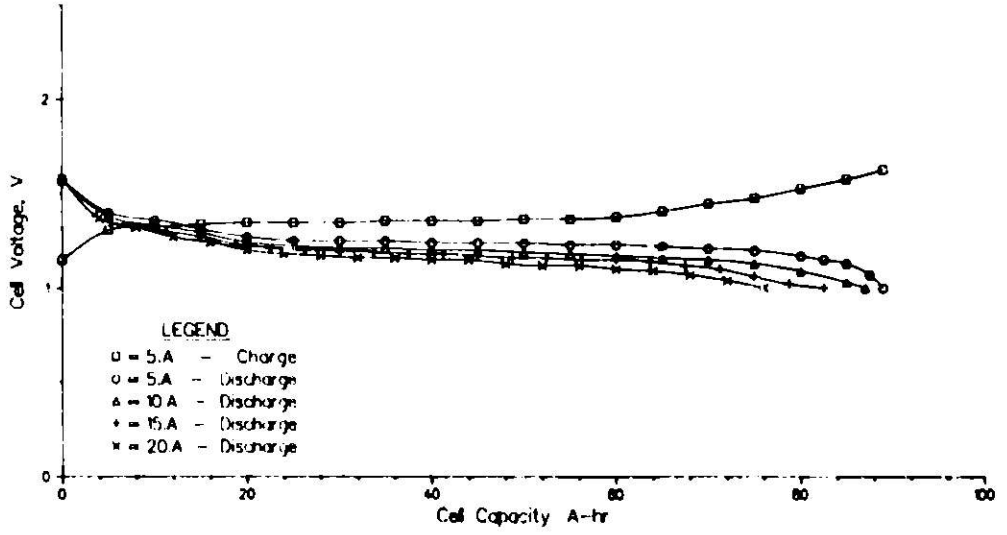

Fig. II-6. Voltage-*vs.*-Capacity Curves for Cell R-7 (theoretical capacity, 112 A-hr)

than 4 mΩ, thereby indicating the advantage of the higher copper level. The coulombic efficiency was above 95% and the energy efficiency was >80% at 10-hr rate; these high efficiencies indicate an electrical performance that is satisfactory for practical application. Maximum specific energies achieved by the most recent cells are in the range from 65 to 100 W-hr/kg. It is believed that the specific energy values can be further improved by making the electrodes more compact.

Figure II-7 shows the capacity of Cell R-7 as a function of cycle life. This cell has been in operation for over 2000 hr and 80 cycles at the time of this writing. In Fig. II-7, one can see periods of high capacities during initial cycles, with a gradual stabilization to a slightly lower value. This is a typical pattern of cell capacity *vs.* cycle life; however, the causes of this type of behavior are not presently known.

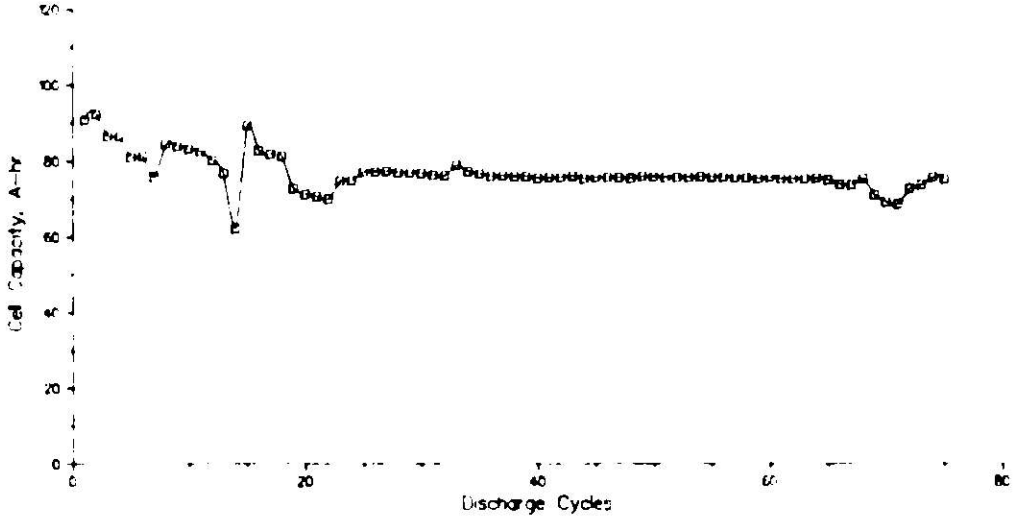

Fig. II-7. Capacity *vs.* Cycle Life for Cell R-7 (theoretical capacity, 112 A-hr)

Cell R-7 has attained much higher specific powers than previous Li-Al/FeS cells, but these values are still substantially lower (about 40%) than those attained by Li-Al/FeS_2 cells. Major improvements in specific power are expected in future cells for both systems.

Swelling and gassing, which were observed in all previous Li-Al/FeS cells, did not occur in the cells of this series. One can postulate that, despite the existence of J phase, swelling does not occur because the positive electrode materials, as initially assembled, are at their maximum volume. Disappearance of the gassing can be attributed to the use of metallic aluminum-fiber plaques instead of powdered lithium-aluminum alloy or electrochemically formed lithium-aluminum alloy, either of which can be easily contaminated by oxygen, nitrogen or moisture during handling and storage.

Further improvements in performance and lifetime are expected to be achieved with this type of cell as improved component materials become available for the cell construction.

D. Entropy Heating Effects in FeS_2 Cells

(T. O. Cooper and W. J. Walsh)

An experiment was performed to test the temperature variations which occur in Li-Al and FeS_2 electrodes as the various charge and discharge reactions proceed. The apparatus was designed with a fast-response thermocouple inserted within each electrode. The electrodes were 5 by 5 cm and were thermally isolated from each other and the cell housing, except for the LiCl-KCl electrolyte which flooded the cell. The electrodes were provided with good current collection to minimize ohmic heating, thus simulating the condition expected in a well-engineered hardware cell.

The results showed that the temperature variations in the Li-Al electrode were very slight on both plateaus during both charging and discharging. It is concluded that the entropy ($T\Delta S$) heating or cooling effect is very small for Li-Al half-cell reactions, and that the ohmic heating is negligible for this electrode. In contrast, the $T\Delta S$ and ohmic (I^2R) contributions were significant in all cases in the FeS_2 electrode. The reactions corresponding to the upper voltage plateau during discharge and the lower plateau during charge were both endothermic; very high current densities were possible without significant temperature escalation, owing to the cancelling effect of the ohmic energy evolved and the $T\Delta S$ energy absorbed. In some cases, closing the circuit resulted in a temperature rise in the Li-Al electrode and a temperature decline in the FeS_2 electrode.

The most significant result of this test was that temperature excursions of up to 40°C were measured in the positive electrode; these occurred during discharge reactions on the lower plateau and during charge reactions on the upper plateau. These temperature rises apparently result from a combination of a $T\Delta S$ energy release and an I^2R ohmic energy release. Several conclusions can be drawn from these results. For example, an upper-plateau FeS_2-type battery could probably operate at high discharge rates with very little need for temperature control; however, during charging, this type of battery might require low current densities or a special cooling system. An FeS_2-type battery utilizing both voltage plateaus would experience significant energy releases during the later portions of the charge and discharge cycles.

E. Development of Fabrication Methods

(W. E. Miller, T. O. Cooper, J. W. Allen, J. D. Arntzen)

Effort on development of fabrication methods during this period was expended in two areas: (1) development of advanced cells with uncharged, hot-pressed electrodes for use in future contract work and (2) assistance to industrial firms in the development of fabrication procedures for cells being built under existing contracts. This latter work involved the design, fabrication, and testing of various versions of the cells to be produced under the Gould contract; these cells had electrodes consisting of porous structures into which powdered active materials were loaded. Several technical improvements were made in cell design, electrode fabrication, and molybdenum joining, and the results were transmitted to Gould before they began construction of cells. In the course of this work, two Li-Al/FeS_2 cells were constructed at ANL to proof-test the fabrication procedures.

The cells having powder-loaded electrodes present fabrication problems including (1) attaining uniform loadings with the desired degree of compactness, (2) immobilizing the powders after loading, (3) sealing each porous structure surface to prevent losses of particles, and (4) obtaining electrodes with good dimensional control. Cells incorporating pressed electrodes or carbon-bonded electrodes appear to be more amenable to industrial fabrication, and work is now being concentrated on cells of these types.

REFERENCES

1. W. J. Walsh, A. A. Chilenskas, E. J. Cairns, and P. A. Nelson, "Modular Electrochemical Cell," U. S. Patent No. 3,887,396 (June 3, 1975).

2. W. J. Walsh, C. C. McPheeters, N. P. Yao, and N. Koura, "Metallic Sulfide Additives for Positive Electrode Material Within a Secondary Electrochemical Cell," U. S. Patent Application 596,044.

3. N. P. Yao and W. J. Walsh, "Discharged Electrochemical Cell," U. S. Patent Application 510,840, September 1974.

4. N. P. Yao, R. C. Elliott, and J. W. Allen, "Development of a Discharged Iron Sulfide Electrode," Extended Abstracts of Battery Division, Electrochemical Society Meeting, New York, October 13-17, 1974, Vol. 74-2, pp. 140-141 (1974).

III. ELECTRODE DEVELOPMENT
(E. C. Gay)

A. Scope

The objective of the investigations in this part of the program is to develop electrodes having the capacity density, power density, and cycle life commensurate with the goals for batteries to be used for off-peak energy storage and electric vehicle propulsion. The major emphasis for development of negative electrodes continues to be on solid lithium-aluminum electrodes, with a smaller effort on other solid lithium-alloy electrodes. The positive electrodes contain FeS_2 or FeS as the active material and various metal sulfide additives. The major emphasis is on development of vertical, rectangular electrodes. The development efforts for the off-peak energy storage battery and the electric-vehicle battery are closely related and, in some cases, development work is carried out in the same series of experiments. The major difference is that the electrodes developed for the electric vehicle battery are thinner and are more suitable for operation at higher current density.

B. Development of Positive Electrodes

1. Considerations of Charged and Uncharged Positive Electrodes

At the present time, a major effort is being directed to the development of carbon-bonded FeS_2 electrodes for the electric-vehicle application and hot-pressed Li_2S-Fe electrodes (FeS electrodes assembled in the uncharged state) for the off-peak energy storage application. A minor effort is being directed to the development of vibratorily loaded FeS_2 and Li_2S-Fe electrodes for the respective applications. The choices of the carbon-bonded and hot-pressed electrodes were made on the basis of performance, projected costs, and ease of fabrication. The considerations leading to the choices of charged FeS_2 electrodes and uncharged FeS electrodes are discussed below.

The FeS-type electrodes are of interest because of the potential for lowering the electrode cost by using low-cost iron current collectors. Performance measurements of FeS-type cells are promising with respect to meeting the goals for the off-peak energy storage application. Although this electrode has exhibited excessive swelling as a result of interaction with potassium in the LiCl-KCl eutectic during discharge of the FeS, several methods of controlling the swelling appear promising. Results of cell chemistry studies (Section V) indicated that this interaction could be eliminated by adding copper sulfide to the FeS. No interaction was observed between the potassium and an electrode of the composition $CuFeS_2$; lower levels of copper addition were effective in controlling the interaction with potassium to a lesser extent. Another means of controlling swelling of the FeS electrode is to assemble the cell in an uncharged state. Related work on cell development (Section II) with hot-pressed Li_2S-Fe-Cu electrodes (uncharged FeS electrodes with copper additive) has indicated that swelling of the FeS electrode can be controlled.

Present efforts include development of uncharged FeS electrodes with copper additive and the development of appropriate forms of uncharge negative electrodes to be used in low cost, compact, welded cells. Earlier studies of uncharged FeS electrodes with no additive indicated that severe corrosion of the

iron current collector and iron housing occurred at electrolyte volume fractions of 0.20 or lower. Effort is also being directed to the design of uncharged FeS-Cu_2S electrodes with sufficiently low corrosion rates of the metal current collector to meet the lifetime goals for off-peak energy storage cells.

The FeS_2-type electrodes are of interest for electric-vehicle application because the power requirements for electric-vehicle cells are high (electrodes containing FeS do not appear capable of meeting power requirements). Positive electrodes of FeS_2, assembled in both the charged and the uncharged state, are being studied. Even though the volume changes observed for charged FeS_2 electrodes are much lower than those for charged FeS electrodes, uncharged FeS_2 electrodes may be more compatible with ceramic paper separators since the volume changes may be reduced. Ceramic papers are rigid and are not expected to be able to accept large volume changes in the electrodes. The assumption is made here that volume changes of the negative electrode can be controlled during charge, when lithium reacts with the aluminum plaque to form the Li-Al alloy. Investigations of charged and uncharged carbon-bonded and pressed FeS_2 electrodes are being conducted for the electric vehicle propulsion battery; the electrodes with the highest performance will be used in the electric vehicle battery cells to be fabricated by industrial contractors. The major question to be answered about carbon-bonded uncharged FeS_2 electrodes is the compatibility of Li_2S with the organic binder used in the fabrication of this electrode.

2. Fabrication Techniques

a. Electrodes with Porous Current Collector Structures (F. J. Martino and E. C. Gay)

The Li-Al/FeS_2 and Li-Al/FeS prismatic cells fabricated at Gould Laboratories (see Section VII) contain porous current collector structures vibratorily loaded with electrochemically active material. These cells and electrode components were delivered to ANL on November 18, 1975. Positive and negative electrode fabrication techniques investigated at ANL provided the basis for the fabrication procedures used by Gould. The following recommendations were accepted for fabrication of the positive electrodes: 1) the positive electrode was divided into two equal halves by a sheet of molybdenum metal (two vertical compartments), 2) each vertical compartment of the positive electrode was divided into five horizontal compartments by layers of graphite cement, 3) vitreous carbon foam was used as the porous current collector structure, and 4) a mixture of positive electrode active material and electrolyte was vibratorily loaded into the porous current collector structure.

The recommendations were based on the results obtained from the operation of Cells S-80 to S-85. All of these cells were vertical, prismatic cells with one positive electrode and two negative electrodes (electrode areas, 170-200 cm^2). The electrodes were sandwiched against the BN separator but the cells were not sealed and the amount of electrolyte was not optimized. The molybdenum separator in the positive electrode prevented excessive lithium deposition in either negative electrode. The horizontal compartments reduced the possibility of slumping of the active material; the mixture of active material and electrolyte was necessary to provide the proper

loading of active material, while maintaining particle-to-particle contact to prevent slumping.

b. Carbon-Bonded Electrodes
(T. D. Kaun, W. A. Kremsner)

The carbon-bonded electrode is formed from a three-component paste of active material, a noncontaminating, volatile substance (e.g., ammonium carbonate), and carbon cement. After the carbon cement is cured and the volatile material is driven off, the rigid, porous structure remaining consists of particles of active material held in a lattice of carbon (Fig. III-1). Usually the carbon occupies about 5 vol % of the structure. The porosity is controlled to allow for volumetric changes in the active material during cell cycling; the porosity can be controlled uniformly to nearly any desired amount by the quantity of volatile material in the paste. This method produces an integrated electrode structure to which a particle retainer (usually zirconia cloth) can be bonded.

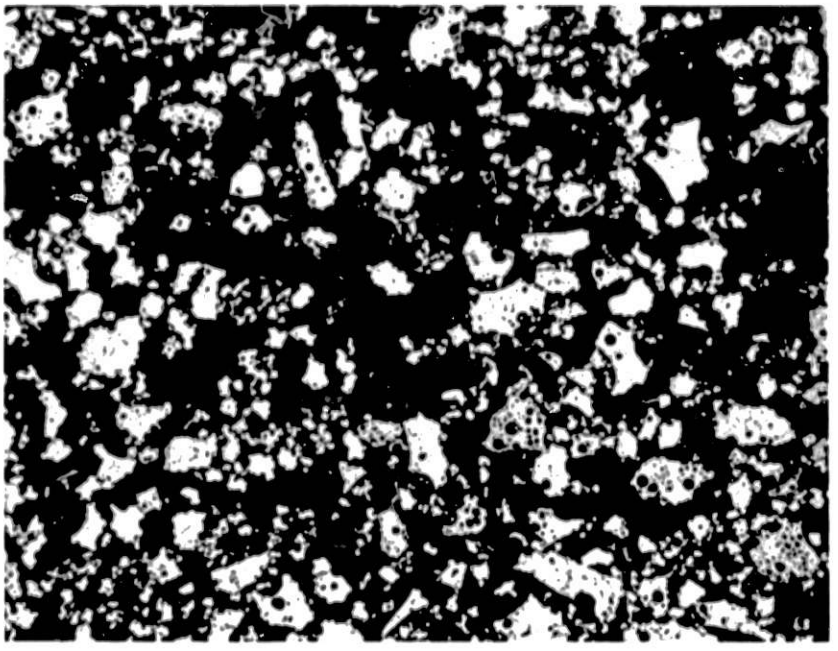

Fig. III-1. Photomicrograph of Carbon-Bonded FeS Electrode (11X; FeS particles are white; carbon bonding is light gray, and voids are dark gray)

The carbon-bonded electrode gives a freedom of cell design. The homogeneous structure can be easily formed into any shape, and is suitable for either charged or uncharged electrodes. This structure shows promise of fulfilling the design characteristics necessary for the vertical electrode: 1) it provides direct support of the active material in a homogeneous dispersion to counter settling, 2) the porosity can be easily controlled to minimize swelling, and 3) current collection is good. Moreover, the material cost is low and fabrication from a paste is simple.

Recent effort has dealt with applying the carbon-bonding technique to various active electrode materials, with the aim of identifying problems that may arise in vertical, prismatic electrodes. Different types of carbon-bonded electrodes have been tested in horizontal, cylindrical cells (5.1 cm in diameter); the electrolyte was LiCl-KCl, and the cells were operated for about 500 hr and 25 cycles at 450°C. In the preparation of these electrodes, Union Carbide Grade C-34 carbon cement was used as the binder and ammonium carbonate as the volatile material. The paste was first cured in air at about 125°C for 3 hr and then at higher temperatures up to 400°C in inert atmosphere for 6 hr. Upon completion, the electrodes had void volumes corresponding to about 50% in the charged state. Electrolyte was infiltrated into the positive electrode under vacuum after the cell was assembled. The types of electrodes tested and the results are given in Table III-1. Utilizations ≥70% of theoretical were achieved at 0.05 A/cm^2 with all electrodes.

Table III-1. Tests of Carbon-Bonded Electrodes in Small-Scale Cells

Cell No.	Starting Active Material	Thickness, cm	Theoretical Capacity, A-hr	% Utilization
TK-3	FeS_2	0.4	8.7	80
TK-6	FeS	0.6	12	75
TK-7	Kennecott matte (iron and copper sulfides)	0.6	9	70
TK-8	Li_2S + Fe + Cu (uncharged FeS)	0.5	8	70

The feasibility of using the carbon-bonding technique for both FeS and FeS_2 electrodes has been demonstrated in vertical, prismatic cells of about 200 cm^2 area. The two cells (KK-1 and KK-2) each had one positive and two negative electrodes. The current collectors were perforated metal trays (Fig. III-2), to which carbon cement bonds well. The pastes were cured in the previously described manner to obtain the positive electrode compact. The cells were operated with restraining plates to eliminate any swelling.

Cell KK-1, in which the carbon-bonded structure contained FeS, was operated with LiCl-KCl electrolyte. Because of the excessive swelling that results from the reaction of these components, operation of this cell was considered to be a stringent test of the carbon-bonded structure. The normal cell operation was at an 8-hr discharge rate (0.04 A/cm^2) at which 54% of the theoretical capacity of both the positive and negative electrodes (matched at 105 A-hr) was utilized at 500°C. The coulombic efficiency was greater than 96%. Cell KK-1 was terminated because of a faulty cell housing after more than 1300 hr and 60 cycles of stable operation. Post-test examination of the positive electrodes showed no electrode swelling or active material settling.

Cell KK-2, which had a carbon-bonded FeS_2 positive electrode, has been operated for over 1500 hr and 75 cycles at 450°C and 0.025 A/cm^2

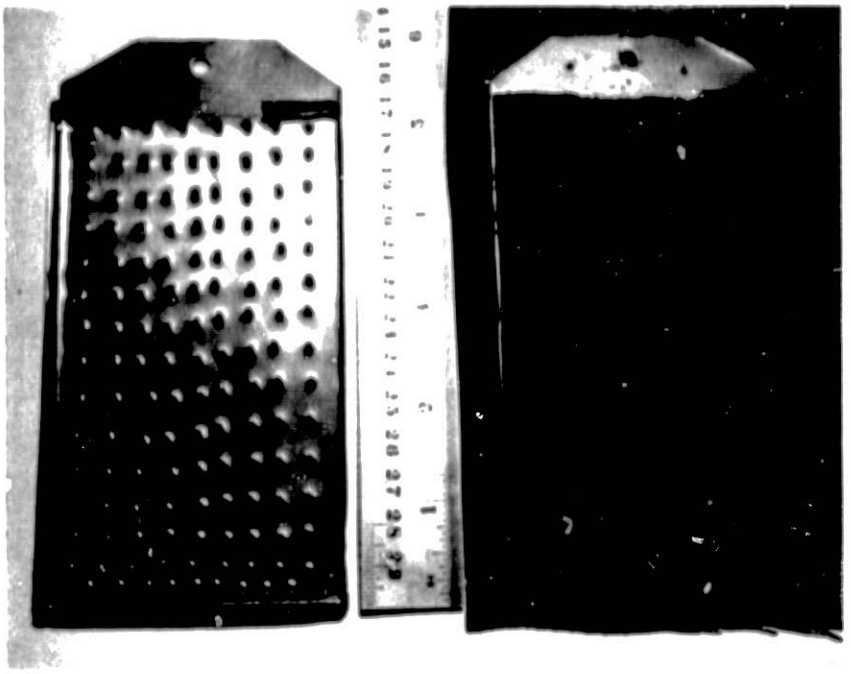

Fig. III-2. Positive Electrode of Cell KK-1 (perforated metal current collector at left, carbon-bonded FeS structure at right)

discharge current density. Charge and discharge cutoff potentials are 2.2 and 0.9 V, respectively. The percentage of theoretical utilization is 52%, with a coulombic efficiency of approximately 95%. Because the positive electrode is relatively thick, 1.2 cm, the addition of CoS_2 should greatly improve utilization. Many such improvements are planned for future carbon-bonded electrode tests.

Studies have been initiated to identify the parameters that affect the performance of the carbon-bonded electrode. Investigations of various carbonaceous binders and volatile materials as well as current collector materials are planned. Some of the parameters to be investigated include 1) percentage void volume, 2) volume percent carbon cement, 3) electrode thickness, 4) additives, 5) initial particle size, and 6) preparation technique.

c. Development of Vertical Prismatic Cells with Hot-Pressed FeS Positive Electrodes
(T. D. Kaun, W. A. Kremsner, N. P. Yao)

The fabrication procedure for hot-pressed FeS positive electrodes was as follows: The active material was FeS with 13 wt % CoS as an additive. A homogeneous mixture (particle size, <177 μm) of 80 wt % active material and 20 wt % LiCl-KCl was prepared by several cycles of melting the salt, cooling, and grinding. To form an electrode compact, the mixture of FeS and LiCl-KCl was hot-pressed onto an iron mesh current collector in a 7.6 cm x 12.7 cm rectangular die for about 4 hr at 370°C and 26 kg/cm^2 pressure. The pressed positive electrode compacts were approximately 0.5 cm thick, and generally flat and strong.

Cell PR-1, the first vertical prismatic cell with a hot-pressed FeS electrode (see ANL-75-36, p. 48), was operated satisfactorily for 1400 hr and 88 cycles at temperatures of 450 to 530°C. The major problems encountered with this cell were positive electrode swelling and temporary cell shorting from an electrolyte surface film (the latter probably resulted from the fact that the cell was not sealed). Post-test examination showed that the FeS positive electrode had swollen to 150% of its original thickness, owing to the J phase formation when an FeS electrode is operated in LiCl-KCl electrolyte. This amount of swelling could not be tolerated in a practical cell because allowance for the swelling would significantly reduce the specific energy (W-hr/kg). The post-test examination also showed that no slumping of the active materials had occurred.

To determine the performance of a hot-pressed positive electrode performance under dimensionally stable conditions, Cell PR-3 was operated with the positive electrode constrained by 0.48-cm-thick steel plates. The face plate was perforated with 0.80-cm-dia holes. Two layers of steel screen and zirconia cloth at the electrode face served as particle retainers beneath the face plate. This positive electrode was cycled against a negative electrode of Li-Al with excess lithium capacity. Operated under nearly the same temperatures and current densities as Cell PR-1, Cell PR-3 gave nearly identical active material utilizations (see Fig. III-3). Post-test X-ray radiograph examinations showed no settling of active material in the FeS electrode. Cell PR-3 demonstrated the feasibility of operating a dimensionally stable, compact, prismatic cell with a hot-pressed FeS electrode.

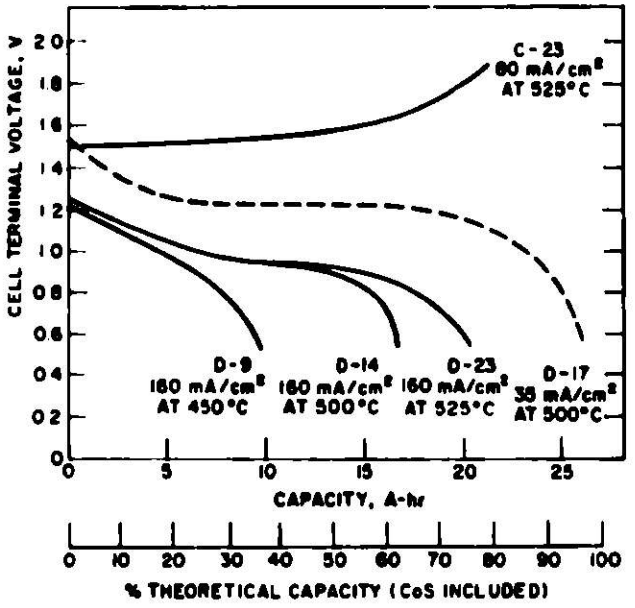

Fig. III-3. Voltage and Capacity of Cell PR-3 as a Function of Temperature and Current Density

Cell PR-4 was designed to eliminate the bulk and weight of electrode housings used in Cell PR-1. Steel sheet and mesh (0.25 mm thick) were replaced by 325-mesh stainless steel cloth for the electrode housing. Details of the design are shown in Fig. III-4. The two Li-Al negative electrodes were formed electrochemically within restraining plates to produce flat, compacts, 0.32 cm thick. The FeS electrode was 0.64 cm thick and had a theoretical capacity of 54 A-hr. The cell, which used LiCl-KCl as the electrolyte, was operated within 1.3-cm-thick steel restraining plates to eliminate any swelling. The cell operating temperature was 450 to 525°C; the IR-included voltage cutoffs were 0.7 V on discharge and 1.75 V on charge; current densities were 0.025-0.10 A/cm^2.

The coulombic efficiency of Cell PR-4 declined to about 60% after a few hundred hours operation. With 400 hr of operation and a leaking cell housing, the cell was dismantled and the components visually examined. A slight amount of positive electrode swelling of the lower third of the positive electrode caused reciprocal compression of the electrochemical Li-Al negative electrode. A film of Fe and FeS particles was found on the inside surface of the BN cloth separator.* Insufficient retention of the very fine FeS particles, formed during the hot-pressing technique, by the zirconia retaining cloth appeared to be the cause of poor coulombic efficiency.

*X-ray diffraction analyses performed by B. S. Tani, Analytical Chemistry Laboratory, ANL.

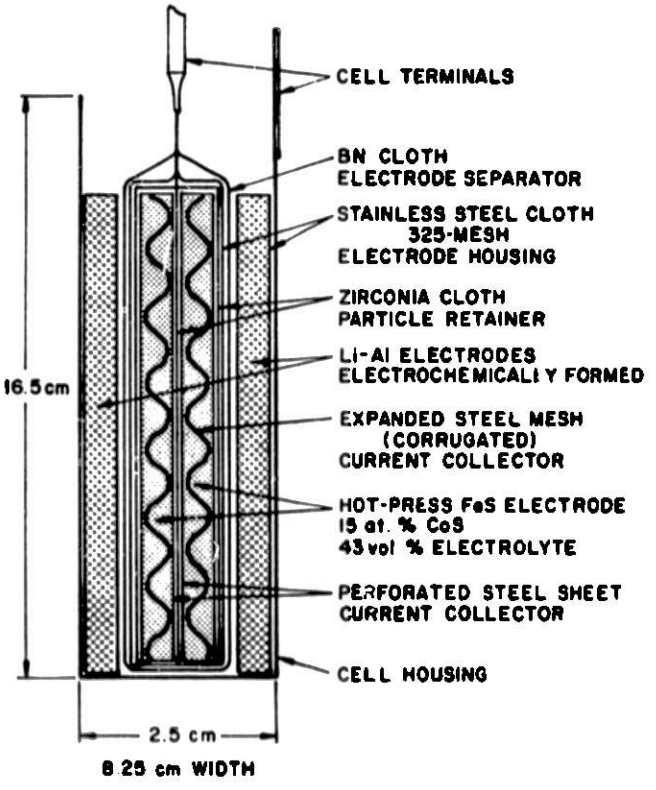

Fig. III-4. Cell PR-4

Cell PR-4 was rebuilt and operated for a total of 1400 hr and 90 cycles, at which time cell operation was voluntarily terminated. The coulombic efficiency was >97%, with positive electrode utilizations of 70% at a 0.025 A/cm^2 discharge rate and 55% at a 0.050 A/cm^2 rate at 500°C.

Post-test examination of Cell PR-4 showed no swelling or settling of the hot-pressed FeS electrode. The examination indicated that after the initial cycle, the hot-pressed FeS electrode in LiCl-KCl electrolyte does not appear to undergo further swelling. A stable electrode structure is set up. These findings indicate that the hot-pressed FeS electrode may be operated in LiCl-KCl electrolyte without excessive swelling if the cell undergoes initial cycling within restraining plates. Unfortunately, the FeS electrode needs to operate at higher temperatures, about 500°C, to obtain good performance, and corrosion problems are accelerated at this temperature.

C. Cell Lifetime and Cycle Life Testing

1. Positive Electrode Cycle Life Studies
(F. J. Martino, E. C. Gay)

Cell S-77. Cell S-77 (previously described in ANL-75-36, p. 40) achieved the longest life of any ANL cell to date, namely, 300 cycles and 6400 hr. The test was terminated after an examination indicated a separation in the stainless steel housing of the negative electrode and a failure of zirconia fabric particulate retainer in the positive electrode. Results of post-operative examinations of this cell and evaluations of various operating conditions have been instrumental in determining factors which appear to be necessary for high performance over large numbers of cycles.

Cell S-77 was a horizontal, cylindrical cell with a negative electrode of pyrometallurgical Li-Al contained in an iron Retimet current collector and a positive electrode of FeS_2-CoS_2 contained in vitreous carbon foam; the electrolyte was LiCl-KCl eutectic. The electrode area was 46.5 cm^2, the theoretical capacity of the Li-Al was 58 A-hr, and that of the FeS_2-CoS_2 electrode was 86.5 A-hr. Under the normal operating conditions, capacity densities of 1.0 to 0.68 A-hr/cm^2 were measured at charge and discharge current densities of 0.075 A/cm^2; the respective cutoff voltages were 2.53 V and 0.7 V (IR-included) for the first 192 cycles and 4300 hr and 2.53 V and 0.9 V for the final 108 cycles. Capacities of 31 to 45 A-hr were typical under these operating conditions, corresponding to Li-Al utilizations of 53 to 80% and FeS_2-CoS_2 utilizations of 36 to 55%. Throughout the operating period, ampere-hour efficiencies of greater than 95% were maintained. The performance history of Cell S-77 is presented in Fig. III-5. During the first 100 cycles, the wide variations in capacity resulted from changes in the charge cutoff voltage. The most noteworthy observation was the stabilizing effect on the capacity of using a 0.9 V discharge cutoff, compared with the previously used 0.7 V; a much lower rate of decline in the capacity resulted when the higher cutoff was used. The estimated rate of decline in the capacity density for the first 191 cycles is approximately 0.001 A-hr/cm^2 per cycle. At the higher 0.9 V cutoff, the rate is reduced to about 0.0002 A-hr/cm^2 per cycle.

Cell S-82. Cell S-82, now being operated for a lifetime test, is a vertical, prismatic cell with two negative electrodes of pyrometallurgical Li-Al in an iron Retimet current collector and a positive electrode of

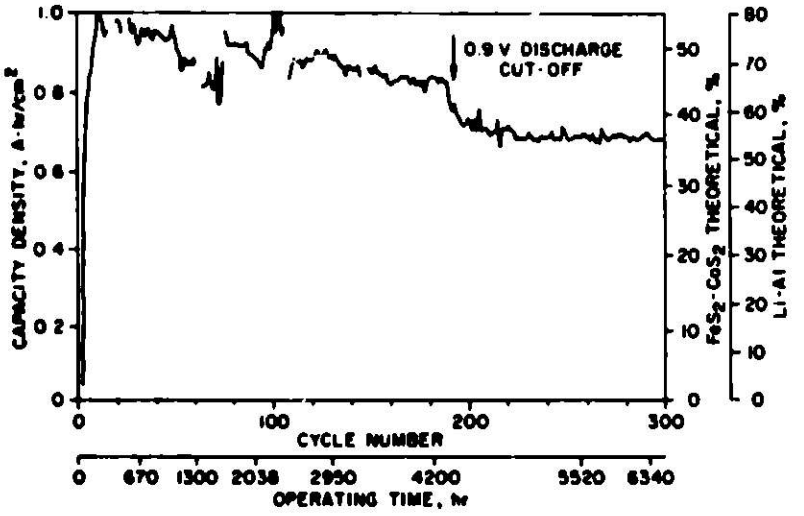

Fig. III-5. Lifetime and Cycle Life Performance of Cell S-77

FeS_2-CoS_2 in vitreous carbon foam. The electrode area is 193.6 cm^2, the theoretical capacity of the Li-Al is 192 A-hr and that of the FeS_2-CoS_2 is 270 A-hr. Because a discharge cutoff voltage of 0.9 V appeared to be favorable for good performance over many cycles for Cell S-77, this voltage was used throughout the operation of Cell S-82. At charge and discharge current densities of 0.052 and 0.075 A/cm^2, respectively, capacities of 117 to 131 A-hr were measured at a charge cutoff voltage of 2.27 V (IR-included). These values correspond to 61 to 68% of theoretical for the Li-Al electrodes and 43 to 49% for the FeS_2-CoS_2 electrode. The performance history of Cell S-82 is shown in Fig. III-6. The reproducible, high performance with cycling observed in this cell is very encouraging. The cell has been operated for over 148 cycles and 3777 hr and operation is continuing.

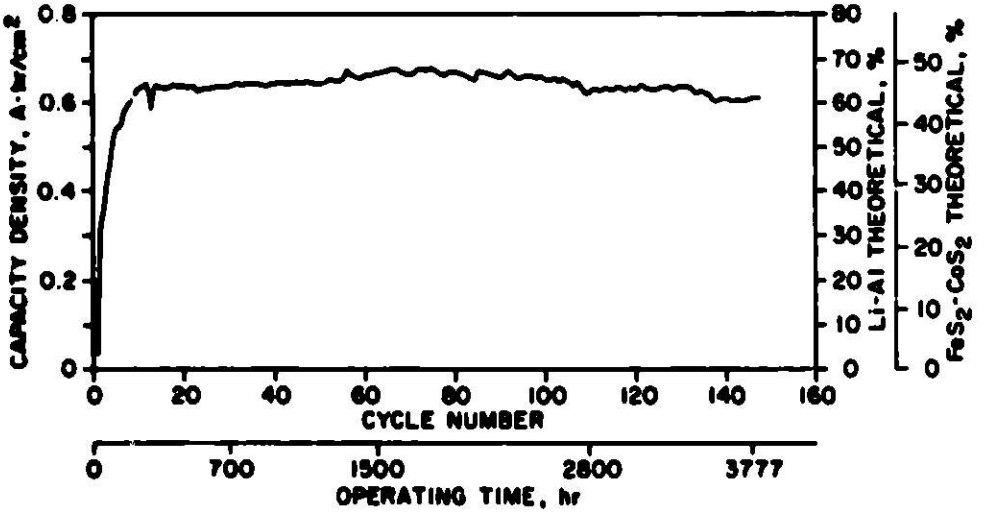

Fig. III-6. Lifetime and Cycle Life Performance of Cell S-82

The post-operative examination of the negative electrodes from Cell S-77 had indicated regions of high lithium concentration near the faces of the electrodes; therefore, Cell S-82 was operated for several hours on open circuit with the aim of eliminating any gradients that might exist in the distribution of lithium in the negative electrodes. Preliminary results indicate that the open-circuit periods have a stabilizing effect on the capacity density with cycling.

From data obtained on Li-Al/FeS_2 cells of vertical, prismatic design, the following electrode design characteristics and operating conditions appear to be favorable for high performance over large numbers of cycles:

1) The separation of the positive electrode into two equal vertical portions by a sheet of molybdenum current collector.

2) The separation of each of the above vertical portions of the positive electrode into horizontal reservoirs (formed with graphite cement in cells with vitreous carbon foam) to prevent slumping of the active material.

3) The use of carbon cloth as particulate retainer in the positive electrode.

4) The use of a discharge cutoff voltage of 0.9 V (IR-included).

5) The operation of a cell for several hours on open circuit after large numbers of cycles, for possible redistribution of the lithium in the negative electrodes.

6) The use of zirconia fabric as a particulate retainer in the negative electrode.

2. Solid Lithium-Aluminum Cycle Life Studies
(W. R. Frost, D. R. Vissers)

The objectives of these studies are to determine the cycle life of the presently available Li-Al alloy electrodes and to identify those factors which limit cycle life. The first variable being studied is the effect of electrolyte purity; the tests are being conducted in Li-Al/LiCl-KCl/Al cells. Cell LT-1, the first test operated in this series, contained polarographic grade LiCl-KCl eutectic from Anderson Physics Laboratory and was used as the base-line cell.

Cell LT-2, the second test in the series, contained LiCl-KCl from Lithcoa; this salt is less expensive and is being evaluated for use in the ANL cells. Cell LT-2 has completed 75 cycles and 1409 hr and has achieved an average utilization of 72.93%. The cell is being operated at a current density of 0.078 A/cm^2 with IR-free cutoff potentials of 0.9 V. Figure III-7 is a comparison of the performance of Cell LT-2 and Cell LT-1 (the fluctuations during initial cycling result from the process of electrode conditioning).

Cycling of Cell LT-2 will be continued until the cell fails, whereupon it will be submitted for post-operative examination. It is believed, however, that more useful data pertaining to the life of a cell will come

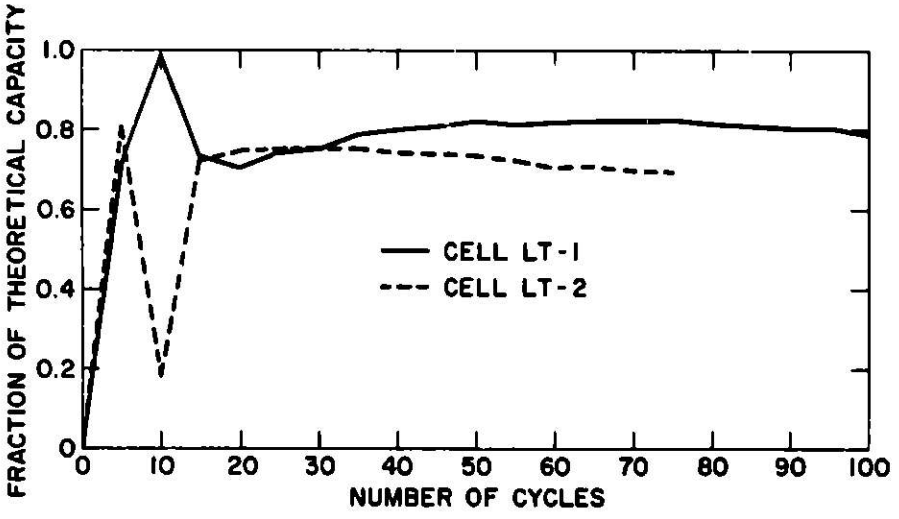

Fig. III-7. Lithium Utilization in Cells LT-1 and LT-2

from an intensive morphology study rather than from operational information generated during the life of the cell. Studies in this area are described in Section D.2, below.

D. Development of Negative Electrodes

1. Solid Lithium-Aluminum Electrode Development

The investigations that have been conducted in this part of the program, to date, have been directed mainly toward the characterization of electrochemically prepared Li-Al electrodes. New fabrication techniques are now being sought, with the aim of eliminating many of the economic and technical problems that are associated with the present Li-Al electrodes. In addition, the performance characteristics of Li-Al electrodes are being investigated in an all-lithium electrolyte, LiCl-LiF-LiI, to determine whether the ion-transport characteristics of the electrolyte affect the performance of the Li-Al electrodes.

a. Cast Li-Al Electrodes
(D. R. Vissers and W. R. Frost)

The feasibility of using cast Li-Al electrodes in Li-Al/FeS_x is being investigated. This type of electrode should be cheaper and less susceptible to contamination during electrode fabrication than those prepared by pyrometallurgical powder techniques, but the electrochemical conditioning of the electrode may be a lengthy process because the alloy is a continuous solid. Accordingly, the performance of a cast Li-Al electrode was studied in a Li/LiCl-KCl/Li-Al cell, JW-2.

In Cell JW-2 the liquid lithium electrode was prepared by loading 23 A-hr of lithium into Type 347 stainless steel Feltmetal. The Li-Al for the electrode was cast* into a disc 0.6 cm thick by 5 cm in diameter. The

*The cast electrode was prepared by T. W. Olszanski and F. C. Mrazek (see Section IV.E, this report).

Li-Al material contained 46 at. % Li, to give a theoretical capacity of 13.7 A-hr (0.876 A-hr/cm^2). The cast Li-Al was inserted into a stainless steel cell housing; zirconia cloth and 16- and 24-mesh screens were used to confine particulate material. Corrugated molybdenum expanded mesh was placed against the back of the cast disc to serve as a current collector and to allow for expansion of the Li-Al.

Cell JW-2 was initially cycled at a current density of 0.015 A/cm^2 and a temperature of 412°C. After the first cycle, when the temperature was increased to 450°C, the amount of lithium cycled increased from ~15 to 94%. After the third cycle, the current density was increased to 0.025 A/cm^2. The lithium utilization at charge and discharge cutoff potentials of 0.15 and 0.70 V was 99.8%. Performance curves for the cell are shown in Fig. III-8. The capacity density of the cell was measured next at charge rates of 0.025, 0.05, and 0.10 A/cm^2 and at discharge rates of 0.05, 0.10 and 0.20 A/cm^2.

A comparison of the performance of Cell JW-2 with that of Cell DK-9 (ANL-75-36, p. 31), which used an electrochemically prepared Li-Al electrode, was 0.64 cm thick and had an electrolyte fraction of 0.2, showed that the performances were quite similar. Actually, at the higher Li-Al electrode charge rate (0.10 A/cm^2), the performance of Cell JW-2 was slightly better than that of Cell DK-9. The cell was operated for 75 cycles; as cycling was continued, a decrease in performance was observed. The cause of this decrease has not been determined.

In conclusion, it appears that the cast Li-Al electrode may be an alternative to the Li-Al electrodes presently used. The incorporation of current collector into the cast electrode may be an improvement in the electrode and will be investigated further in this program.

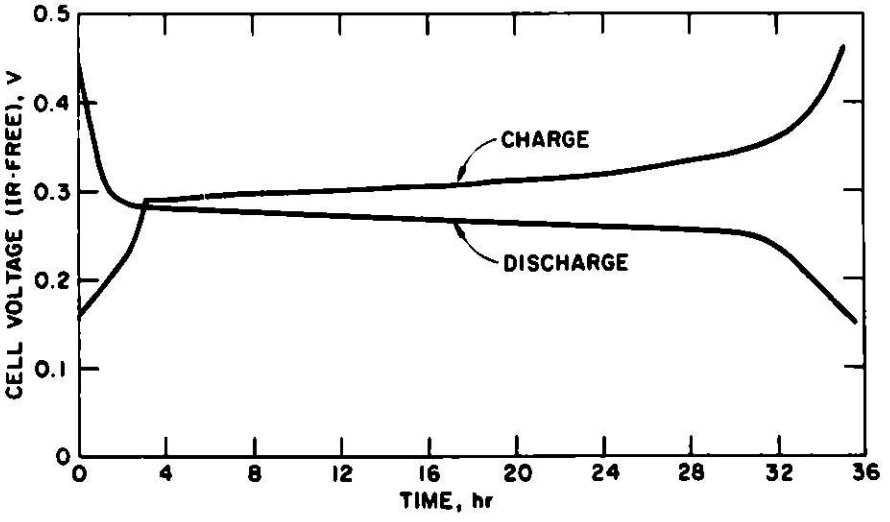

Fig. III-8. Performance Characteristics of Cast Li-Al Electrode in Cell JW-2 (temperature, 450°C; current density, 0.025 A/cm^2)

b. Uncharged Aluminum Foil Li-Al Electrodes
(D. R. Vissers)

Aluminum foil is being evaluated as a possible low-cost material for uncharged Li-Al electrodes. Earlier work indicated that an electrode prepared from pressed aluminum foil 0.32 cm thick by about 5 cm dia showed good performance (ANL-75-1, p. 45). Preliminary studies to date with a thicker (0.7 cm) aluminum foil electrode indicate that its performance is comparable to that of a similar uncharged Li-Al electrode prepared from pressed York aluminum mesh (Cell DK-9, ANL-75-36, p. 31).

c. Characterization of Li-Al Electrodes in Li/LiCl-LiF-LiI/Li-Al Cells
(D. R. Vissers and K. E. Anderson)

The increase in lithium utilization of Li-Al electrodes with decreasing volume fraction of electrolyte suggests that the performance-limiting factor is diffusion of lithium in the solid phase of the electrode rather than Li^+ ion transport in the electrolyte. In an effort to establish the performance-limiting mechanism, the role of the electrolyte is being examined in the operation of a Li/Li-Al cell having an all-lithium-ion electrolyte, LiCl-LiI-LiF, which melts at <400°C. This electrolyte has a higher concentration of lithium (29.1 M) than LiCl-KCl eutectic (17.7 M). If the limiting mechanism is Li^+ ion transport in the electrolyte, the electrode should perform much better in the all-lithium-ion electrolyte.

The design of the Li/LiCl-LiI-LiF/Li-Al cell (DK-24A) was similar to that of a previous Li/Li-Al cell, DK-19 (see ANL-75-36, p. 29). Liquid lithium was contained in Type 347 stainless steel; the aluminum matrix for the Li-Al electrode was prepared by vibratorily loading granular aluminum into a two-layered structure of iron Retimet 0.76 cm thick. The volume fraction of electrolyte in the Li-Al electrode at full charge was ~0.48. The theoretical capacity density was 0.7 A-hr/cm^2 (0.73 A-hr/cm^3).

The electrical performance of the Li-Al electrode was evaluated by determining the capacity density at several charge and discharge rates and at several charge and discharge cutoff voltages. The charge rates were 0.025-0.010 A/cm^2 and the discharge rates, 0.05-0.30 A/cm^2. During the Li-Al electrode charge cycle, the cutoff potential* was 0.15 V, and the discharge cutoff was 0.40 or 0.70 V. With the exception of 0.70 V, these cutoff potentials are believed to be quite conservative (see ANL-75-36, p. 29).

The performance of Cell DK-24A was compared with that of Cell DK-19 (ANL-75-36, p. 29), an identical cell except for the electrolyte, which was LiCl-KCl. The performance characteristics of the two cells were nearly identical under all conditions, except when the discharge cutoff was 0.40 V and the charge current density was 0.025 A/cm^2. In this case, the Li-Al electrode in Cell DK-24A showed a higher performance than the Li-Al electrode in Cell DK-19. Thus, the electrolyte appears to affect the performance of a relatively thick (0.76 cm) Li-Al electrode only at a low charge rate, 0.025 A/cm^2, and a low discharge cutoff, 0.40 V. These results further suggest that solid-state diffusion of lithium into the Li-Al electrode is the performance limiting mechanism.

*All cutoff potentials are IR-free voltages *vs.* lithium.

2. Morphology Studies of Li-Al Electrodes
(D. R. Vissers, W. R. Frost)

Recently a study was begun of the morphology of aluminum particles in Li-Al electrodes under controlled conditions. An understanding of the changes in morphology that take place under specified conditions is expected to be useful in determining mechanisms for cell failure, in designing improved Li-Al electrodes, and in developing models of electrode behavior.

The study has initially centered on the relationship of particle morphology and discharge current density during deep discharge (~75% utilization). A series of Li/LiCl-KCl/Li-Al cells, all identical in design, are being operated at predetermined current densities for twenty cycles. Operation of the cells is then terminated with the Li-Al electrode in the discharged state, and morphology data is obtained from photomicrographs of the electrode cross sections, as well as electron photomicrographs of the individual aluminum particles or sections of the electrode.

A Li-Al electrode consists initially of aluminum powder in a porous nickel Retimet structure, 4 mm thick and 5 cm in dia. The electrode is supported by a stainless steel housing and screen, and zirconia cloth serves to contain particulates. The cell have a liquid-lithium counter electrode and are operated at ~425°C.

Several cells have been operated at discharge current densities from 0.025 to 0.20 A/cm^2. Photomicrographs show a random particle distribution, and the particles are very irregular in size and have very high surface areas. The average particle size, however, varies markedly with current density; particle break up increases with increasing discharge current density. The smaller the particle becomes, the greater the internal electrode resistance owing to increasing particle-to-particle contact and decreasing particle-to-Retimet contact. Scanning electron photomicrographs yielded similar information (the particles were sponge-like and had extremely high surface areas) and also showed that the particles in contact with the Retimet tended to take on its contours.

Further studies of Li-Al particle morphology under other cell operating conditions are planned.

IV. MATERIALS TESTING AND FABRICATION
(J. E. Battles, R. O. Ivins)

The fabrication of various cell components such as electrical feedthroughs, insulators, electrode separators, current collectors, and cell housings requires a variety of metallic and ceramic materials. Because of the corrosiveness of the environment of Li-Al/metal sulfide cells and the need for lightweight, low-cost components, extensive evaluations of materials are required for the selection of materials suitable for use in the various cell components. This report discusses not only the corrosion testing of potentially useful materials of construction, but also the fabrication and evaluation of electrical feedthroughs, development of ceramic insulators, studies of electrode separators, studies of the Li-Al phase diagram, and postoperative examinations of cells.

A. Electrical Feedthrough Development
(K. M. Myles, J. L. Settle)

The electrical feedthrough required for Li-Al/metal sulfide cells must be hermetically tight, lightweight, compact, inexpensive, and compatible with the cell environment. Two general types of feedthroughs are being developed. These are classified according to the method of making the seal between the metal and ceramic members; in one method the seal is produced mechanically, and in the other, it is a metallurgical bond.

1. Mechanical-Type Feedthrough

Two types of mechanical seals are being developed: (1) a compression type, wherein loose BN powder is compacted within a relatively heavy-walled metal fitting to effect the seal, and (2) a ram type, wherein a high strength BeO ceramic body is forced into a thin-walled metal tube to produce high hoop stresses and a seal.

The compression type is a modification of the commercially available Conax thermocouple seal. As currently used, the upper insulator is made from high purity Al_2O_3 and the lower insulator is machined from hot-pressed BN. This feedthrough has been successfully used in ANL cells and will be installed in all of the commercial cells now being fabricated. The main limitations of this feedthrough are the lack of sufficient leak tightness, and bulkiness. High strength insulators of BeO and Y_2O_3 are being fabricated as replacements for the intrinsically weak BN insulator. In an effort to reduce the size and weight, the metal parts of the feedthrough were redesigned. Cost estimates for manufacturing the feedthrough were solicited for various quantities ranging from 250 to 100,000 units, representing both immediate and future needs. The cost of the feedthrough in relatively large volumes (100,000 units), without the BN powder, was estimated to be about $1.85 (the cost of BN powder in limitied-quantity purchases is about $0.24). This projected cost is reasonable in relation to our cost goals.

The ram-type feedthrough (shown schematically in ANL-75-36, p. 57) is being developed for ANL by Ceramseal Inc. A photograph of a completed feedthrough is shown in Fig. IV-1. Metal members of the feedthrough were selected to insure that high hoop stresses would be retained at cell operating

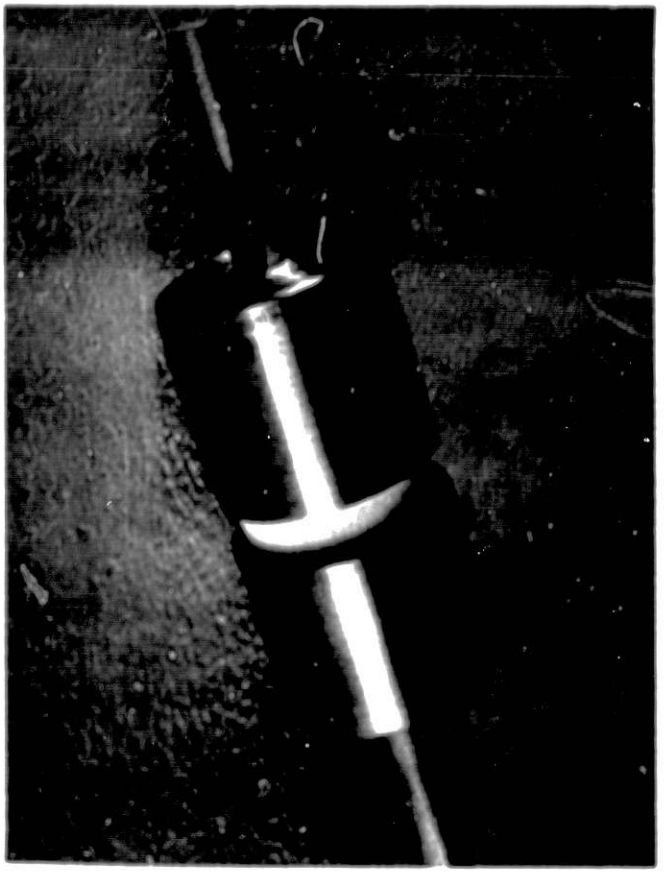

Fig. IV-1. Ram-Type Feedthrough Produced by Ceramaseal, Inc.

temperatures. Prototypes have been supplied with leak rates as low as 1×10^{-9} cm^3 He (std)/sec and these have sustained a vacuum of about 1×10^{-9} torr. Various tests, including thermal cycling, will be performed on these feedthroughs at ANL. The feedthrough design will be optimized in terms of size and weight, and the improved feedthrough will then be tested in large-scale cells.

2. Bonded-Type Feedthrough

The principal problem encountered with metallurgical bonding of the ceramic and metal components is that most braze materials are not compatible with the cell environment. The most common modes of failure are oxidation of the bond material upon charging, reaction of the bond material with the sulfides in the positive electrode, and galvanic corrosion because of the electrochemical dissimilarity of the bond material and the adjacent metal parts.

Efforts are under way to develop a suitable bonded-type feedthrough, utilizing the technical experti e of three commercial feedthrough manufacturers. Feedthroughs with BeO insulators have been produced by the 3M Corporation using three different conventional braze techniques. Because the brazes themselves were not expected to exhibit reasonable lifetimes in the cell environment, a protective coating of nickel or gold was plated on the braze. Corrosion tests are being conducted at ANL to evaluate the effectiveness of this approach.

ILC Technology has developed several Nb-base active metal brazes for BeO and has produced feedthroughs with brazes of Nb-Ni, Nb-Cu, Nb-Ag, and Nb-Au. Niobium was selected as the base metal because it is not expected to oxidize at reasonable cell charge potentials, *i.e.*, 2.0 V (IR-included). A schematic representation of the feedthrough is shown in Fig. IV-2A. A recent design, which closely resembles that used by Eagle-Picher Industries, Inc. in their nickel-cadmium batteries (see Fig. IV-2B), appears ideally suited for use in the ANL prismatic cell. Discussions are under way with ILC Technology for the purchase of some of these feedthroughs for in-cell evaluation. Some design modifications have also been made by ILC to minimize the cost of the feedthroughs. In one such design, shown in Fig. IV-2C, two of the three BeO insulator rings are replaced with a single Al_2O_3 ring. Because BeO represents a large fraction of the total cost of the feedthrough, the substitution of Al_2O_3 yields a significant cost reduction. Preliminary efforts to produce such a geometry have been encouraging.

The most recent effort involves the development of Y_2O_3 ceramic bodies and a nonmetallic braze to molybdenum metal by Coors Porcelain Company. The development of Y_2O_3 insulators is viewed as a back-up effort, which is prompted by the possibility that, at some future time, the use of BeO in electric vehicles will be prohibited because of its toxicity. The raw material costs for Y_2O_3 are somewhat greater than for BeO, but the fabrication costs are lower because special handling facilities are not required. ILC Technology has also been asked to consider developing brazes for Y_2O_3; however, this effort awaits the results of compatibility tests at ANL on Y_2O_3 bodies produced by Ceradyne, Inc.

A facility has been assembled for screening feedthroughs prior to in-cell testing. The procedure is as follows: the feedthroughs are sealed into half-cells of Li-Al/LiCl-KCl at 450°C, and the variation in resistance across the ceramic insulators is determined by monitoring the current level under a constant applied potential of 2.00 V. The tested feedthroughs will also be examined by metallography and scanning electron microscopy to determine possible failure mechanisms.

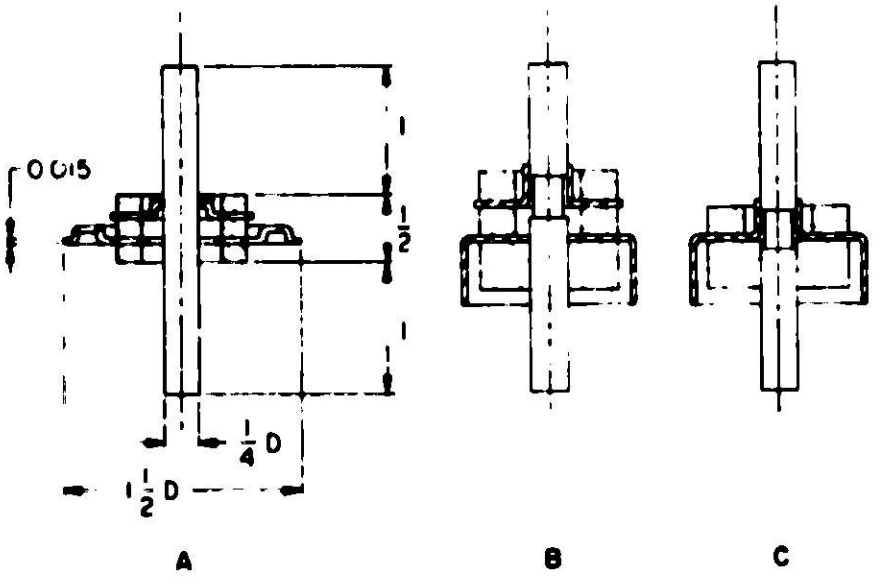

Fig. IV-2. Designs of ILC Technology Brazed Feedthroughs. ANL Neg. No. 308-76-57 R-1.

B. Ceramic Insulator Development
(W. D. Tuohig, J. T. Dusek)*

Work is continuing on the processing and fabrication of pure Y_2O_3 in an effort to eliminate the large irregular flaws reported previously (ANL-75-36, p. 59). Specimens in the form of rectangular bars (~5 by 0.5 by 0.5 cm) have been prepared using a variety of schemes; some of these are shown in Fig. IV-3. These specimens will be broken in a four-point bend test to ascertain the flexure strength. The data will be correlated with variables related to both processing and microstructure and will ultimately be used to establish permissible design stresses for Y_2O_3 components.

To date, the most promising Y_2O_3 bodies have been prepared according to the scheme outlined in Table IV-1. The relatively high binder concentration requires that care be taken during the initial heating; however, it appears likely that lower percentages of binder can be used without adversely affecting the pressing characteristics. Final densities have ranged from 90 to 96% of theoretical. Although the bars appear quite sound, the presence of any flaws will not be apparent until the fracture surfaces have been examined.

*Materials Science Division, ANL.

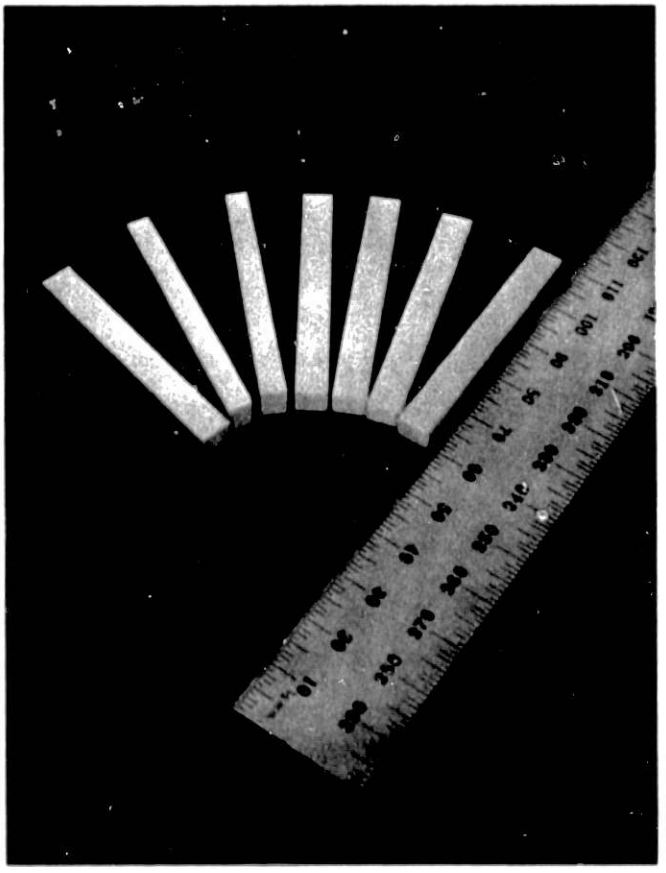

Fig. IV-3. Specimens of Y_2O_3 Prepared for Flexure Strength Measurements

Table IV-1. Procedure for Preparation of Y_2O_3 Bodies for Testing

Make slurry of Y_2O_3 powder, 8% stearic acid, and 4% acrylic resin in CC_4
↓
Blend in jar mill for 12 hr
↓
Evaporate to dryness under constant agitation
↓
Vacuum dry at 100°C
↓
Crush, granulate
↓
Screen to size

Prototype insulators for the compression-type feedthroughs have been prepared by an isostatic pressing technique. Figure IV-4 shows the isostatic mold, with a pressed insulator in place on the steel mandrel. A preweighed charge of granulated powder (-60 +170 mesh) containing 3.5% of the stearic acid-acrylic resin binder is vibratorily loaded into the mold cavity and the assembly is then pressed at 172 MN/m^2 (25,000 psi). The green form is then

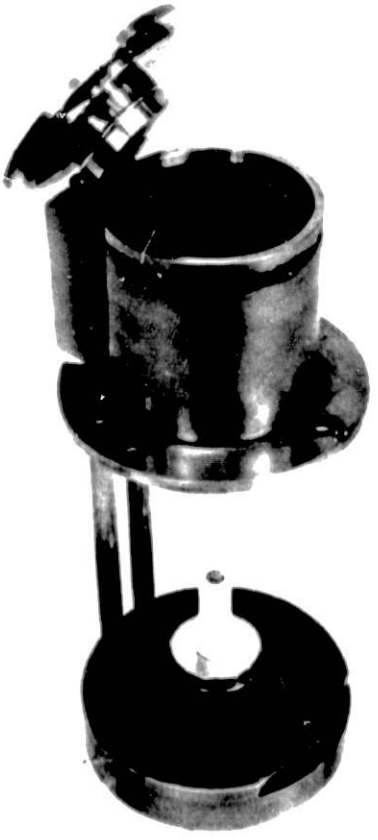

Fig. IV-4. Isostatic Mold Assembly for Fabrication of Y_2O_3 Feedthrough Insulators

fired at 1500°C, after which it is readily machinable to the prefired dimensions. The part is finished by firing at 1750°C in vacuum followed by oxidation at 1500°C. Although required dimensional tolerances can be obtained routinely, the insulators are only 90-91% of theoretical density and are likely to contain the fabrication flaws discussed previously. Any change in the processing, however, would affect the firing shrinkage and thus necessitate tooling alteration. These changes will be made when the final results of the fabrication study became available.

In a preliminary developmental effort, high-density polycrystalline MgO wafers suitable for corrosion testing were produced from MgO powder from two different sources. Powder 1 (grade MJ-30, Iwatani Ltd., Japan) was a high-purity material (>99.9%) of extremely fine particle size. This powder was calcined at 800°C for 35 hr and milled in the presence of a 5% binder solution for 40 hr; the product was then vacuum dried and granulated for dry pressing. Powder 2 (reagent grade, Matheson Coleman and Bell, Cincinnati, Ohio; reported purity >99%) was treated identically except that no calcining was required. Firing at 1500°C in air for 48 hr produced a density greater than 96% of theoretical. Both the grain and the pore sizes were larger in the specimens prepared from Powder 1, thus indicating the relative level of impurities.

Specimens of both materials were immersed in molten lithium at 500°C for 300 hr, along with a specimen of a commercial BeO.* The MgO specimen prepared from Powder 1 exhibited the best results observed to date for polycrystalline MgO, namely, a weight loss of only 4% (for comparison, the weight loss of single-crystal MgO under similar conditions was <1%). The specimen produced from Powder 2 was severely deteriorated and exhibited a nominal weight loss of >40%. These results suggest that additional testing, in a lithium-aluminum/electrolyte environment, may be warranted for MgO specimens produced from Powder 1; no further work with Powder 2 is planned.

The BeO specimen underwent very little attack in the molten lithium and exhibited a weight loss of 0.1%. These results compare favorably with those obtained for a more expensive, higher-purity material from the same source. Additional specimens will be included in long-term (5000-hr) tests.

C. Electrode Separator Development

(J. P. Mathers, T. W. Olszanski)

Boron nitride fabric has been used successfully as the electrode separator in ANL test cells for up to 6400 hr, but its present cost is too high for use in commercial cells. The cost of a separator could be reduced by using papers having less fiber per square foot of separator or by using a less expensive fiber. Because no low-cost fibers are presently available that are expected to be stable in the cell environment, efforts have been concentrated on the development of paper separators.

Organic binders are normally used in preparing ceramic papers (such as Al_2O_3) to provide greater strength and improve the handling characteristics. However, organic binders are unstable at the cell operating temperature (425°C) and are effective only during handling and assembly operations. Inorganic binders which are stable in the cell would have the added advantage of helping

*K 151, National Beryllia Corp., Haskell, N.J.

to maintain the structure of the paper during cell operation, as well as during handling and assembly operations.

Papers made from fibers of BN and Al_2O_3 were obtained either commercially or through development contracts with the Carborundum Company and the University of Florida.* These papers, which contained either an organic or inorganic binder, were tested as separators in a Li-Al/LiCl-KCl/FeS cell. Several had sufficient strength for handling and assembly; however, all of the papers failed in the cell tests owing to deterioration of the binder and subsequent separation of the paper.

Work is continuing on the development of a binder that is stable in the cell. In particular, Carborundum is continuing with the development of a stable BN binder. It is felt that the BN binders already tested may have contained some residual B_2O_3 which reacted with the molten salt. The University of Florida is working on composite papers which consist of BN fibers and fillers of powders which are stable in the cell. It is hoped that the fillers will aid in holding the paper together in the cell and also reduce the effective pore size to aid in the retention of electrode particles. These papers also utilize a small amount of asbestos fiber which is unstable in the cell, but greatly improves the handling characteristics of the paper.

D. The Lithium-Aluminum Phase Diagram
(J. L. Settle, K. M. Myles)

Work has continued on delineating the phase relationships of the lithium-aluminum alloy system. Methods of preparing the alloys and determining the phase transformation temperatures by differential thermal analysis were described in previous semiannual reports (ANL-8109, ANL-75-1, and ANL-75-36). Also described were the chemical and X-ray diffraction analyses and the metallographic examinations that were performed on the alloys.

The results of the investigations to date are shown in Fig. IV-5. Recent features that have been added to the diagram are the peritectic formation of Li_9Al_4 at 335°C and the polymorphic transition of Li_9Al_4 at 275°C. Other new details include the location of the solubility limit of α-Al in β-LiAl at 48 at. % lithium and the formation of Li_3Al_2, rather than Li_2Al, as previously reported.

Future efforts will be concentrated on establishing the solid-solubility limit of α-Al, the solubility of Li_3Al_2 in β-LiAl, and the high-temperature crystal structure of Li_9Al_4.

E. Development of Solid Li-Al Electrodes
(T. W. Olszanski, F. C. Mrazek)

Small diameter, solid Li-Al electrodes were prepared for in-cell testing and evaluation in the electrode development effort. These electrodes were prepared by casting molten Li-Al alloy into a mold of the desired size and configuration (flat disc). A flat plate was placed on the surface of the still-molten alloy and light pressure applied to insure a flat surface on the electrode.

---

*R. D. Walker, Jr., Dept. of Chemical Engineering; directly funded by ERDA.

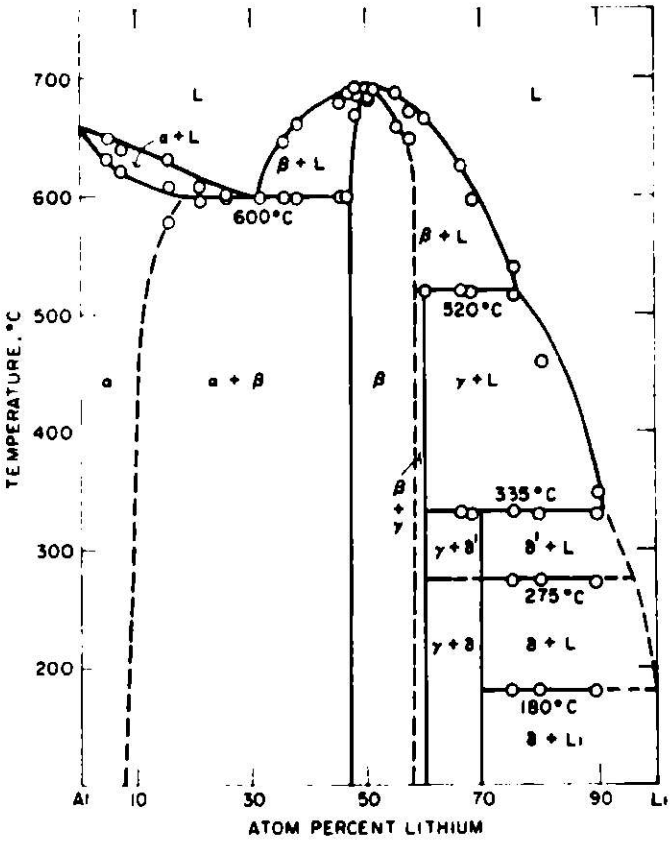

Fig. IV-5. Tentative Phase Diagram of the Lithium-Aluminum System (α = Li, β = LiAl, γ = Li_3Al_2, δ = δ' = Li_9Al_4). ANL Neg. No. 308-76-56.

This type of electrode was evaluated in Cell JW-2 which was operated at 420°C for 75 cycles (see Section III.D, this report). Post-operative examination showed that the electrode had increased from the original 9 mm thickness to 11 mm. Metallographic examination showed that most of the reaction (charge-discharge) was occurring in the portion of the electrode nearest the positive electrode. Some minor reaction had also occurred in the back portion of the electrode. The increase in thickness for a fully reacted electrode of this type would be much greater than the increases for more conventional electrodes, *i.e.*, those prepared from Li-Al powder or from aluminum structures electrochemically loaded with lithium and approximately 50 vol % electrolyte.

The feasibility of a new method for incorporating a metal current collector into a solid Li-Al alloy electrode was also investigated. The technique of loading a macroporous metal structure, (*e.g.*, Retimet) with molten Li-Al would eliminate the need for crushing, sizing, and vibratorily loading powdered alloy into the macroporous structure, as is now being done.

In the initial preparation,* weighed amounts of lithium and aluminum corresponding to a 40 at. % Li alloy were placed in a tantalum crucible and heated to slightly above the liquidus temperature. The macroporous metal

*Z. Tomczuk, Cell Chemistry Group, assisted in these preparations and conducted the cell test.

discs of nickel were immersed for about 15 sec and then removed. Because of surface tension effects, the molten alloy was retained and essentially filled the structure. Thus, the attempt to retain the macroporous structure was not completely successful. Nonetheless, the electrodes fabricated from these discs were tested in small cells with good results.

After testing, one of the electrodes, comprising two Li-Al discs, was examined metallographically. The examination showed that the Li-Al alloy in the disc farthest from positive electrode was relatively unreacted, but the alloy in the disc nearest the positive electrode was well broken up and uniformly dispersed. The microstructure of the latter disc was typical of that in a well-cycled electrochemically or pyrometallurgically prepared electrode. Also, some reaction had occurred between aluminum and nickel; the reaction products were identified as $NiAl_3$ and $NiAl_2$.

The solid Li-Al alloy electrode with the self-contained metal current collector offers a very attractive and viable alternative to previously constructed negative electrodes because of its ease of construction, reduced susceptability to oxide and impurity attack, ease of handling, and the fact that any size or shape electrode can be made. This type of Li-Al electrode, as well as the cast solid described above, are being studied further by Catalyst Research for use in contractor-produced cells.

F. Corrosion Studies

(J. A. Smaga, J. E. Battles)

Extensive materials-evaluation studies of both metals and ceramics are conducted to provide data for the selection of suitable materials for constructing various cell components. Although the performance of materials can be evaluated fully only in operating cells, many candidate materials can be eliminated from further consideration by relatively simple corrosion tests in an environment that approximates their intended application. Generally, materials behavior, as determined in static compatibility tests, has closely paralleled that found upon postoperative examinations of cells.

1. Corrosion Studies in the Negative Electrode Environment

Further studies have been conducted to establish conditions under which a reaction occurs between aluminum in the negative electrode and the cell housing. This reaction was observed previously in postoperative examinations of cells operated at or above 500°C, and the mechanism was identified as a galvanic couple that occurs near the end of a discharge cycle when the Li-Al alloy is depleted of lithium (ANL-75-36, pp. 64-66). The intermetallic compounds formed in this reaction were brittle and fractured under small stresses. Prolonged development of such reaction layers would result in the premature failure of a cell.

In the present tests, high-purity aluminum was used as the anodic member of the couple to simulate the discharged state of a Li-Al negative electrode. An aluminum member was mechanically joined to a cathodic member (a candidate material of construction) and the couple was immersed in LiCl-KCl eutectic salt, contained in a quartz crucible, ~10 days at either 400 or 500°C. The LiCl-KCl used in the tests was from two different sources, namely, Applied Physics Laboratory (APL) and Lithium Corporation of America (Lithcoa). The

APL salt, which has been used in most major ANL cells, is of high purity (polarographic grade), whereas the Lithcoa salt, which is less expensive, contains some anionic impurities. All seven materials were tested in the APL salt, and selected materials were tested in the Lithcoa salt.

The results of the tests are presented in Table IV-2. In all of the tests, the weight loss of the aluminum member was matched by a similar weight gain for the cathodic member. A comparison of the results at 400 and 500°C for the tests conducted in the APL salt reveals that at the higher temperature, the rate of aluminum pickup by all seven materials evaluated as cathodic members increased by more than an order of magnitude. The compositions of the reaction layers formed on four of the cathodic members exposed to the APL salt at 500°C, determined by electron microprobe analysis, are also given in Table IV-2 (column 6). The ratios of aluminum to cathodic metal in the intermetallics were about 1:1 or 2:1. These results are in complete agreement with the postoperative cell examinations.

Table IV-2. Reaction of Dissimilar Metal Couples in LiCl-KCl

Couple	Rate of Al Pickup by Cathodic Member, mg/cm^2)(yr)				Intermetallic Formed in APL Salt at 500°C
	In APL Salt[a]		In Lithcoa Salt[b]		
	400°C	500°C	400°C	500°C	
Fe/Al	7.8	95	1.6	3.2	$FeAl_2$
	30	514	-	14	
304 SS/Al	2.0	55	1.2	8.0	-
	7.5	44	-	-	
316 SS/Al	0.8	224	-	3.6	Inner, $(Cr_{0.2}Fe_{0.8})Al_2$ Outer, $(Ni_{0.1}Cr_{0.3}Fe_{0.6})Al_2$
Ni/Al	4.9	337	-	11	NiAl or Ni_2Al_3
Ni-20Cr/Al	2.5	106	-	27	-
E-Brite/Al	3.4	41	-	-	$(Cr_{0.4}Fe_{0.6})Al$
1008/Al	55	90	-	-	-

[a]LiCl-KCl eutectic from Anderson Physics Laboratory.

[b]LiCl-KCl eutectic from Lithium Corporation of America.

The results of tests at 500°C using LiCl-KCl from Lithcoa were unexpected. The weight gains of the cathodic members were considerably lower than in the APL salt. Dissimilar metal couple tests were repeated for both Armco electromagnet iron and Type 304 stainless steel using both types of LiCl-KCl salt under identical time and temperature conditions. The results of these retests, also given in Table IV-2, confirmed that the reaction rate was significantly reduced in the Lithcoa salt. It is postulated that an anionic impurity (OH^-, $O^=$, $CO_3^=$) in the Lithcoa salt retards the kinetics of this reaction. One or more of these anions could be involved in the formation of a passivating film on the aluminum anode surface. The APL salt is slightly acidic, with a pH of about 5.8, whereas the Lithcoa salt has a pH of about 10.

If one assumes that a material with an aluminum pickup rate of 20 mg/(cm^2)(yr) (a layer about 0.08 mm thick) or less under these idealized test conditions will be serviceable in actual cell use, some conclusions can be drawn. None of the materials evaluated in this study would be acceptable at a cell operating temperature of 500°C if APL salt is used as the electrolyte; even at 400°C in the APL salt, Armco Electromagnet iron and 1008 steel may be unsatisfactory. With the Lithcoa salt, Armco iron and 1008 steel would be acceptable at temperatures up to 500°C, provided that the passivating impurities did not become involved in other cell reactions.

2. Corrosion Studies in the Positive Electrode Environment

Corrosion tests have been conducted on a number of metallic materials at 500°C to determine their suitability for use in both FeS and FeS_2 electrodes. Some of these materials were previously evaluated at 400°C, but information on their corrosion behavior at the higher temperature was needed because some cells are being operated at higher temperatures. A second group of materials, not previously tested, is a series of iron-molybdenum-nickel alloys. Interest in this ternary system stemmed from results of an earlier corrosion study, which showed that the corrosion rate of iron-molybdenum alloys decreased when the molybdenum concentration was increased to 6 wt %.

The following commercial materials were tested: Armco Electromagnet iron, nickel, molybdenum, niobium, Hastelloy B (65Ni-28Mo-5Fe-1Cr) and Hastelloy C (57Ni-17Mo-5Fe-16Cr-4W). A number of iron-molybdenum-nickel alloys, which were prepared at ANL,* were also tested. These materials were evaluated in equal-volume mixtures of FeS_2/LiCl-KCl and FeS/LiCl-KCl, with the exception of Armco Electromagnet iron which was tested in the FeS environment only. The samples, which had surface areas of 0.6-0.7 $in.^2$, were removed for examination after time intervals of 500 and 1000 hr. The results of the tests are summarized in Tables IV-3 and -4, which give the corrosion rates and metallographic observations for the FeS and FeS_2 environments, respectively.

The FeS corrosion study indicates that the following materials have acceptable reaction rates at 500°C: molybdenum, Hastelloy B, Hastelloy C, niobium, nickel, Fe-10Mo-20Ni, Fe-15Mo-20Ni, and Fe-15Mo-30Ni. For both nickel and niobium, an adherent layer of iron was formed on the surface of the samples; no metal sulfide layers were observed. In the case of the two Hastelloys, the FeS reacted with the alloy to form a molybdenum sulfide band, and the iron formed by the reaction deposited on the outer surface of the sulfide band. Nickel (and chromium in the case of Hastelloy C) diffused through the sulfide band and into the outer layer of iron. Armco Electromagnet iron and the iron-base ternary alloys, with the exception of Fe-6Mo-20Ni, were susceptible to intergranular attack. The latter showed a band of surface porosity and internal molybdenum sulfide particles.

As expected, at 500°C the corrosion rates in FeS_2/LiCl-KCl were much higher than those in FeS/LiCl-KCl. Molybdenum, the only material that showed an acceptably low reaction rate at both exposure times, reacted to

*The addition of nickel, combined with the proper heat treatment, makes it possible to increase the molybdenum concentration and still maintain a solid-solution alloy.

Table IV-3. Results of Corrosion Tests in FeS/LiCl-KCl at 500°C

Material	Corrosion Rate, μm/yr[a] 500 hr	1000 hr	Comments
Armco iron	480	340	General attack with intergranular penetration 1-2 grains deep.
Nickel	+58	+39	Iron-nickel reaction layer.
Molybdenum	8.7	11.6	Minor surface attack.
Niobium	+18	+30	Iron-niobium reaction layer.
Hastelloy B	+9	+12	Weakly adherent reaction layer of an internal molybdenum sulfide band and a plated iron layer. Localized areas of intergranular attack.
Hastelloy C	+26	+9	Similar reaction layer but no apparent intergranular attack.
Fe-6Mo	110	130	Intergranular attack resulted in grain fallout.
Fe-6Mo-7Ni	25	79	Surface attack after 500 hr with intergranular penetration after 1000 hr.
Fe-6Mo-20Ni	74	90	Internal sulfidation of molybdenum resulted in a band of porosity 30 μm deep after 1000 hr.
Fe-10Mo-20Ni	17	+14	Localized areas of intergranular attack after 500 hr; reaction layer on some areas after 1000 hr.
Fe-15Mo-20Ni	32	26	Intergranular attack resulted in grain fallout.
Fe-15Mo-30Ni	59	21	Intergranular attack was more severe for the 500-hr sample.

*Numerical values preceded by "+" represent the formation rates of reaction layers.

Table IV-4. Results of Corrosion Tests in FeS_2/LiCl-KCl at 500°C

Materials	Corrosion Rate, μm/yr[a] 500 hr	1000 hr	Comments
Nickel	>6600	-	Completely reacted after 500 hr.
Molybdenum	+20	+11	Uniform but weakly adherent MoS_2 reaction layer.
Niobium	4500	-	Completely reacted after 500 hr.
Hastelloy B	4100	>3900	General attack with some intergranular penetration; porous reaction zone and an outer shell of NiS_{1+x}.
Hastelloy C	3000	3300	Same form of attack as above; >90% of the 1000-hr sample reacted.
Fe-6Mo	>22000	-	All samples reacted throughout their entire thickness; external reaction shells consisted of various sulfides; porous substrates were depleted in Fe and mechanically weak.
Fe-6Mo-7Ni	>22000	-	
Fe-6Mo-20Ni	>22000	-	
Fe-10Mo-20Ni	>22000	-	
Fe-15Mo-20Ni	>22000	-	
Fe-15Mo-30Ni	11000	11000	Same form of attack as above but at a lower rate (50% reaction after 500 hr, 90% reaction after 1000 hr). Reaction band had three distinct zones: an outer sulfide shell, a highly porous zone depleted in Fe and Ni, and a less porous zone depleted in Fe.

*Numerical values preceded by "+" represent the formation rates of reaction layers. Values preceded by ">" represent the minimum corrosion rates based on initial thicknesses.

form a 5 μm-thick surface layer. Electron microprobe and X-ray diffraction analyses* of the surface layer indicated that it was MoS_2, similar to one found on the current collector of Cell W-9 (ANL-75-36, p. 70). Although the layer was quite uniform it was not strongly adherent; thus, the role of MoS_2 in the corrosion protection of molybdenum is questionable. At 400°C in the FeS_2 environment, no surface film was detectable on molybdenum and the average corrosion rate was 2 μm/yr.

The two Hastelloys underwent severe attack in FeS_2/LiCl-KCl at 500°C; the corrosion rates were also higher than at 400°C--approximately 50 and 20 times higher for Hastelloy B and C, respectively. These alloys reacted with the FeS_2 to form nickel sulfide layers; outward diffusion of nickel continued through the developing sulfide layer. As a result, the interior of these samples showed porous zones depleted in nickel. The attack on the iron-base alloys paralleled this form of corrosion. In the case of the Fe-15Mo-30Ni alloy, a band of MoS_2 formed on the original surface, with mixed iron and nickel sulfides also present. Outward diffusion of iron and nickel through the forming sulfide layer again left porous internal reaction zones; the external layer of mixed sulfides was weakly adherent.

Similar corrosion tests will be conducted to screen additional materials. Those materials which show promise will undergo further evaluation.

G. Postoperative Cell Examinations
(F. C. Mrazek, J. E. Battles)

Postoperative examinations are conducted on test cells primarily to evaluate the performance of various construction materials; in particular, feedthroughs, current collectors, electrode separators, and cell housings. These postoperative examinations provide important information, not only on the compatibility of cell components with the cell environment, but on the performance and behavior of the lithium-aluminum and metal sulfide electrode materials. The examination procedures were described in a previous semiannual report (ANL-8109, p. 72).

Postoperative examinations were conducted on prismatic Cells PR-1, R-1, and R-2, all of which were prismatic, vertically oriented cells, to determine materials behavior and to obtain information on the performance and behavior of the lithium-aluminum and metal sulfide electrodes. These examinations included microscopic, X-ray diffraction, chemical, and electron microprobe analyses. Cell PR-1 (Li-Al/FeS-CoS) was voluntarily terminated after 1386 hr and 88 cycles of operation; some of the results of the postoperative examination were presented previously (ANL-75-36, p. 73). Cell R-1 (Li-Al/FeS_2-CoS_2) was terminated after 52 cycles and 1010 hr of operation because of an internal short circuit. A cross section of the cell is shown in Fig. IV-6, with the area of the short circuit circled. Although Cells R-1 and R-2 were similar in construction, the electrodes were prepared differently. In Cell R-1, the Li-Al electrodes were formed electrochemically by the deposition of lithium into an aluminum wire plaque. The entire electrode assembly (including the

*Electron microprobe analyses performed by C. A. Seils, Chemical Engineering Division, ANL; X-ray diffraction analyses performed by B. S. Tani, Analytical Chemistry Laboratory, ANL.

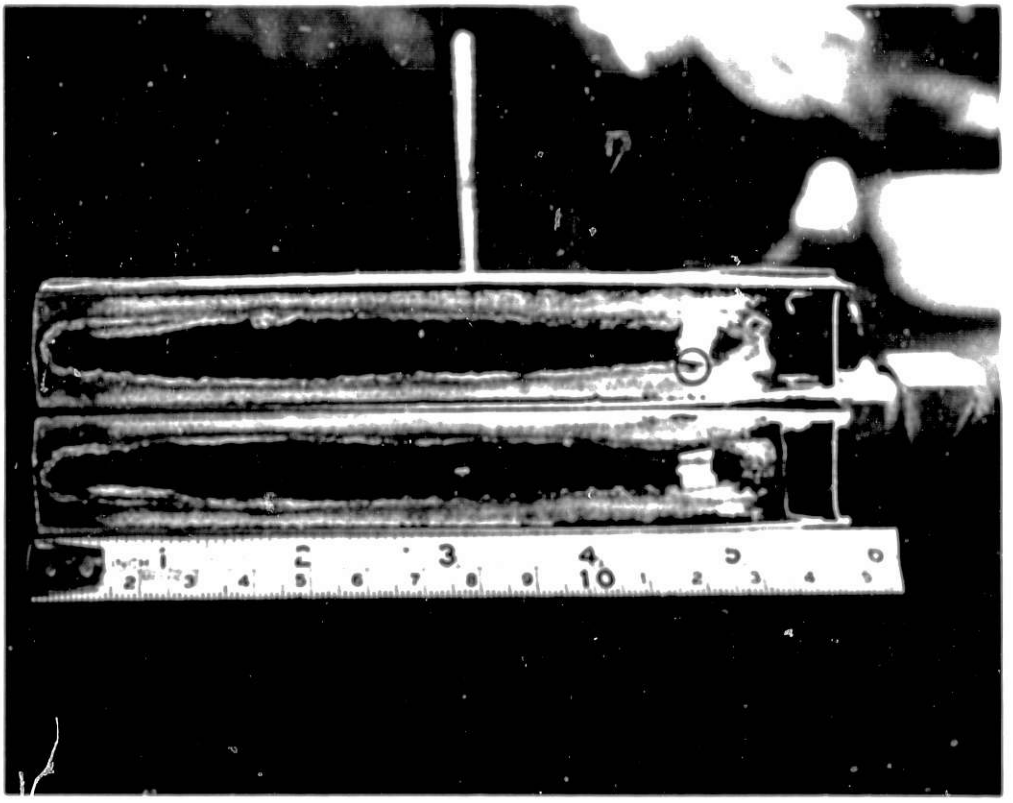

Fig. IV-6. Cross Section of Prismatic Cell R-1 (the short circuit occurred in the region indicated by the circle). ANL Neg. No. 308-4135

FeS_2 electrode) was then electrochemically discharged before installation in the cell case. Cell R-2 was assembled in the cell case as a fully uncharged cell, *i.e.*, with negative electrodes of aluminum wire plaques and a positive electrode of Li_2S and Fe powder. Cell R-2 was terminated after 1406 hr (143 cycles) because of an internal short circuit. Examination showed that positive electrode material had extruded to fill a void space initially present below the electrode. Because the overlap in BN fabric separator at the bottom of the electrode was forced apart, an electrical short circuit resulted.

Macro examination of the vertical cross section of each cell showed no evidence of electrode slumping, which had been a major concern in the design of vertically oriented cells. Cell PR-1 was unrestrained and showed considerable electrode swelling; the mechanical restraint used on the other cells prevented swelling. The observation that electrode slumping did not occur in these cells is supported by microscopic examination and by results of sulfur and iron analyses performed on samples of the positive electrodes of Cells PR-1, R-1 and R-2.* The sulfur distributions from top to bottom of the positive electrodes, presented in Table IV-5, indicate no evidence of increased sulfur contents at the bottoms. In fact, the results for R-1 and R-2 show a slight trend for a greater concentration of sulfur in the upper portion of the electrode.

*Sulfur analyses performed by W. E. Streets, Analytical Chemistry Laboratory.

Table IV-5. Results of Sulfur and Iron Analysis of Vertical Positive Electrodes

Cell No.	Sulfur,[a] wt %	Iron, wt %	S/Fe Ratio
PR-1	7.60	-[b]	-
	11.55	-	-
	12.48	-	-
	11.33	-	-
	7.85	-	-
R-1	27.9	23.9	2.04
	25.8	22.7	1.98
	17.8	19.2	1.80
R-2	6.67	6.16	1.89
	19.73	17.87	1.92
	19.51	18.78	1.81
	17.89	17.75	1.76
	16.66	17.07	1.71
	15.84	13.98	1.98

[a]Approximately equal size samples were obtained, starting at the top of the electrode.

[b]Not analyzed for iron. Cell PR-1 had an iron current collector in the positive electrode. Cells R-1 and R-2 had molybdenum current collectors.

Metallographic examination of the negative electrodes from each cell showed considerable nonuniformity in the microstructure of the electrochemically formed Li-Al electrodes (unreacted or partially reacted aluminum wire). Also, the lithium concentration was greater at or near the negative/positive electrode interface. This behavior is typical of electrochemically formed Li-Al electrodes, and the variations in lithium content have been confirmed by chemical analyses (ANL-75-36, p. 75). Also, the finer particle structure in the region of the interfaces indicates that the bulk of the cycling reactions had occurred in this region.

Microscopic examination has shown evidence of Li-Al alloy reaction with the low-carbon steel or stainless steel cell housings and negative electrode current collectors (the reaction mechanism was discussed in Section F). The reaction products have been examined by electron microprobe analysis; the intermetallic compound $FeAl_2$ is the typical reaction product. As expected, the reaction is more prominent at elevated temperatures (>450°C); at lower temperatures the reaction appears to be negligible.

The postoperative examinations of these cells led to the following general observations:

1. The electrodes must extend to the bottom of cells (or have adequate support to prevent extrusion) and the separator must be positioned to prevent the positive electrode from contacting the cell housing.

2. Restraining of the cell as a means of preventing swelling and distortion of electrodes should be reevaluated in view of the extrusion of material observed in Cell R-2 and to a lesser extent in Cell R-1.

3. The mechanical restraint on cells may be a factor in forcing fine particles of Li-Al or Al into the BN fabric separator; this could lead to cell failure if a bridge is formed between the negative and positive electrodes.

4. Additional development is necessary to obtain a more complete and uniform formation of Li-Al in the negative electrode when cells are started from the discharged state.

5. Additional studies of cell fabrication and cell operating parameters (charge rate, composition, conductivity, etc.) appear warranted to insure that the concentration of lithium in the interfacial region of the negative electrode does not become high enough during charging to allow the formation of a liquid Li-Al alloy.

V. CELL CHEMISTRY
(R. K. Steunenberg)

The objectives of the cell chemistry studies are (1) to provide solutions to specific chemical and electrochemical problems that arise in the electrode and cell development work, (2) to conduct investigations that are expected to lead to innovations and improvements in the electrode and cell designs, and (3) to develop a basic understanding of the processes that occur within the cells.

A. Investigations of Overcharge and Overdischarge Reactions
(Z. Tomczuk, A. E. Martin)

In the operation of a battery, it is possible that cells will become overcharged or overdischarged because of unmatched capacities or other reasons. The use of cell tests and cyclic voltammetry studies to investigate the overcharge reaction products in FeS_2 electrodes was reported previously (ANL-75-36, pp. 80-84). These studies have been extended to include the overcharge reactions of FeS electrodes and the overdischarge reactions of Li-Al electrodes.

1. Overcharge Reactions of FeS Electrodes

The effort thus far on the overcharge reactions of the FeS electrode in Li-Al/FeS cells has consisted of charging four such cells to successively higher cutoff voltages; plans have been made to supplement this work with cyclic voltammetry measurements. The results of earlier Li-Al/FeS cell tests had indicated that the following phases are formed as the FeS electrode is charged:

I. Fe + Li_2S (fully discharged condition)

II. J phase* (normal full charge, 1.65 V)**

III. FeS (full charge above 1.7 V)

In this earlier work, the maximum charge cutoff voltage was 1.90 V. The present study involved higher charge cutoff voltages ranging up to 2.38 V.

The results of this work indicated that the increase in charge cutoff voltage resulted in considerably greater porosity of the FeS electrode, but that the effect on coulombic efficiency was negligible up to a cutoff voltage of 2.36 V (see Table V-1). X-ray diffraction† and metallographic results indicated that FeS (somewhat hyperstoichiometric in sulfur) was the only sulfide phase present in the positive electrode of the fourth cell; this result, however, has not yet been confirmed by X-ray diffraction data.

* Approximate composition, $Li_{0.4}K_{2.8}Fe_{12}S_{13}$ (ANL-75-36, p. 96).

** All voltages in this section are IR-free, unless indicated otherwise.

† Performed by B. S. Tani, Analytical Chemistry Laboratory, ANL.

Table V-1. Results of Charging Li-Al/FeS Cells to Successively Higher Cutoff Voltages

Cell No.	Charge Cutoff Voltage, V	Average Coulombic Efficiency, %	Porosity of Sulfide Electrode	Phases Present in FeS Electrode[a]
1	1.76	100	Normal	$Fe_{1-x}S$
2	2.15	99	Increased	$Fe_{1-x}S$
3	2.30	98	Increased	$Fe_{1-x}S$
4	2.36	75	Increased	FeS_2(?)

[a]Based on X-ray diffraction and metallographic results.

The increased porosity of the positive electrodes in the last three cells (charged to $\geq$2.15 V) suggests that a gaseous product was formed at the higher cutoff voltages. This product is suspected to be sulfur vapor, which could be produced by the overcharge reaction

$$FeS + 3Cl^- \rightarrow S + FeCl_3^- + 2e^-. \quad (1)$$

The voltage-*vs.*-capacity curves obtained during the discharge of these cells showed four voltage plateaus, in contrast to the curve for the first cell (charged to 1.76 V), which had only one plateau. The four plateaus, shown in Fig. V-1, are attributed to the successive formation of different phases as the electrode was discharged. Further work is needed to identify these phases.

2. Overdischarge Reactions of Li-Al Electrodes

Investigations were conducted to determine a minimum discharge cutoff voltage for Li-Al/FeS_x cells. This work was initiated by the observation that the performance of engineering-scale cells was higher at a discharge cutoff voltage of 0.9 V than at 0.7 V. These results suggested that the aluminum in the Li-Al electrode was being discharged to form aluminum ions in the electrolyte. To investigate this possibility, cell tests were made, using negative electrodes either of high-purity aluminum or of aluminum demister wire, which contains about 5 wt % magnesium and has been used frequently for the preparation of Li-Al electrodes for the engineering-scale cells. The positive electrode material was Li_2FeS_2. The experimental conditions were selected to simulate as closely as possible the conditions of the engineering-scale cell tests, particularly for the case in which the capacity of the Li-Al electrode is less than that of the FeS_x electrode.

The high-purity aluminum negative electrode could not be discharged at a cell potential of 0.7 V (the open-circuit voltage was 0.58 V), but the cell test with the demister wire aluminum showed that this electrode could be discharged at the 0.7-V level (open-circuit voltage, 0.82 V). Since the

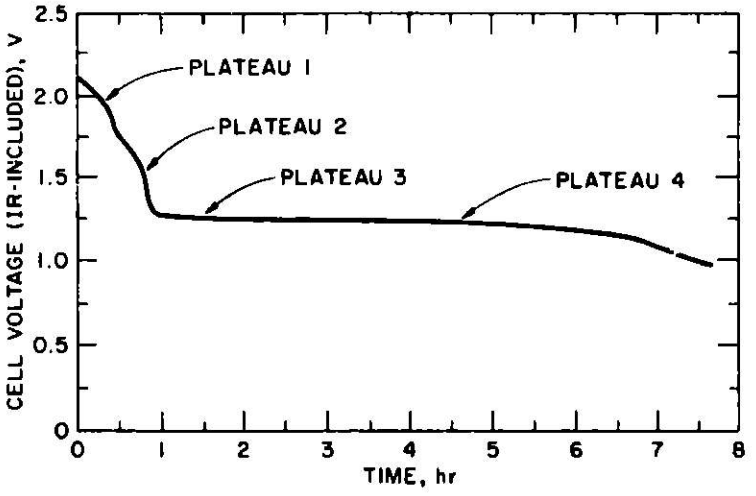

Fig. V-1. Voltage-*vs.*-Time for the Discharge of Cell Li-Al/FeS

essential difference in the two electrodes is the magnesium content of the demister wire, the extra capacity observed at 0.7 V is attributed to the discharge of magnesium to form magnesium ions in the electrolyte. To avoid this reaction, a minimum discharge cutoff voltage of 0.9 V is recommended for cells having a negative electrode made from the demister wire.

B. Studies of Initially Uncharged Cells
(Z. Tomczuk, A. E. Martin)

Several laboratory-scale Li/FeS cells were started from the uncharged condition to explore the practicality of this approach, which may simplify the cell construction and minimize expansion of the electrodes. The negative electrodes of these cells consisted of stainless steel Feltmetal* partially loaded with lithium metal. The positive electrodes utilized either a mixture of Li_2S powder, which was made from Li_2S sintered at 950°C, and iron powder, or a mixture of Li_2S and iron powders obtained by sintering the combined Li_2S and iron powders at 1200°C and grinding the product. Both types of cells exhibited excellent performance after an initial break-in period.

The eventual success of the above concept will depend in large part upon the availability of an adequate supply of high-purity Li_2S at a reasonable cost. The present process for producing Li_2S is too costly for this purpose. On the basis of information in the literature, promising methods for the production of Li_2S included the reaction of Li_2CO_3 with H_2S or H_2S-hydrogen mixtures and the reduction of Li_2SO_4 by hydrogen or carbon. Some preliminary small-scale tests were conducted on the reduction of Li_2SO_4 by graphite. The results showed that Li_2S can be prepared satisfactorily by this reaction either under a vacuum ($\sim 10^{-2}$ Torr) at about 820°C, or under a helium atmosphere at 1000-1100°C.

*A product of the Brunswick Corp.

C. Electrolyte Studies

The principal impurities in the LiCl-KCl electrolyte used in the Li-Al/FeS_x cells appear to be water, hydroxide ion (OH^-), oxide ion (O^{2-}), and particulate material, which has not yet been identified. Cyclic voltammetry was investigated as an analytical method for the soluble impurities, and this method was used to evaluate the effects of various purification procedures. Investigations were also directed toward alternative molten-salt electrolyte systems for Li-Al/FeS cells.

1. Determination of Impurities in Molten LiCl-KCl
(C. A. Melendres)

Studies were conducted on the development of an analytical method for determining impurity levels in LiCl-KCl electrolyte and the effect of these impurities on cell performance. The main contaminant studied was water and its reaction products, OH^-, and O^{2-}. The electrochemical behavior of water in the molten LiCl-KCl was examined by cyclic voltammetry in a platinum cell, using platinum working and counter electrodes. A Li-Al alloy (39 at. % Li) inside an alumina compartment was used as the reference electrode.

Voltammograms were taken at water concentrations of 1.45, 4.36, and 6.87 mM and at two temperatures, 390 and 480°C. Two reversible peaks that were observed were identified as resulting from the reduction of water (see Fig. V-2) and OH^-, respectively. The diffusivity of water, calculated from plots of peak current *vs.* square root of the scan rate, using the first order theory of Nicholson and Shain,[1] is 3.1×10^{-5} cm^2/sec at 390°C and 8×10^{-5} cm^2/sec at 480°C. Peak currents for water and OH^- reduction were both proportional to the concentration of the species. Further measurements of the diffusivity of O^{2-} yielded the values 2.8×10^{-6} cm^2/sec and 7.0×10^{-6} cm^2/sec, respectively, at the above temperatures.

A preliminary study of the effect of impurities on the performance of the Li-Al electrode indicated that the amount of lithium incorporated into aluminum is less in the presence of OH^-.

2. Purification of LiCl-KCl Electrolyte
(J. P. Ackerman, J. W. Sim)

The following methods of purifying the LiCl-KCl eutectic electrolyte were investigated: (1) filtration, (2) drying of LiCl and KCl individually in a fluidized bed, and (3) electrolysis. Filtration through a quartz frit having a pore size of 5-10 μm effectively removed all of the visible solid material,* and is considered to be a necessary step in the purification process. Molten LiCl-KCl eutectic, prepared directly from anhydrous LiCl and KCl as received from commercial sources in plastic bags, contained ∿21 ppm O^{2-} and ∿30 ppm OH^-, determined by cyclic voltammetry. (Most of the water present in the as-received material is driven off by the heating required to melt the eutectic, which has a melting point of 352°C.) When the same constituents were dried by fluidization with helium at temperatures up to 400°C, the molten eutectic, after filtration, contained ∿14 ppm O^{2-} and ∿26 ppm OH^-. Electrolysis of this salt lowered the impurity concentrations to about

*All LiCl except that from Anderson Physics Laboratories seems to contain this particulate.

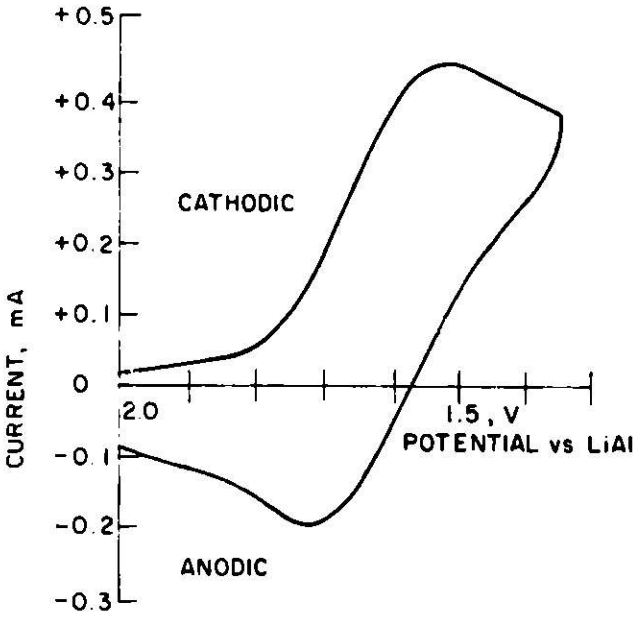

Fig. V-2. Voltammogram of Water in LiCl-KCl (Pt working electrode, area = 0.48 cm^2; C_{H_2O} = 4.36 mM; scan rate = 50 mV/sec; T = 390°C)

3 ppm O^{2-} and 8 ppm OH^-. Highly purified LiCl-KCl eutectic from the Anderson Physics Laboratories contained ∿10 ppm each of O^{2-} and OH^- according to the voltammetric analyses. These results indicate that the fluidized-bed drying is unnecessary and that filtration followed by electrolysis should be an effective purification procedure for the electrolyte.

3. Alternative Molten-Salt Electrolyte Systems
(J. P. Ackerman, J. W. Sim)

A search for alternative molten-salt electrolyte systems has been initiated. The LiCl-KCl eutectic, which is generally satisfactory with respect to cost, density, and melting point, has been used in nearly all of the cell work. However, the potassium content (41.8 mol %) of this electrolyte is high, and the reaction of potassium with FeS to form J phase results in swelling of FeS electrodes. For this reason, and because a higher lithium-ion content in the electrolyte may improve negative electrode (Li-Al) performance, the ternary mixture, 22 mol % LiF-31 mol % LiCl-47 mol % LiBr, is being used in some Li-Al/FeS cells. Although the cell performance is improved, this electrolyte has the disadvantages of high density (2.19 g/ml at 500°C *vs.* 1.63 g/ml for LiCl-KCl), a higher melting point[2] (432°C *vs.* 352°C for LiCl-KCl), and higher cost.

Molten salts that are richer in chloride generally have lower densities and are less expensive. Investigations to date have shown that such mixtures have higher liquidus temperatures than the ternary lithium halide system cited above, but the substitution of potassium ion for some of the lithium ion results in substantially lower liquidus temperatures. For

example, a salt sample of the approximate composition 16 mol % LiF-50 mol % LiCl-34 mol % LiBr had an observed liquidus temperature of ∿481°C, whereas a salt of the same composition, but with potassium ions substituted for 10% of the lithium ions, had a liquidus temperature of ∿427°C. Although the thermocouple used for these measurements has not yet been calibrated, the depression of the liquidus temperature caused by the addition of a relatively low concentration of potassium ions is clear. The concentrations of potassium ion (or other cations) that can be tolerated in cells having FeS electrodes are not yet known, but the results of this work are expected to provide a basis for engineering trade-off decisions.

D. Wetting Characteristics of Molten Salt Electrolytes
(J. G. Eberhart)

The cloth separators and particle retainers in Li-Al/FeS_x cells must be wet by the molten LiCl-KCl electrolyte for lithium ions to pass easily through the separator as the cell is charged and discharged. To investigate this aspect of the cell operation, molten salt penetration tests were performed with boron nitride cloth (used as a separator) as well carbon and zirconia cloths (used as particle retainers); wetting experiments were conducted on solid surfaces of these same materials.

In the initial penetration tests, a sample of the cloth was fastened over the lower end of a vertical boron nitride tube (in drumhead fashion) and this assembly was lowered to a depth of 3 cm in molten LiCl-KCl eutectic in a crucible that was located in the furnace well of a helium-atmosphere glovebox. In the helium atmosphere and at a temperature of 400°C, the zirconia cloth was penetrated immediately by the molten salt. When the assembly was raised and lowered, the salt passed easily back and forth through the cloth pores. After the test the zirconia cloth, which was originally soft and flexible, was rigid as a result of permeation by the salt, which had solidified upon cooling. When a boron nitride or the carbon cloth was similarly lowered into the molten salt, no penetration occurred, even over a period of several days. To achieve penetration of the boron nitride or carbon cloth, it was necessary to cover the upper surface of the cloth with a layer of the molten salt, and then, with the assembly lowered into the salt in the crucible, to evacuate and repressurize the system. During the repressurization step, the salt penetrated the cloth and passed easily through the cloth in either direction. The boron nitride and carbon cloths were penetrated and permeated only in those regions where the upper and lower surfaces were both in contact with the molten salt. There appeared to be no lateral wicking to regions of the cloth where one or both surfaces were not in contact with the salt. The zirconia cloth, in contrast, exhibited lateral wicking, even to those regions where neither surface was in contact with the salt.

The boron nitride and carbon cloths behaved as nonwettable surfaces on first contact with the salt, but once the salt was made to penetrate the cloths, they behaved as wettable surfaces. This behavior suggested the possibility of contact-angle hysteresis in these systems. Accordingly, the advancing and receding contact angles of molten LiCl-KCl were measured on solid plaques of boron nitride, glassy carbon, and zirconia at 375°C. The advancing and receding configurations of a sessile drop were obtained by adding or removing salt. The respective advancing and receding contact

angles were 138° and 54° on boron nitride, 117° and 55° on glassy carbon, and 105° and 45° on zirconia. These results show that boron nitride and carbon do indeed behave as nonwettable surfaces on first contact with the salt and as wettable surfaces on subsequent contact. Hysteresis is generally attributed to surface roughness and/or chemical heterogeneity. The solids used in these tests have some degree of roughness and porosity. One source of hysteresis in this system probably is the deposition of salt in the indentations and pores in the solid surface as the drop recedes. This solid surface would then behave as a composite of the original solid and the salt residue and would therefore be expected to be more wettable than the original solid. This principle is probably operative in penetration of the cloth, that is, much of the space between the fibers is filled during the first penetration and subsequent penetrations are much easier.

To obtain wetting of a boron nitride separator in a practical cell configuration, at least a thin layer of the molten-salt electrolyte must be present on each side of the cloth. In compact engineering-scale cells, the separator is in close contact with the two electrodes, and wetting of the separator is difficult. To simulate this situation, a boron nitride cloth was sandwiched between two stainless steel plates, and the assembly was then secured with iron wire and immersed in molten LiCl-KCl. Evacuation and repressurization of the system produced no wetting of the cloth because of the absence of salt on its two surfaces. However, a convenient means of providing the two salt layers has been developed in collaboration with the engineering personnel. A zirconia cloth, which is readily wettable, is placed on each side of the boron nitride cloth. When this "three-layer separator" is placed between the two stainless steel plates and the assembly is immersed in molten salt, the salt wicks laterally through both zirconia cloths and provides a salt layer on both sides of the boron nitride cloth. Evacuation and repressurization of the system then results in penetration of the boron nitride cloth. A similar test, in which two 325-mesh stainless steel screens were substituted for the zirconia cloth, was equally successful.

E. Alternative Secondary Cell Systems

(M. F. Roche, S. J. Preto, L. E. Ross, A. E. Martin, Z. Tomczuk, H. Shimotake, L. G. Bartholme)

The objective of these studies is to investigate new electrochemical couples and electrolyte combinations that may lead to secondary batteries constructed of low-cost, abundant materials. The major effort is focused at present on cells consisting of a calcium-alloy negative electrode, a metal-sulfide positive electrode, and a molten-salt electrolyte (see ANL-75-36, p. 88). Cells of this type are now approaching engineering-scale tests, but other systems such as Mg/FeS_2 are also being studied actively in small-scale tests. The general approach in identifying new systems is to prepare small experimental cells of 1 to 15 A-hr capacity from promising combinations of electrode materials and electrolytes and operate them through charge-discharge cycles to obtain immediate information on their pertinent electrical characteristics (voltage, power, usable capacity, and reversibility). The poorer systems are thereby eliminated quickly, and the more promising ones, such as the calcium alloy/FeS cells, undergo further chemical, electrochemical, and engineering studies. The main emphasis is on molten-salt and solid-electrolyte cells operating at temperatures from about 200 to 500°C.

The calcium/metal sulfide cells being studied fall into two categories. In one, the cells contain no lithium. In the other, the cells have electrolytes containing lithium salts, mainly as a freezing-point depressant. In both types of cells, the negative electrode materials, *e.g.*, Ca_2Si, are either prepared pyrometallurgically or generated in place by starting the cell from the uncharged state. The electrodes are prepared by prewetting the starting materials with the appropriate electrolyte, regrinding the mixture, and vibratorily loading this mixture into a porous iron current collector.

For the lithium-free cells, one electrolyte being studied has the composition 41.9 mol % NaBr-5.1 mol % KF-53.0 mol % $CaCl_2$, and freezes at 457-460°C; the use of this salt permits cell operation at 500-510°C, a temperature that is 50°C lower than that for cells having an electrolyte of NaCl-$CaCl_2$ eutectic (mp, 506°C). Efforts to produce a negative electrode of very high calcium content (Ca_2Si) during charging of this cell have resulted in poor cell performance, including erratic jumps in the cell voltage and poor coulombic efficiencies during attempts to charge the cell fully. The charging problems appear to have occurred because (1) the highest voltage plateau in the Ca_2Si/FeS cell is at a potential too close to that for sodium production (∿1.65 V *vs.* a calculated value of 1.83 V for sodium production), and (2) the thick (∿0.7 cm) electrodes which were used to obtain a high theoretical capacity density, polarized excessively during charge. (The $CaAl_4$ electrode, which was found in earlier studies to have satisfactory cycling characteristics, has a relatively low specific capacity because of its high equivalent weight.) The maximum capacity density achieved with the Ca_2Si electrode was 50% of the theoretical value (0.6 A-hr/cm^2) at a discharge current density of 20 mA/cm^2, and the cells had poor charge-discharge characteristics as noted above. Metallographic examinations indicated poor penetration of the reaction zone into the depth of the electrode. Consequently, studies involving this electrolyte are being shifted toward the development of thinner negative electrodes.

Work on calcium-alloy/FeS cells with an electrolyte that contains lithium ion (55.4 mol % LiCl-39.8 mol % KCl-4.8 mol % $CaCl_2$) has progressed in a more satisfactory manner. Open laboratory-scale cells (15 A-hr) having negative electrodes of either $CaAl_2$ or Ca_2Si have been operated for more than 30 cycles and have achieved integrated discharge capacities of more than 250 A-hr with nearly 100% coulombic efficiency and little capacity decline. The maximum capacities have been about 70% of the theoretical value at a current density of 20 mA/cm^2 (50% at 40 mA/cm^2) in the laboratory cells constructed thus far, but improved performance is anticipated with optimization of the electrode compositions and thicknesses.

The calcium-alloy cells, with both types of electrolytes, generally have voltages about 0.1 V higher than comparable cells with lithium-alloy negative electrodes, and are thus capable of high energy densities. At present, the positive electrode in these cells is FeS; however, the studies are being expanded to include positive electrodes of FeS_2 and Fe_3O_4. The better cells from this family of electrode-electrolyte combinations will be subjected to engineering tests of large-scale cells.

F. Statistical Treatment of Li-Al Electrode Polarization

(M. F. Roche, D. R. Vissers, K. E. Anderson)

A statistical model for the resistance of a randomly packed bed of active material has been developed to treat the polarization behavior of Li-Al electrodes. Other models, such as the diffusion model presented earlier (ANL-75-36, p. 84) have been unable to reproduce the detailed polarization data collected during the operation of Li/LiCl-KCl/Li-Al cells at 425°C. The Li-Al electrodes in these cells were 15.6 cm^2 in area, 0.32 to 0.75 cm thick, and had electrolyte fractions ranging from 20 to 50 vol % at full charge. Metallographic examination of these electrodes showed that on cycling they develop a random structure of Li-Al particles, about 10^{-3} cm in diameter, embedded in the electrolyte. In the statistical model, the overpotentials (both charge-transfer and concentration) are assumed to be small enough to be ignored during either charge or discharge of each active particle within this structure. As individual particles reach full charge or discharge, their emfs change to limit their further participation in the reaction. The assumption of low overpotential gives rise to a reaction front whose motion is dictated by the conduction properties of the electrode, *i.e.*, electrolyte conductivity in the pores, and particle-to-particle electronic conduction. Tiedemann and Newman,[3] in their model, assumed low overpotentials together with the additional assumption of a strictly planar reaction front. The overall result is a bed resistance that increases linearly with electrode utilization. However, the observed polarization in the present case, although it behaves as a resistance in the sense that it is proportional to current at a particular degree of utilization, is a distinctly nonlinear function of utilization. Our statistical model, which relaxes the planar-reaction-front assumption, gives rise to a bed resistance that is a cumulative lognormal function of utilization. This model shows good agreement with the experimental Li-Al electrode polarization data.

The statistical model assumes a reaction front that first involves material associated with the lowest resistance paths of the randomly distributed channels. Progressively less available material along the higher resistance paths is then included as the reaction proceeds. Consideration of the reaction as proceeding in a series of steps along progressively longer, narrower, and more tortuous channels lead to the expression

$$\Delta R_n = \Delta R_{n-1} (1 + a_n) \qquad (2)$$

where ΔR_n and ΔR_{n-1} are the changes in resistance during step n and step $n-1$, and a_n is a small, random variate with a positive expectation value. Aitchison and Brown[4] show in their general derivation that an equation of this type leads to a lognormal distribution for the variate, ΔR. Consequently, R itself is a cumulative lognormal function of the fractional utilization, U. The appropriate continuous function is as follows:

$$U = \frac{1}{\sqrt{2\pi}\,\sigma} \int_{-\infty}^{X} \exp\left(\frac{-x^2}{2\sigma^2}\right) dX \qquad (3)$$

where

$X = \ln (R_B/R_M)$

σ^2 = normal-distribution variance

R_B = bed resistance

R_M = median bed resistance (at U = 0.5).

Because of the power of the central limit theorem of statistics, the derivation is quite insensitive to distortions of underlying variates that may arise from the simple linear form given for the multiplier in Eq. 3. Convergence to the lognormal distribution is guaranteed provided that the distribution for a_n in Eq. 2 has a mean and a variance. The reasonable assumption that the randomly packed bed also has a random distribution of resistive paths thus leads in a very general way to the cumulative lognormal distribution function.

The bed resistance, R_B, in Eq. 3 is calculated from the continuous cell voltage (V) and current (I) curves, recorded as the cell underwent galvanostatic charges and discharges, as follows:

$$R_B = \left(\frac{V - E_o}{I}\right) - R \qquad (4)$$

where R is the electrolyte resistance external to the porous bed (measured by current interruption and found to be nearly constant throughout charge and discharge), and E_o is the emf of the Li-Al/Li couple. The value of E_o is about 300 mV,[5] except near the end of charge or discharge, where shifts occur toward the lithium or aluminum potential, respectively. The sign of I is chosen to be positive for Li-Al discharge ($V > E_o$) and negative for Li-Al charge ($V < E_o$), so that R_B is always positive. Although equations describing the collapse of resistive polarization within the porous bed have not yet been developed, it is reasonable to assume that this polarization collapses slowly because of differences in the emf between particles at the reaction front and particles that had reacted earlier. Thus, separation of external resistance from bed resistance by current-interruption methods becomes possible.

An example of a cumulative lognormal fit to experimental Li-Al electrode data is shown in Fig. V-3 (discharge) and Fig. V-4 (charge). The data are plotted as a function of actual ampere-hours discharged and charged, and the bounds on fractional utilization, U, were adjusted to cover the same region on discharge and charge (the cell voltage plateau). The fact that the same model curve parameters fit both discharge and charge is surprising, because the volume of solid at the end of discharge is a factor of two smaller than that at the end of charge.

The data near the end of discharge in Fig. V-3 were corrected for the increase in emf of the electrode as its average lithium content decreased below that required for saturation of the alpha phase (about 10 at. % Li, see Li-Al phase diagram in Sect. IV). At the beginning of charge, corrections in the corresponding region of high emf were avoided by including data only for the region beyond the zone of changing emf. The dashed curve in Fig V-4

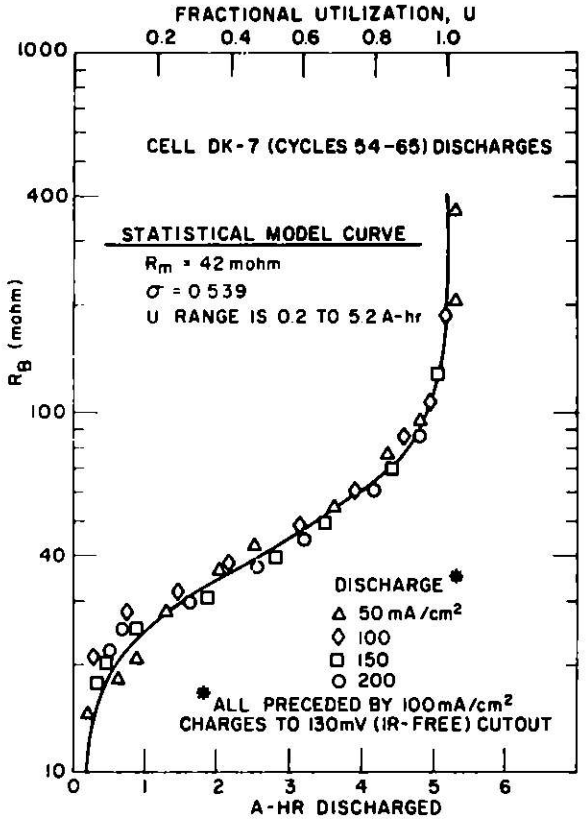

Fig. V-3.

Bed Resistance for Discharge of Li-Al Electrode. ANL Neg. No. 308-76-45.

Fig. V-4.

Bed Resistance for Charge of Li-Al Electrode. ANL Neg. No. 308-76-50

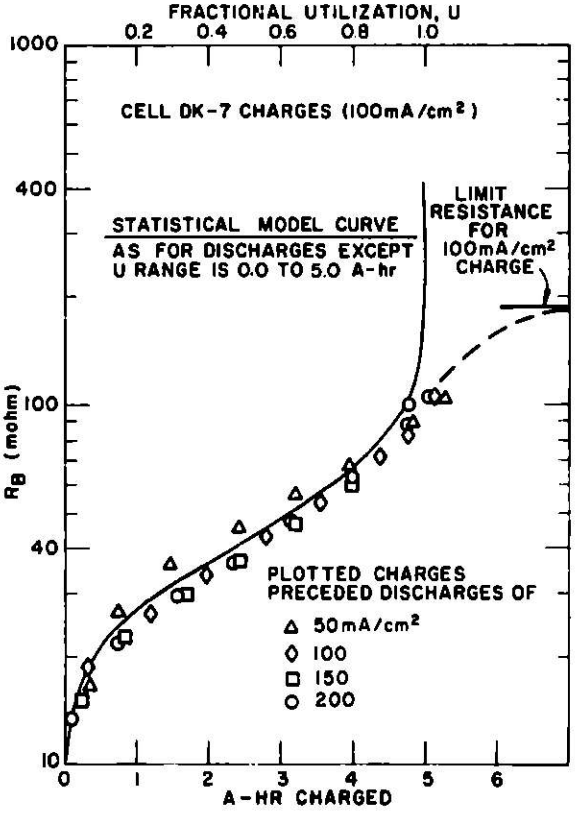

indicates qualitatively how the charge data are expected to deviate from the model at the end of charge as the electrode becomes lithium-rich and approaches a limit resistance governed by liquid lithium formation. (The limit resistance is the emf difference between Li-Al and lithium divided by the charge current.)

The model has been applied, over a range of cycling conditions, to both thin (0.32-cm) and thick (0.75-cm) Li-Al electrodes of differing porosities, with good results. In the case of thick electrodes, deviations from the model occur under some charge conditions. These deviations appear to result from morphological changes that occur during cycling.

The statistical model will be applied next to Li-Al/metal sulfide cell data to determine whether it has more general utility for electrode modeling.

G. Related Physical Research*

1. Phase Studies of Metal Sulfide Systems
(A. E. Martin, Z. Tomczuk)

To understand the electrochemical processes that occur during the charging and discharging of metal sulfide electrodes, it is necessary to characterize the various intermediate phases that are formed. In Li-Al/FeS cells, an interaction occurs between the active material in the FeS electrode and the KCl in the electrolyte to form a material designated as J phase, which causes swelling of the electrode. As described in ANL-75-36, p. 96, the J phase can be prepared by the direct chemical reaction of iron with Li_2FeS_2 in the presence of LiCl-KCl eutectic salt at 400°C. Eight grams of the J phase was prepared, using iron in the form of 10-mil sheet, so that its composition and properties could be characterized. X-ray diffraction results** showed that only J phase was present after the excess iron sheet was removed and the product was leached with water. Differential thermal analysis showed that this material begins to decompose irreversibly at about 560°C. Chemical analysis** of the material gave the following results (in wt %): Fe, 54.69; K, 9.44; S, 32.82; Cl, 1.37; Li, 0.29. These results are in good agreement with the analysis obtained on a sample of J phase that was isolated earlier from the positive electrode of a Li-Al/FeS cell (ANL 75-1, p. 100). A sample of the recently prepared material will be examined by neutron diffraction in an attempt to establish its structure. (X-ray diffraction is incapable of determining the location of light atoms such as lithium.)

---

*This work was supported by the ERDA Division of Physical Research.

**X-ray diffraction analyses performed by B. S. Tani and chemical analyses by K. J. Jensen, Analytical Chemistry Laboratory, ANL.

The Li_2FeS_2 ($Li_2S \cdot FeS$) phase, which has often been identified by X-ray diffraction in the positive electrodes of partially charged Li-Al/FeS_2 cells, has also been detected in a modified form in FeS-Cu_2S electrodes. The latter phase is now believed to have an approximate composition of $2Li_2S \cdot 3FeS \cdot Cu_2S$, on the basis of the following indirect evidence. A series of Li_2S-FeS-Cu_2S preparations of differing compositions were annealed at 400°C and analyzed by X-ray diffraction. One of the preparations, namely, one with the composition $2Li_2S \cdot 3FeS \cdot Cu_2S$, was essentially single phase and had an X-ray diffraction pattern nearly identical to that of the material recovered from FeS-Cu_2S electrodes. These studies of Li_2S-FeS-Cu_2S preparations also disclosed (1) the existence of several compounds that are formed between Li_2S and Cu_2S, and (2) a significant solid-state solubility of Cu_2S in Li_2S at 400°C.

2. Electrochemistry of the Li-Al Electrode
(C. A. Melendres)

An investigation of the kinetics of lithium deposition on aluminum and Li-Al alloys is being conducted to identify the slow processes that limit the performance of the Li-Al electrode in Li-Al/LiCl-KCl/FeS_x cells. A galvanostatic-pulse or current-step technique is being used initially, and the measurements are being made in LiCl-KCl eutectic electrolyte at 400°C. The potential-time transients for the discharge of lithium onto aluminum at low current densities (<5 mA/cm^2) have shown an ohmic overpotential at short times (<10 μsec) and a gradual polarization from the aluminum potential of ~1.25 V *vs.* Li-Al to zero at long times. At high current densities, a marked overpolarization was observed for times less than 1 msec, followed by a gradual depolarization back to the Li-Al potential at long times. The latter behavior was also observed in the deposition of lithium onto a Li-Al electrode.

The observed overpotentials have been considered in the light of the following probable steps involved in the incorporation of lithium into the aluminum:

$$Li^+ \text{ (solution)} \rightarrow Li^+ \text{ (interface)} \quad (5)$$

$$Li^+ \text{ (interface)} + e^- \rightarrow Li \quad (6)$$

$$Li + Al \rightarrow \text{solid solution of Li in Al} \quad (7)$$

$$Li + Al \rightarrow LiAl \quad (8)$$

$$\text{Li diffusion to interior of metal or LiAl layer} \quad (9)$$

There seems to be no mass-transport limitation in the electrolyte phase, and the charge-transfer process is fast. The solid-state diffusion of lithium in aluminum is likely to be the rate-controlling process. The overpolarization at high current densities may result from slow formation and crystallization of the LiAl (β) phase. It may also be pseudo-ohmic because of a film of impurities on the electrode surface. Potential-step experiments and microscopic studies are being undertaken to investigate the

process further. Kinetics studies on other alkali and alkaline earth metals in molten salts and other nonaqueous electrolytes are being contemplated for the future.

3. Electrochemistry of the Iron Sulfide Electrode
(C. A. Cajigas, C. A. Melendres)

The objective of this work is to gain an understanding of the mechanisms and rates involved in the operation of the iron sulfide electrode. Cyclic voltammetry is being used initially to investigate the electrochemical behavior of iron in molten LiCl-KCl containing Li_2S. Typical voltammograms taken at 450°C with two different switching potentials and at a Li_2S concentration of 1×10^{-2} molal are shown in Fig. V-5. The oxidation-reduction peaks at about 1.6 V *vs.* Li/Li^+ are the ones that are involved in the charging and discharging of the FeS electrode. These waves are characteristic of the formation and subsequent cathodic stripping of a surface layer. The reaction is believed to be

$$Fe + S^{=} \rightleftarrows FeS + 2e^{-} \qquad (10)$$

At higher Li_2S concentrations, the anodic overpotential became resistive, presumably as a result of thickening of the film or accumulation of the dissolution product in the solution. At lower Li_2S concentrations, an anodic wave at ~1.5 V and a cathodic peak at ~1.3 *vs.* Li/Li^+ also became prominent.

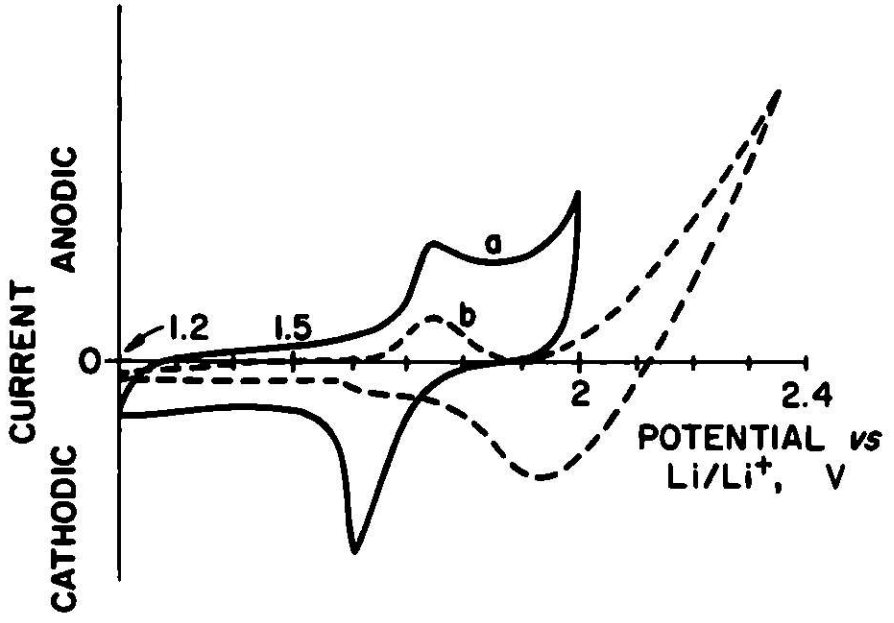

Fig. V-5. Voltammogram of Li_2S in LiCl-KCl on Iron Working Electrode
(a) 100 mV/sec
(b) 20 mV/sec; current scale 10X that in (a)

From Fig. V-5 it is evident that the anodic overpotential again became resistive when the switching potential was increased beyond 2 V. This behavior is attributed to dissolution of the iron with a resulting accumulation of $FeCl_2$ or $KFeCl_3$ in the vicinity of the electrode. This effect has been observed when the FeS electrode is overcharged (see Section V.A.1). Potentiometric measurements are being made to verify the hypothesis that this electrode behaves as a "covering layer" type of electrode (called an electrode of the second kind).

Potentiostatic and galvanostatic pulse experiments will be undertaken to determine kinetic parameters and to study the nucleation and growth of the surface film on the above electrode. This work will be supplemented by microscopic and X-ray diffraction or electron diffraction studies.

4. Emf Studies of Li-Al Alloys
(C. G. Cajigas, J. R. Selman, C. A. Melendres)

The objective of this study is to define more clearly the emf-composition relationships in the lithium-rich portion of the Li-Al system. Further emf measurements have been made at various temperatures, using a coulometric method, on alloy compositions ranging from 70 to 90 at. % lithium. At 510°C, just below the Li_3Al_2 peritectic decomposition, a break in the emf-composition curve was observed (see Fig. V-6). This break corresponds to a liquidus composition of 85.5 ± 0.5 at. % lithium, and occurs at a potential of 23.2 mV *vs.* $Li°/Li^+$.

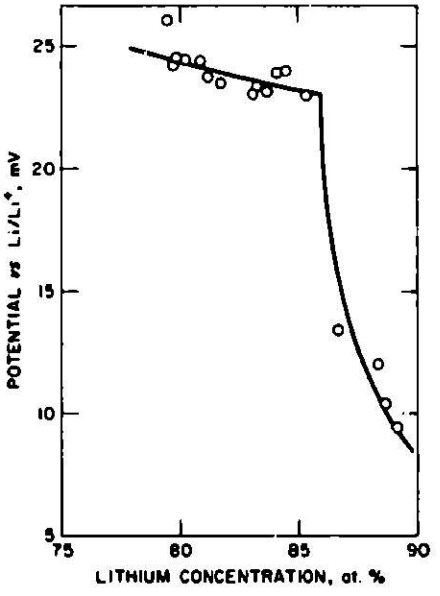

Fig. V-6. Emf of Li-Al Alloys at 510°C

Measurements were also made with a sample containing 77.5 at. % lithium at temperatures from 510 to 650°C. The values that were obtained are 565 ± 5°C for the liquidus temperature, 21.5 mV *vs.* $Li°/Li^+$ for the emf, 0.74 for the lithium activity and 0.96 for the activity coefficient.

The above alloy compositions are being checked by chemical analysis. No further experimental work is planned.

5. Emf Series in Molten LiF-LiCl-LiBr Electrolyte
(L. A. Schaum,* C. A. Melendres)

This study is aimed at establishing an emf series in molten LiF-LiCl-LiBr electrolyte (composition: 22-31-47 mol %), which is of interest as an alternative for Li-Al/FeS batteries. The electrode potentials of a number of metals were measured at 400°C in alumina or zirconia cells against a lithium pool (in a beryllia crucible) or against solid (α + β) Li-Al alloy as the reference electrode. The metal ions were generated coulometrically by anodic dissolution of the metal. Potential readings were made after the system had come to equilibrium, normally about 15 to 30 min after the metal ions were generated. Nernst plots were constructed of the measured potential *vs.* log $[M^{+n}]$, where $[M^{+n}]$ is the metal ion concentration in molality and n is the valence. From these plots, values were obtained for the standard potential, E°, at $[M^{+n}]$ = 1 molal and for the number of electrons involved in the reaction. Preliminary results are given in Table V-2. The standard potentials in the LiF-LiCl-LiBr electrolyte do not differ widely from those reported for the LiCl-KCl eutectic, and there is a similar trend in the series. The temperature coefficient of the emf for Cu/Cu^+ was also measured, with a resulting value of -0.93 mV/degree.

Table V-2. Electrode Potentials in Molten LiF-LiCl-LiBr Electrolyte at 450°C

Couple	E° *vs.* Li-Al, V	E°' *vs.* Li/Li^+,[a] V	No. of Electrons	E°' *vs.* Li/Li^+ in LiCl-KCl,[b] V
Fe/Fe^{++}	1.944	2.258	2.17	2.148
Cu/Cu^+	2.079	2.393	0.91	2.364
Ag/Ag^+	2.102	2.316	1.00	2.578
Pd/Pd^{++}	2.767	3.081	1.92	3.106

[a] Corrected to a Li^+ ion concentration of 10.6 molal for comparison with the E°' values in LiCl-KCl, which has this Li^+ ion concentration.

[b] Data from Ref. 6.

* Undergraduate Research Participant Program.

REFERENCES

1. R. S. Nicholson and I. Shain, Anal. Chem. 36, 706 (1964).

2. A. G. Bergman and A. S. Arabadyham, Zhur. Neorg. Khim. 8, 1228 (1963).

3. W. Tiedemann and J. Newman, J. Electrochem. Soc. 122, 1482 (1975).

4. J. Aitchison and J. A. C. Brown, The Lognormal Distribution, Cambridge University Press, London (1966).

5. N. P. Yao, L. A. Heredy, and R. C. Saunders, J. Electrochem. Soc. 118, 1039 (1971).

6. J. A. Plambeck, J. Chem. Eng. Data 12, 77 (1967).

VI. BATTERY DESIGN AND ENGINEERING
(A. A. Chilenskas, R. O. Ivins)

A. Systems and Cost Studies

Studies are being continued to define goals for the application of high-temperature batteries to electric-vehicle propulsion and utility load-leveling. The goals thus defined become the basis for cell and battery specifications to help guide the near-term development as well as the longer-term commercial application of these batteries.

1. Driving Range of Automobiles Powered by a Lithium/Iron Sulfide Battery
(A. A. Chilenskas)

Present plans call for the first full-scale battery to be ready for a test automobile in 1978; an improved battery, for demonstration of program goals in 1981; and a commercially produced battery, for demonstration in 1985. Calculations have been made to estimate the range of electric automobiles that are powered by lithium/iron sulfide batteries at these various stages of development. The bases for the calculations and the performance characteristics are given in Table VI-1. In addition to the assumptions shown in the table, a 10% reduction of aerodynamic drag of the vehicle is assumed for 1985. As is shown, the driving range of a subcompact at highway speeds (60 mph) can be expected to increase from 62 miles to about 175 miles as the development of the lithium/iron sulfide battery proceeds from the 1978 test battery to a mass-produced battery in 1985. Also, the larger automobiles show an increase in range potential from greater than 70 miles to greater than 200 miles.

A study is now under way to examine the potential range of battery-powered vehicles in more detail. Included in the study are considerations of the economic and technical aspects of extending the range of electric vehicles by (1) battery exchange, (2) quick recharge, (3) battery/internal combustion engine hybridization, and (4) road electrification.

2. Economic Comparison of an Electric-Powered and a Gasoline-Powered Vehicle
(G. J. Bernstein)

A comparison has been made of the costs of owning and operating a vehicle powered by a Li-Al/iron sulfide battery and a vehicle powered by gasoline. The comparison takes into consideration differences in capital costs as well as differences in operating and maintenance costs and life expectancy of vehicles and batteries. A 10-yr period is used for comparison since this is the usual standard selected for gasoline-powered vehicles.[1] However, allowance is made for the greater durability of electric vehicles by charging a lower annual maintenance cost and amortizing the capital costs over a 13-yr period. Allowances were also made for increases in costs of fuel and maintenance over the 10-yr period.

Table VI-1. Driving Ranges of Electric Automobiles at Constant Speeds

Basis

Gross Vehicle Weight (including battery), kg		Battery Output, W-hr/kg	
Subcompact	800	1978	80
Compact	1136	1981	143
Family Car	1818	1985	164
Battery/Vehicle Weight Ratio		**Conversion of Battery Output to Power at Wheels, %**	
1978	0.35		
1981	0.35	1978	75
1985	0.40	1981	75
		1985	80

Vehicle Class	Constant Speed, mph	Range at Constant Speed, miles 1978	1980	1985
Subcompact	40	95	171	267
	60	62	112	175
Compact	40	107	190	294
	60	76	135	209
Family	40	117	210	325
	60	79	141	219

The base costs assumed for the comparison are shown in Table VI-2. In addition, as indicated in the table under "Variation from Basis Conditions," the effects of variations in fuel, maintenance, and capital costs as well as driving use and battery lifetime were considered. Cost comparisons were based upon differences in costs for like charges rather than upon absolute costs. These costs comparisons were calculated as annual cost differences and then summed to give the 10-yr differences. As shown in the table, the cost advantage lies with the electric vehicle over the range of selected conditions when the initial cost of the electric vehicle does not exceed the cost of the gasoline-powered vehicle by more than about $2000.

B. Design Studies

Design studies covering a wide range from conceptual sketches to detailed designs are continuing requirements in the ANL battery program. Described below are (1) a reference design of a prismatic cell that served as the basis for development/fabrication of cells by three industrial firms under contract with ANL, and (2) a conceptual design for a 30 kW-hr electric vehicle battery utilizing a prismatic cell design.

Table VI-2. Differential Cost of Operation of a Gasoline Vehicle (GV) and an Electric Vehicle (EV) over a 10-yr Period

Basis

Vehicle driven 10,000 miles/yr
GV: 24 miles/gal
EV: 0.38 miles kW-hr/miles

Base Cost: $4200

GV depreciation over 10 yr = $420/yr
EV depreciation over 13 yr = $323/yr
Δ = $97/yr

Any additional cost of EV amortized over 13 yr at 6% interest = $113/yr for each $1000 added cost

Li/FeS_2 battery cost = $1225 ($35/kW-hr)
amortized over 10 yr at 6% interest = $167/yr
Battery life: 1000 cycles at 35kW-hr/cycle

Initial GV maintenance, $120/yr higher than EV and increases at 8%/yr

Gasoline cost, 60¢/gal and increases at 10%/yr

Electricity cost, 3¢/kW-hr and increases at 6%/yr

	Variation from Basis Conditions	Cost Advantage[a] of EV over GV (10-yr Total), $
1.	None	3543
2a.	8000 miles/yr; Initial Maintenance, Δ = $100/yr	2929
b.	7000 miles/yr; Initial Maintenance, Δ = $90/yr	2588
3a.	Initial Cost of Electricity = 4¢/kW-hr	2947
b.	Initial Cost of Electricity = 5¢/kW-hr	2465
4.	Battery Cycle Life = 500 cycles	
a.	10,000 miles/yr; Electricity, 3¢/kW-hr	2223
b.	10,000 miles/yr; Electricity, 5¢/kW-hr	1235
c.	7000 miles/yr; Electricity, 3¢/kW-hr	1998
d.	7000 miles/yr; Electricity, 5¢/kW-hr	1343

[a]Deduct $1130 for each additional $1000 of initial cost of EV.

1. Design of Prismatic Test Cell for Industrial Development and Fabrication
(V. M. Kolba)

The reference design to be used as a basis for development and fabrication of cells by industrial firms under contract to ANL was presented in the preceding semiannual report (ANL 75-36, p. 121). The specifications for this design were developed as a result of an intensive review of cell-design and operating experience in all areas of the ANL program. Given below is a summary of the work that led to the design for the contractor-produced cells.

The basic design criteria that were adopted are as follows:

1. The cell has one positive electrode and two facing negative electrodes, and is of vertical, prismatic configuration.

2. Specific energy goals are 80 W-hr/kg at the 10-hr rate for FeS-type cells and 130 W-hr/kg at the 5-hr rate for FeS_2-type cells.

3. The design accommodates a variety of electrodes and electrode thicknesses, with a maximum amount of common hardware.

4. The positive electrode housing is at the negative electrode potential, *i.e.*, the active materials in the positive electrode are electrically isolated from the housing by the separator and retainer cloths.

5. A modified version of the Conax compression-type feedthrough is used for the positive lead.

6. The design provides for electrolyte filling after assembly.

7. The electrode design permits use in future multiplate cell designs.

The prismatic shape of the cell permits better space utilization and the vertical orientation permits the cells to be packaged into a battery configuration similar to a lead-acid automobile battery. The design also provides a gas space above the cell plates that reduces the contact between the positive feedthrough and the cell electrolyte. This latter specification is believed to be important in terms of improving cell lifetime.

Two types of cells were designed. One type, designated "A", has thin electrodes to comply with the high performance requirements for an electric vehicle. The second type, designated "B", has thick electrodes to meet the requirements for a storage system for load-leveling on utility networks. The electrode thicknesses and electrolyte volume fractions used in these designs were based on recommendations received from the various groups for the specific performance desired for an "A" or "B" type of cell.

A schematic of the prismatic test cell, previously presented in ANL-76-9, p. 121, is shown in Fig. VI-1 for reference. The electrode and cell specifications are given in Table VI-3. The negative electrode is

Table VI-3. Prismatic Test Cell Specifications

	Type A	Type B
Negative Electrode (each)		
Dimensions of Porous Structure, cm		
Length and Width	12.86	12.86
Thickness	0.30	0.70
Electrolyte Volume Fraction		
Pyrometallurgical Li-Al	0.25	0.30
Electrochemical Li-Al	0.25	0.30
Theoretical Capacity, A-hr		
Pyrometallurgical Li-Al	36	80
Electrochemical Li-Al	38	84
External Dimensions, cm		
Length and Width	12.90	12.90
Thickness	0.33	0.73
Positive Electrode		
Dimensions of Porous Structure, cm		
Length and Width	12.48	12.48
Thickness	0.6	1.2
Electrolyte Volume Fraction		
FeS-type electrode	0.55	0.64
FeS_2-type electrode	0.66	0.71
Theoretical Capacity, A-hr		
FeS + Cu_2S	92	151
FeS_2	109	184
Cell Housing		
External Dimensions, cm		
Height	15.64	15.64
Width	13.10	13.10
Thickness	1.97	3.37
Wall Thickness, cm	0.06	0.06
Total Height to Top of Negative Current Lead, cm	19.69	19.69

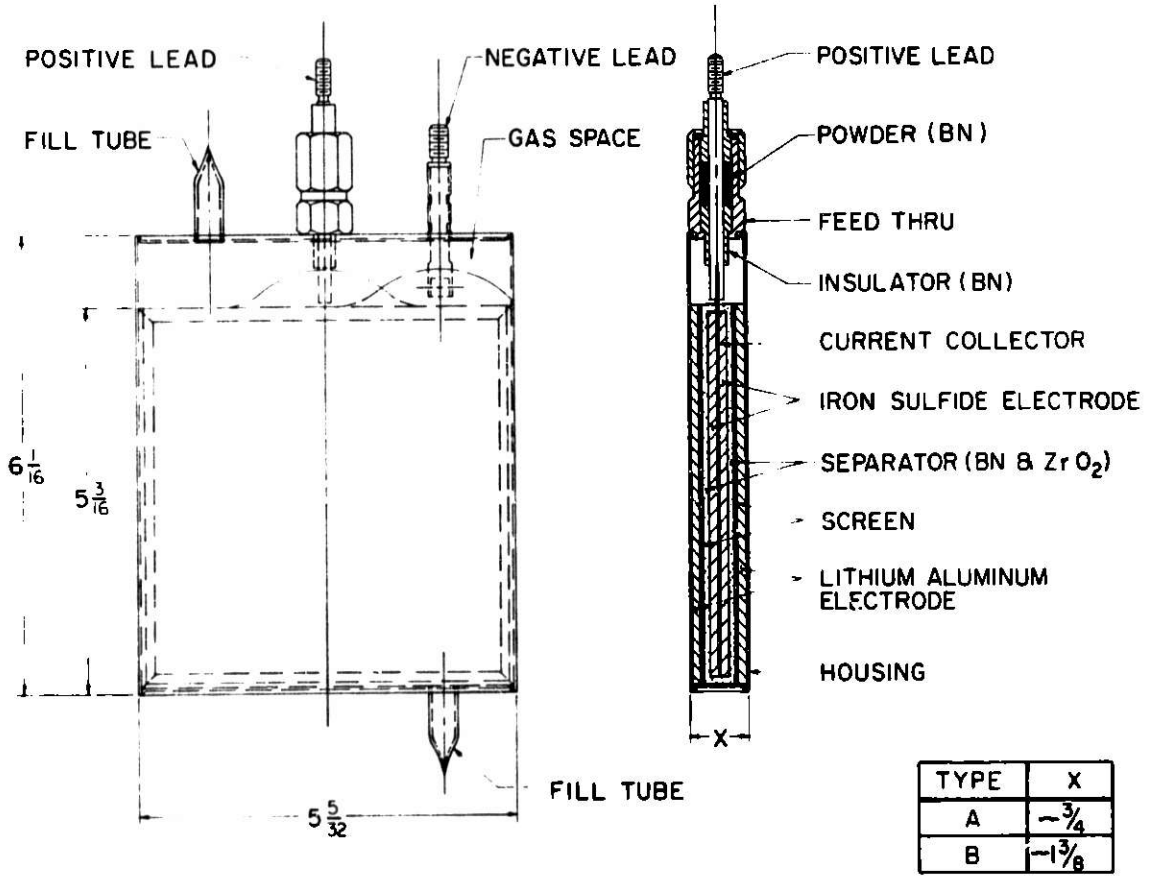

Fig. VI-1. Design of Prismatic Cell for Industrial Contracts (dimensions in inches)

designed to accommodate either an electrochemically formed structure or a porous metal structure loaded with lithium-aluminum alloy powder. The current collecting structures are attached to a backing plate. The lithium concentration in the Li-Al alloy is specified as 43 at. %. Particle retention in the negative electrode is provided by a 325-mesh stainless steel screen at the face of the electrode. The positive electrode utilizes a current collecting structure of porous metal (for FeS) or porous carbon (for FeS_2). These structures are located on each side of a central current collector plate. The current collector plate separates the two sides of the positive electrode to promote uniform reaction between the electrode halves and the facing negative electrodes. Powders of FeS or FeS_2 in combination with any required additives, are loaded into the porous structures. Particle retention in this electrode is provided by a ZrO_2 cloth. A BN cloth is used as the electrode separator. These cloths are held against the loaded porous structure of the positive electrode by a 60-mesh screen on the faces of the electrode and by a thin metal band around the periphery of the electrode.

The cell housing is low carbon steel; penetrations are provided for the positive lead (modified Conax), the negative lead, and the electrolyte fill tubes. In the early design, shown in Fig. VI-1, a bottom inlet/top outlet filling arrangement was used; a later design utilized only a single top-fill tube.

2. Conceptual Design of a 30 kW-hr Electric Vehicle Battery With Prismatic Cells
(V. M. Kolba, A. A. Chilenskas)

A battery program goal is to design, develop, and fabricate an electric vehicle battery of about 30 kW-hr output that can be tested in a compact-sized automobile in 1978. The automobile would seat four passengers, weigh about 1136 kg (2500 lb) including a 400 kg battery, and have an urban driving range of about 100 miles.

To meet the short time schedule, a design effort has been started to determine the cell size and overall battery configuration that will permit utilization of the present prismatic design with minimum cell scale-up requirements.

In the scale-up calculations, five cases were examined; cell sizes varied from the present 12.7 x 12.7 cm prismatic cell being fabricated by the industrial contractors to a size of 16.5 x 23 cm. Cell specifications for the five cases are given in Table VI-4 for cells utilizing an active positive electrode containing FeS_2 plus CoS_2. Only a small increase in specific energy with increasing cell size is obtained owing to the need for increasing the weight of current conductors in the larger plate size. It is believed that the design calculation assumptions were somewhat conservative and, with actual scaled-up cells, larger gains in specific energy can be achieved than those calculated in Table VI-4. The battery parameters for each of the cell sizes are shown in Table VI-5.

Table VI-4. Cell Parameters for Scale-Up Studies

	Case				
	I	II	III	IV	V
Plates					
Nominal size, cm	12.7x12.7	12.7x19	12.7x19	15.2x15.2	23x16.5
Cells					
Thickness, cm	2.5	2.5	2.5	2.5	2.5
Width, cm	13	13	13	15.7	23.5
Height, cm	19	25.4	25.4	21.6	23.5
Capacity, A-hr					
Theoretical	155	233	221	215	363
Usable (at 75% util.)	116	175	166	161	272
Average voltage, V	1.3	1.3	1.3	1.3	1.3
Energy Output, W-hr	151	227	216	209	354
Weight, kg	1.4	2.1	2.0	1.9	3.1
Specific Energy, W-hr/kg	108	108	108	108	113

Table VI-5. Battery Parameters

	Case				
	I	II	III	IV	V
Battery					
Weight, kg					
Cells	277	277	280	279	263
Battery	347	347	350	349	329
Specific Energy, W-hr/kg at 5-hr rate	86	87	86	86	91.5
Modules/Battery	66	66	70	2	1
Cells/Battery	198	132	140	144	85
Voltages, V					
E max. (charge limit)	132	132	140	144	170
E operating average at 5-hr rate	86	86	91	94	110
E min. (discharge limit)	66	66	70	72	85
Assembled Module Envelope Size					
Length, cm	197	189	200	206	243
Width, cm	40.6	26.4	26.0	15.7	23.5
Height, cm	19.0	25.4	25.4	21.6	23.5
Volume, m^3	0.15	0.13	0.13	0.07[a] 0.14[a]	0.13
Battery Envelope Size					
Length, cm	205	196	208	213	251
Width, cm	45.7	31.4	31.4	-	28.6
Height, cm	24.1	30.5	30.5	-	28.6
Diameter, cm	-	43.8	38.1	31.8	40.0
Volume, m^3	0.23	0.29	0.24	0.17[a] 0.34[a]	0.31

[a]Two required per vehicle.

In Case I, representing the present 13 x 19 cm prismatic cell, the cells are placed in modules comprising 3 cells in parallel and 66 modules in series. In Cases II and III the cells are the same size (13 x 25.4 cm), except that for Case III a corner has been cut off the bottom of each cell to allow more efficient packaging. This concept is shown in Fig. VI-2. Two cells are connected in parallel and the array connected in series down the length of the container. Case IV (15.6 x 21.6 cm cells) represents the concept of two separately insulated modules. Each module could be integrated into the structural frame of the vehicle. Case V represents a large cell (23.5 x 23.5 cm) which in overall sectional configuration is a square and is more easily accommodated in a cylindrical battery container than arrays of the other cells.

Tentatively, the first design is to be based upon the cell size described by Case III (13 x 25.4 cm) within a cylindrical battery case having a vacuum annulus of about 2 cm to contain the high-efficiency multifoil insulation. The space between the cell walls and the inner cylinder wall will be used for bus bars and connectors, instrumentation leads, voltage taps, and air cooling pipes.

C. System/Component Development

The emphasis during the past year has been upon the development of bus bars and connectors that meet the needs for high-temperature batteries and upon the development of procedures and equipment that simplify cell fabrication and assembly.

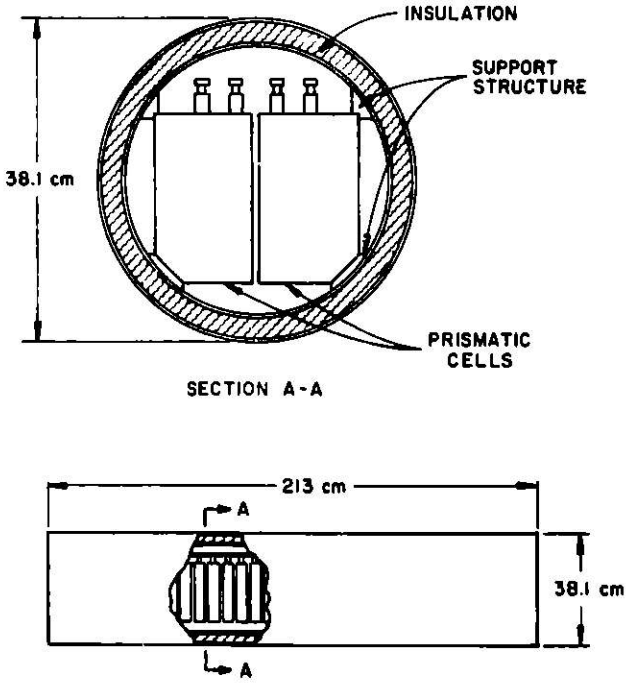

Fig. VI-2. Proposed Battery Module For an Electric Vehicle

1. High-Temperature Bus Bars and Connectors
(M. A. Slawecki*)

A more detailed study of the Li-Al/FeS_x battery for the Battery Energy Storage Test (BEST) Facility is in progress; previous work on this design was presented in ANL-75-1, pp. 124-134. The objective of the present study is to better define the allowable resistances for cell, module, and battery current conductors.

An estimated total energy loss of 1200 kW-hr for each 4.8 MW-hr battery string is expected for the BEST Facility battery on the basis of 80% efficiency. About half of this loss (600 kW-hr) is in the internal resistance of the individual cells with the remainder in all cell, module, and battery connections and bus. An earlier preliminary study of allowable losses in the battery had assumed approximately 30% of the total losses (360 kW-hr) in all connections of the battery, with the remaining 20% (240 kW-hr) in the metal bus of the battery.

A study of the various bus connections required has shown that, regardless of the final geometry of the battery, three basic types of connections (excluding individual cell internal connections) will be required:

1. Cell pole-to-submodule** bus connections
2. Submodule-to-submodule connections
3. Module-to-module† connections.

Various connection test pieces are being fabricated for mock-up and testing. The first units will be made from #102 OFHC copper†† and #150 zirconium-copper.†† Those pieces required for connections outside the sealed submodule will be nickel-plated for corrosion protection.

A test facility is presently being constructed to perform connection-resistance tests. The facility will consist of two furnaces--one for tests of all bus connections made outside the battery submodules (air atmosphere) and one for tests of connections inside the submodule (inert atmosphere). This facility will be used to perform connection-resistance tests on all battery systems designed, including those for electric vehicle use.

2. Salt-Filling Apparatus
(G. J. Bernstein, J. E. A. Graae§)

An apparatus has been designed to demonstrate the filling of cells with electrolyte without the need for inert-gas gloveboxes. The apparatus

---

*Installations Group, Chemical Engineering Division, ANL.

**Submodule-parallel connection of any number of cells in a sealed case (BEST battery requires 6 cells per submodule).

†Module-series connection of any number of submodules (initial design of BEST battery requires 5 submodules per module).

††Copper alloys from Copper Development Assoc.

§Consultant to ANL Battery Program.

comprises a resistance-heated furnace which contains a salt-melting tank, a sintered stainless steel filter, a cell positioner, and appropriate valves. The apparatus provides for melting of the salt at ∿450°C, degassing of the cell under vacuum, and filling of the cell with filtered molten salt. The apparatus also provides for adjustment of the final salt level in the cell within specified limits.

Under present plans, the LiCl-KCl from Lithcoa will be filtered. However, if electrolytic purification of salt is necessary, space is available within the furnace for addition of a purification tank.

D. Battery Testing

The main emphasis in the past year has been centered upon the planning and construction of a battery testing laboratory. The laboratory, which is now completed, provides the facilities for electrical/electronic circuit development, battery testing, and space for development of components such as the salt-filling apparatus. Because of the limited floor space in this laboratory, only two-cell, three-cell and six-cell batteries are to be tested here. Additional laboratory space is being acquired for the larger sized batteries that will need to be tested in the future.

1. Battery Test Facilities and Test Plans

(V. M. Kolba, E. C. Berrill, G. W. Redding, T. E. Hickman,* T. A. Morgan*)

Plans are being implemented to provide the capability for testing single and multiple cell arrangements without the need for inert-atmosphere gloveboxes. Three small test chambers (15.2 cm diameter) have been installed for single cell tests; these can be interconnected to provide for series or parallel testing of up to three cells. Two larger test chambers (30.5 cm diameter), which provide for testing six cells in series or parallel in each unit, have been completed.

Both sizes of test chambers are equipped with flanges that accommodate leads for cell current, cell voltage, cell heater power, and temperature measurements. The current leads will permit external coupling of the cells for series or parallel arrangement, or elimination of a defective cell without breaching the inert atmosphere containment. The voltage leads permit the monitoring of individual cell voltages and the voltage equalization of individual cells. The heater power leads are connected to the individual start-up heater tapes. The temperature of each cell is monitored, as well as the temperature of the chamber. Spare leads are provided for special temperature measurements.

The status of other equipment items is as follows. Two furnace-control consoles--one for control of the three small test chambers and the other for control the two large chambers--have been designed and fabricated. Two cyclers for control of the charge/discharge of the cells and batteries have been designed. The small cycler (250 A at 20 V) for up to three cells

---

*Co-op Program Students, University of Cincinnati.

has been completed, checked out, and installed. The large cycler (250 A at 40 V) for up to 12 cells, is being fabricated. A console for equalizing the charging of up to four cells has been designed and is being fabricated; this console will be interconnected to the small cycler during testing.

Test measurements of voltage, current, time, temperature and number of cycles will be fed to a data acquisition system and stored on tape. These data will be used to calculate desired quantities, which may be displayed in tabular or graphical forms.

The cells to be used in this test program are of the prismatic type currently being fabricated for ANL through industrial contracts. Some of the important battery performance parameters to be determined are as follows:

1. Capacity as a function of constant current at various current levels during charge and discharge.

2. Capacity as a function of constant-power discharge.

3. The effect of various charging procedures upon battery capacity and energy efficiency.

4. The effect of cell-capacity mismatch upon battery capacity.

5. The efficacy of the battery charging/equalization circuits being developed.

6. The effect of various fault conditions upon battery operation *i.e.*, short circuit, shorted cells, open cells.

7. The effect of nonisothermal conditions upon battery capacity and power output.

2. Battery Charging/Equalization Circuits
(F. Hornstra, J. Cox*, W. W. Lark, E. C. Berrill)

As described in a previous semiannual report (ANL-75-1, p. 134), one of the requirements for Li-Al/FeS_x batteries is close control of the cell voltages within the batteries. Two methods are being pursued to effect voltage equalization among battery cells.

In the first method, conceived for laboratory use, individual, isolated, adjustable power supplies are connected to each cell of the battery. The power supplies operate individually in a constant-current or constant-voltage mode. Depending upon terminal conditions, each supply automatically changes from one mode to the other. For example, when the cell voltage is lower than the set voltage, the supply for that cell will operate in a constant-current mode until the cell voltage reaches the set voltage; then the supply operates in a constant-voltage mode with the current monotonically decreasing to the self-discharge current of the cell. As an adjunct to this system, a cell voltage monitor is being constructed which will terminate the

*Industrial Participant from Gulton Industries.

main battery charger when any cell reaches the set cutoff voltage. This action can also turn on the cell-voltage equalizing circuit to complete the charging process.

A second method is being developed for use in the battery of an electric vehicle. Here, cost and weight are important considerations. J. Cox, an industrial participant in tne ANL program from Gulton Industries, Inc., has been focusing attention on this application. A preliminary analysis indicates that a system which will be acceptable for use on an electric vehicle can be built. The design and construction of a laboratory test model for a six-cell battery is being proposed by Gulton.

3. Multicell Cycler
(E. C. Berrill, W. W. Lark, F. Hornstra)

The increase in number of cells now being tested, along with the planned increase in the fabrication of cells by industrial suppliers, has created a need for a simple, low-cost system for testing large numbers of cells. To date, the most expensive element of such a system has been the cell cycler. This device controls and regulates the charge/discharge current of a cell under test and ensures that preset limits on high and low cell voltage are not exceeded. To meet these immediate needs and provide for future expansion, a new cell cycler has been designed and tested through a working prototype stage.

The new cell cycler is of modular design (43.2 cm long by 20.3 cm wide by 25.4 cm high), weighs about 13.6 kg, and has solid-state components. Each module is capable of independently cycling a single cell. In the first application, ten of the modules will be combined in a cabinet to form a multicell cycler system. The cabinet contains meters that will allow a status determination of any of the ten cells. The cabinet and the individual modules are also provided with a computer-interface plug so that the cell readings can be monitored and recorded by an existing data-acquisition system. Charge/discharge currents are independently adjustable up to ±25 A and can be regulated to better than ±1%. Upper and lower cell voltage limits are adjustable and can be held to any value up to 3 V within ±10 mV. Front panel controls also provide for open-circuit testing and manual override of automatic cycling at any time.

A contract with a commercial electronics manufacturer, Paraplegics Mfg. Co., Bensonville, Ill., has been negotiated to assemble 26 modules and one equipment cabinet plus all interconnecting cables. The modules cost about $500 each, in lots of five. This represents a considerable saving in cost over similar electromechanical cycler equipment used heretofore, and an improvement in accuracy, reliability, and versatility is expected.

REFERENCES

1. L. L. Liston and R. W. Sherrer, Cost of Operating an Automobile, U. S. Department of Transportation (April 1974).

2. M. A. Hind, in "Electric Vehicle (for Industry)" p. 12, June 1973.

VII. COMMERCIAL DEVELOPMENT
(R. O. Ivins)

To accelerate the commercial availability of lithium-aluminum/iron sulfide batteries requires a rapid and efficient transfer of technology to industry. Toward this end, the participation of industrial firms capable of manufacturing components, electrodes, cells, and batteries has been sought at an early stage in the development program. Commercial development is being implemented by contracting with industrial firms to develop (1) components such as insulated battery casings, electronic circuitry for charge control, electrical feedthroughs, and ceramic separators and (2) manufacturing techniques for electrodes and cells.

A. Industrial Participation in ANL Program

A program is being carried out in which scientists and engineers from industrial firms spend from three months to a year working in the ANL battery program. This program is bringing industrial experience in battery design and manufacture to the laboratory cell-development efforts. This direct participation has also provided the participating firms with the knowledge that they need in bidding on contracts to develop manufacturing techniques for electrodes and cells. To date, six industrial firms have assigned highly qualified personnel to ANL. These are Gould Inc., Globe Union, Inc., C & D Batteries, Inc., Catalyst Research Corp., Eagle-Picher Industries, Inc., and Gulton Industries, Inc.

B. Cell and Battery Procurement
(R. F. Malecha,* V. M. Kolba)

Development contracts have been made with industrial firms to develop fabrication techniques and to fabricate test electrodes and cells. The purposes of these contracts are to (1) transfer ANL technology on lithium-aluminum/iron sulfide cells to industrial firms, (2) provide industrial capability for manufacturing test electrodes and individual cells in the quantity necessary for the ANL battery development program, and (3) develop manufacturing techniques and procedures applicable to mass-manufacture of cells and batteries.

The developmental cells to be fabricated in the contracts are a prismatic type having a positive center electrode with a negative electrode at each face (see Fig. VI-1). Two thicknesses of electrodes and cells will be fabricated. The thin type (A) is applicable for use in electric vehicles, whereas the thick type (B) is applicable for use in utility off-peak energy storage systems. For each application, several techniques will be used to prepare Li-Al, the active material for the negative electrodes. Moreover, several techniques will be investigated for fabricating positive electrodes; the positive electrode materials to be used are FeS-Cu_2S and FeS_2-CoS_2. Details of the electrode and cell design specifications are given in Section VI.B.1., this report.

As discussed in the preceding report (ANL-75-36, p. 120), requests for proposals to develop manufacturing techniques for electrodes and cells were

*Chemical Engineering Division, ANL.

issued in January 1975, and contracts were signed on April 1, 1975, with Gould Inc., and on May 1, 1975 with Eagle-Picher Industries, Inc. A third contract--with Catalyst Research Corp.--became effective on October 1, 1975.

1. Contract Support and Management

A contract steering committee provides technical direction to the contracted efforts. The committee is composed of five members, three of whom are technical monitors, one for each contract. The committee reviews the progress on the contracts on a weekly basis to identify problem areas. Having defined a problem, recommendations are made on areas that should be investigated by the contractor or by ANL to resolve the problem. A plan for evaluation and testing of contractor-supplied electrodes and cells was developed and is being implemented.

At approximately six-week intervals, joint meetings on updates in technology and contractor progress are held between the contractors and ANL. Mutual areas of concern are discussed, *e.g.*, equipment for monitoring glovebox atmospheres, materials, new techniques for cell assembly, modifications in the design of electrodes or cells, etc. As a part of this effort, various changes have been made during this period to maintain the industrial effort at a level that is current with the advancing laboratory technology at ANL. Some of the changes that have been made are as follows:

1) The nominal composition of the Li-Al alloy was changed from 50 to 43.5 at. % Li.

2) Methods of particle retention were modified. ZrO_2 cloth was added to the negative-electrode side of the BN separator cloth. In the Gould cells, the ZrO_2 paper or cloth in the positive electrode was replaced with carbon cloth.

3) The positive electrodes were divided into compartments.

4) The electrolyte volume fraction in the positive electrodes was increased.

5) Provisions were made for mechanical as well as metallurgical connections of molybdenum components in the positive electrode.

6) Provisions were made for carbon-cement bonding of vitreous carbon and graphite structures.

7) Holes were added in the top segment of the positive-electrode frame to aid in filling the electrode with electrolyte.

As part of the continuing technical administration of these cell contracts, a significant number of design changes have been developed by both the contractors and ANL. Examples of contractor developments which were approved shortly after ANL conducted design reviews are as follows:

1) A method was devised for making connections to the negative electrode.

2) Designs were established for electrical insulation of the positive electrode current collector above the electrode.

3) Honeycomb-type current collectors were incorporated into cold-pressed positive electrodes.

4) Hardware designs required for separator and particle retainers around the positive electrodes were established.

Examples of ANL-generated changes which were accepted by the contractors are as follows:

1) Specifications for impurity levels in the glovebox atmosphere were modified at an early stage to <3ppm H_2O, <5ppm O_2, <5ppm H_2 and <5ppm N_2. (As a general rule, these requirements have been met using commercially available equipment; however, some difficulties have been encountered in monitoring the water level at this level.)

2) Detailed specifications for materials were developed by ANL as part of a continuing effort.

3) Quality assurance requirements were up-graded and clarified.

Because of an early decision that ANL would supply all cell active materials (and certain other critical items), several types of support work involving ANL personnel were required. For example, the FeS_2 was processed to remove a significant fraction of silica grains that were present as an impurity; this was done in a joint effort among ANL, Gould, and the University of Minnesota. In addition, the commercial LiCl-KCl selected for cell use was filtered prior to its use in cells; preparation of electrolyte is an area of continuing effort.

2. Gould Contract

This contract, which was described in the preceding semiannual (ANL-75-36, p. 122), covers the development of electrodes having porous current collector structures which are loaded with powders of the active materials alone or with additives. During this reporting period, the contractor completed installation and check-out of equipment at his site; proceeded with development work; and delivered the following electrodes and cells: 24 aluminum plaques; nine Li-Al powder electrodes; nine Li-Al electrochemically formed electrodes; six $FeS_2 + CoS_2$ electrodes; six $FeS + Cu_2S$ electrodes; six cells having positive electrodes of $FeS_2 + CoS_2$ and negative electrodes of Li-Al powder; and six cells having positive electrodes of $FeS + Cu_2S$ and negative electrodes of Li-Al powder.

3. Eagle-Picher Contract

This contract became effective May 1, 1975 and covers the development of electrodes having compartmentalized structures which are loaded by cold-pressing powder mixtures of the active material, any additives, and the electrolyte salt. In this reporting period, the contractor completed installation and check-out of equipment at his site and development work on

the compartmentalized structure and cold-pressing of powders into this structure. Development work on methods of joining molybdenum is continuing. Electrodes and cells are scheduled for delivery by mid-January 1976.

4. Catalyst Research Contract

In negotiations that preceded this contract, the scope of work was developed with the contractor, detailed drawings and specifications were prepared, and a pre-award contract meeting was held, in which the drawings and specifications were discussed and a work statement was agreed upon. The contract, which became effective October 1, 1975, covers the development of a cast or dipped alloy in a porous structure for the negative electrode and a powder-loaded positive electrode similar to that in the Gould contract. Catalyst Research will also develop the capabilities for cycling test cells and conducting post-test examinations of the cells. About two-thirds of the cells fabricated will be tested by Catalyst Research and the remaining one-third will be sent to ANL for testing. During this reporting period, development work on loading a Retimet structure with Li-Al by dipping or casting was started. Design of cycling equipment and temperature control systems for testing cells is also in progress.

C. Component Development
(J. E. Battles)

1. Electrode Separators

A compact, lightweight cell requires a porous electrode separator that is resistant to the cell environment, is low in cost, maintains electrical isolation of the electrodes, and permits close electrode spacing. (Work on separator development is discussed further in Section IV.) Boron nitride fabric from the Carborundum Co. has been used successfully in test cells; however, present cost ($515/ft^2) and projected cost (~$10-15/ft^2) of BN fabric preclude its use in low-cost commercial cells. One method of lowering costs is through the use of papers that require less fiber per square foot of separator area. Therefore, efforts are being concentrated on the development of papers prepared from BN or other stable, ceramic fibers. The preliminary specifications for the separators are as follows: 1) porosity, about 85%; 2) thickness, 0.75-1.5 mm; 3) pore size, ~5 μm; and 4) adequate strength during cell fabrication. Development contracts have been initiated with the Carborundum Co. and the University of Florida (funded directly by ERDA) to develop improved separators. Also, contract discussions are under way with other manufacturers of ceramic fibers and papers.

Initial efforts at Carborundum were concentrated on the fabrication of a BN paper using commercial organic and inorganic binders. These binders were unsuccessful because of decomposition of the organic binders at cell operating temperatures (~450°C) and chemical attack of the inorganic binders (colloidal SiO_2 and Al_2O_3) in the cell environment. However, new cell designs providing mechanical support to the fiber separator may allow use of these materials even though the binders lose integrity. Presently, efforts are concentrated on developing a BN paper using BN as a binder; such a separator would be compatible with the cell environment and current cell designs.

Initial results have been encouraging and appear to warrant increased effort. Carborundum has projected a cost of about $50/lb for BN fiber at an annual production rate of 50,000-100,000 lb per year. Based on the specifications listed above, the projected cost of BN paper would be $2-5/ft^2, depending on the fiber content and thickness of the separator. Further reductions in cost can be expected at much higher production rates (*e.g.*, 10^6 lb per year).

The major emphasis of the development contract with the University of Florida is on the fabrication of composite-type separators using various combinations of fibers and ceramic powders. Separator papers have been prepared using BN and asbestos fibers with particulate fillers of BN, MgO, or $LiAlO_2$ powders. In these preparations, the ratio of BN and asbestos fibers was varied to determine the effect of asbestos concentration on mechanical properties. Also, the quantity of particulate filler was varied. Initial results indicate that the addition of asbestos fibers and MgO powders substantially strengthens papers made of BN fibers. Future efforts will be directed toward improving the composite-type separators and characterizing them in terms of pore size, porosity, permeability, etc. Also, new combinations of materials (fibers and powders) will be evaluated.

2. Electrical Feedthroughs

The effort to develop an electrical feedthrough has been expanded to include work by several commercial manufacturers of ceramic bodies and feedthroughs (see Section IV).

A compression-type feedthrough (modified Conax fitting) has been successfully used in many ANL test cells. The main limitations of this feedthrough are size, weight, and insufficient leak-tightness. Replacment of the lower BN insulator with a higher-strength insulator of BeO or Y_2O_3 is expected to improve the leak-tightness. Also, the metal body was redesigned to achieve a reduction in size, cost, and weight. Cost estimates from commercial vendors indicate that the feedthrough can be produced in large quantities (100,000 units) for about two dollars per unit.

Efforts are under way to develop a brazed-type feedthrough utilizing the technical expertise of three commercial feedthrough manufacturers. The 3M Corporation has prepared feedthroughs with BeO insulators using conventional brazing techniques. Because the braze material is not compatible with the cell environment, the braze joint was plated with either nickel or gold. ILC Technology has developed several Nb-base active metal brazes for BeO and has produced feedthroughs with Nb-Ni, Nb-Cu, Nb-Ag, and Nb-Au brazes. Niobium was selected as the base metal because it is not expected to oxidize at reasonable cell charge potentials. The most recently started program is with Coors Porcelain Company for the development of Y_2O_3 ceramic bodies and a nonmetallic braze. The raw materials cost of Y_2O_3 is somewhat more than that of BeO, but the fabrication costs are lower because special handling facilities are not required.

Prototype feedthroughs have been received from each of the commercial firms discussed above. Mechanical tests and tests in a simulated cell environment are being conducted; these tests will enable modes or mechanisms of failure to be determined. The results from these evaluations will eliminate the less favorable concepts and will also provide necessary information for improving feedthrough designs.